MAGYAR TUDOMÁNYOS AKADÉMIA

Műszaki Fizikai Kutató Intézete

MFKI '80

YEARBOOK

of the

Research Institute for Technical Physics
of the Hungarian Academy of Sciences

Институт Технической Физики
Венгерской Академии Наук

Forschungsinstitut für Technische Physik
der Ungarischen Akademie der Wissenschaften

MAGYAR TUDOMÁNYOS AKADÉMIA

Műszaki Fizikai Kutató Intézete

MFKI '80 YEARBOOK

RESEARCH INSTITUTE FOR TECHNICAL PHYSICS
OF THE HUNGARIAN ACADEMY OF SCIENCES

Budapest, Hungary, 1981

Published by the

RESEARCH INSTITUTE FOR TECHNICAL PHYSICS
OF THE HUNGARIAN ACADEMY OF SCIENCES

Postal address:

H-1325, Budapest, Ujpest 1., P.O.Box 76.

Responsible publisher:
Elemér NAGY, director

Editor:

Béla SZENTPÁLI

Publisher's readers:

Erzsébet BARTA

Mihály GÁL

Editorial board:

Edit KOVÁCS

Mrs. Éva LAJOS

ISSN–0139–4363

Hozott anyagról sokszorosítva

8112670 MTA KESZ Sokszorosító, Budapest. F. v.: dr. Héczey Lászlóné

PREFACE

Dear Reader!

Having the second issue of our Yearbook in your hand, it is of course natural that you make a comparison with the previous one. The past two years brought about much change in the organization and funding of research in our country, the most notable being the preferred treatment of that kind of research which leads to new products and technologies. This preferred treatment means that this type of research is not a merely academic effort, but the Ministry for Industry, the State Committee for Technical Development and the end user factories are also funding it.

Most of our research falls into that category.

Some people would say that this kind of research is not true research at all. I tend to disagree with them: it is true research but subject to severe constraints in respect of topic selection. The conditions to be met are numerous indeed. The task should not be too big, since there is no hope for solution within a resonable time with the manpower, equipment and funding available. The results of the research must be introduced into industry, manufactured and marketed. This is of course the overwhelmingly largest part of the total expenditures. So it can lead but to a waste of funds and a waste of credibility to do research with strongly subcritical means. On the other hand a supercritical research team is in fact too conservative, the economical results do not warrant the exaggerated expenditures.

It is very hard to find the possible compromise between these extremes, I personally would shift towards aggressiveness, because fundamental research can lead sometimes to real breakthroughs.

Our two main tasks are now GaAs based devices on one hand and the theory and practice of sintering on the other.

The selection is motivated in the first case by our country's gallium resources, in the second case by the lack of an adequate statistical theory of sintering.

Two other lines which are also followed is the instrumentation in steel manufacture and photometry. We feel that we have competent specialists in both fields and both researches contribute in a special way to the saving of energy.

That's about all and should the scientists speak for themselves

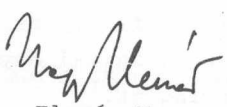

Elemér Nagy
corr.member of the
H.A.S.

CONTENTS

SEMICONDUCTOR RESEARCH DIVISION

METAL RESEARCH DIVISION

STRUCTURE RESEARCH DIVISION

DIVISION OF OPTICS AND ELECTRONICS

INTERNATIONAL SCIENTIFIC ACTIVITIES

I.C. Szép

Nowadays as science has become worldwide, scientific and research organisations need a well-considered scheme of international relations, partly to be informed about new accomplishments, new trends in scientific disciplines of interest, partly to disseminate new results, discoveries made by the respective organisation. Publishing /and also reading/ papers in periodicals, writing /and reading/ monographs can serve both purposes in the same way as attending /and talking at/ conferences.

Unfortunately, the number of publications and also of scientific gatherings have risen to levels uncomprehensible by the individual, as well as has grown the irresistible sub- and subdivision of scientific disciplines.

However, with careful selection one can compromise possibility with reality, and this was the way our Institute has tried to arrange its relations with the scientific world outside. In brief, during 1979-80 some 200 original papers were published in international journals, nearly 50 talks were given at international conferences by coworkers of our Institute. For their outstanding scientific achievements quite a lot of our members have been regularly invited to act as advisers and referees in organizing and programm committees of various international events. For instance, Dr. L. Bartha has acted as member of the Organizing Committee and also as invited speaker at the 2nd Symposium on Incandescent Light Sources, held at Enschede in 1979; Dr. P.B. Barna was invited to the Advisory Committee of the 8th International Vacuum Conference in Cannes /1980/, and also of the 6th International Congress on Crystal Growth in Moscow, 1980; Dr. J. Schanda took part in the Organizing Committee of the 8th IMEKO Congress in Moscow, 1979.

Some have been elected as officers of international scientific organisations: Dr. J. Schanda has been elected vice-

president to the Executive Board of Comité International de l'Éclairage /CIE/; Dr. P.B. Barna became a member of the Executive Council of the International Union for Vacuum Science, Technique and Application /IUVSTA/, and also a member of the Scientific Council of the International Center for Electron Microscopy in Halle /GDR/.

A number of internationally recognized scientific events took place here in Hungary with active participation or even initiation by our Institute. So, for instance, symposia on coloristics in 1979 and 1980, the "optica '80" conference, the VIIth conference on Rare Metals, the Austro-Hungarian Vacuum Conference /Győr, 1979/ have seen many members of our Institute as organizers, reviewers, etc., and of course, as speakers.

The idea of the International Summer School on the Processes of Thin Film Formation, held at Fonyód /1980/ was put forward by our Institute, likewise the International Autumn School on MIS Systems /Dobogókő, 1979/ and the International Summer School on New Developments in Semiconductor Physics /Szeged, 1975/. To these "schools" lecturers of international renown have been invited and an audience between 100-200 from home and neighbouring countries attended. Selected items served both to upgrade and to summarize knowledge of the participants, which was aimed at, by organizing this type of gathering.

Beside these activities, in past two years succesful efforts were also made to extend our direct cooperation with research organizations abroad. Regular exchange of research workers for shorter or longer periods took place with institutions in the Soviet Union, Czechoslovakia, the German Democratic Republic, the Federal Republic of Germany, Sweden, France and Italy. Agreements on scientific cooperation signed by the Hungarian Academy of Sciences and respective authorities of the countries concerned made up the frame for this kind of exchange, as well as the system of schloarships granted by the Ministry of Education.

All these activities have well supported the work done here, made possible, to a great extent, to keep pace with scientific progress abroad, to join efforts with other research organisations, and also to draw attention of the international scientific community to the achievements of our Institute.

SEMICONDUCTOR RESEARCH DIVISION

SEMICONDUCTOR RESEARCH IN THE 1978-80 PERIOD

E. Lendvay

To a large extent our work in the 1978-80 period has been based on semiconductor technology worked out in our laboratories during the last five years. This technological ability allows us to produce GaSb, GaAs and different ternary and quaternary compounds as GaAlAs, GaAlP, GaAsSb, GaAlAsSb and their homo- and heteroepitaxial combinations. As for the Si based MOS and MNOS devices a variety of technologies was also required and developed producing high quality oxide and nitride layers and their combinations.

Epitaxial structures of GaAs and related compounds are in the focus of our activites. They have applications in microwave and optoelectronic devices. For example our GaAs VPE technology produces pure /$n < 10^{15}$ cm^{-3}/ and as well as doped /10^{14} $cm^{-3} \leq n \leq 10^{18}$ cm^{-3}/ GaAs layers for particular microwave applications such as Gunn and Schottky diodes.

To grow LED and laser structures we have built an automatized vertical liquid phase epitaxial system. Using these equipment GaAsSb/GaAlAsSb double heterostructures and GaAlAs/GaAs laser structures were produced.

For laser production an integrated heat sink technology and the metallization of our samples using AuBe and AuGe were developed. Our present DH laserdiodes have a broad-contact geometry with a 5-6.6 kA/cm^2 threshold at room-temperature. Another very interesting technological result is the preparation of GaAlP/GaP:N DH structure. This system is very promising for the study of the superinjection in indirect semiconductors.

Simultaneously with the development of $\lambda > 1.0$ μm LED-s and laser structures the problem of infrared detectors working beyond 1 μm /at around 1.2-1.5 μm/ has emerged. After the recognition of the applicability of $A^{III}B^{V}$ antimonides for both light sources and detectors GaSb single crystal growth was performed by a modified Stockbarger method. The produced GaSb

crystals were of higher structural perfection than the ones pulled with the usual Czochralski method. These experiments together with InSb and GaAs growth /"Eötvös-experiment"/ were repeated on board of the Soyuz-6 space laboratory during the flight of the first Hungarian astronaut. Both in normal and space experiments the wall-effect was found to play a major role in seed formation.

As another possibility for IR detection PbS and PbSSe detectors have been developed using slow chemical precipitation methods. Modifiying the concentrations and the precipitation rate we prepared detectors having the spectral sensitivity maximum between 1.7-2.6 μm and the responsivity of $0.7\text{-}1.5.10^4$ V/W.

A wide range of techniques is also available for characterizing the physical, electrical and optical properties of our materials and structures. The most sophisticated method used in our Department is the deep level transient spectroscopy /DLTS/ which has provided special information about the nature of different defects existing in the most important LED structures, such as GaP and GaAsP. The DLTS spectrometer built in our laboratory is a custom designed equipment characterized by high sensitivity $/\Delta C/C \sim 10^{-6}/$ wide rate window interval $/2\ s^{-1} < en < 5.10^3\ s^{-1}/$ and great versatility. Combining this method with single shot capacitance and photocapacitance transient experiments, nonexponential processes have been observed and explained as a long range lattice distortion in GaP and GaAsP LED-s.

In the field of microwave devices a concentrated effort to achieve good quality, high power Gunn diodes, GaAs Schottky mixers and detectors was made. To meet these requirements a higher level in material technology, design tolerances and manufacturing processes was established. It was determined that for Schottky diode preparation a special requirement is the formation of thin 3 nm thick native oxide, which has no free charges. For Gunn diodes among the processing steps the metallization is one of the most important factor determining the power output, lifetime and other important diode parameters.

The sintering and alloying of contacts using mono- and multi-layer metallization were examined by mass-spectrometry and "in situ" resistance measurements. As it was published earlier the loss of V. column element through the metal layer is the determining factor in contact-resistance changes. Using molecular beam of the particular element /eg. As_2; P_2/ we pointed out the reversibility in the latter process. More than 20 metals and composites /multilayer metallization/ have been examined on GaAs and GaP. Using Au based contacts an anomalous peak of As or P loss was observed from the $A^{III}B^{V}$ semiconductor above a relatively low temperature. Schottky contacts /eg. Al, Pt, Ni, CrAu etc./ and Ag-based metallization show low V. component loss without a peak in temperature dependence.

Regarding our MOS devices we improved our technology for double-gated /silicon-aluminium/ structures and linear CCD-s have been prepared. This MSI level device can be applied to delay analog signals, and recursive filters were constructed and built. This technological progress is partly due to examination of the formation and structure of oxides on Si, using different techniques as electron diffraction and ELMI techniques, TSC /Thermally Stimulated Currents/, ellipsometry and capacitive methods. We observed eg. a 0.35 eV TSC peak which is probably connected with hydrogen in the oxide. The peak was found to be characteristic to the oxide-water interaction. The study of the chemical and thermal oxidation of silicon resulted in higher quality oxides in which the life time was extremely good /400 μs at 310 K in 152 ohmcm n-type material/.

Similar investigations in the oxide-nitride system have proved the importance of built-in hydrogen in MNOS structures, too. With the successful combination of our MOS and MNOS technology, as a test circuit, a fully decoded 64 bit MNOS memory array was produced. During this work we had to solve the problem of contradictory conditions for "write in" and "retention" properties. To measure the static characteristics of these memories an automatic "on line" measuring system was designed and built.

HIGH RESOLUTION THERMAL ANALYSIS OF MICROCIRCUITS USING THE NEMATIC LIQUID CRYSTAL METHOD

G. Aszódi

By the so called nematic liquid crystal method[1] one can map the temperature field of surfaces of microscopic objects with the help of nematic - isotropic phase transitions of liquid crystals. The scope of our work was:

- to improve the accuracy of determining isotherms and to consider the applicability to very small surface thermal gradients
- to analyse the resolution and error of the measurements when heat sources are at some depth from the surface
- to study the effect of a detector layer covering the sample surface
- to examine the nematogen detector material properties.

/For details of the above mentioned problems see Ref. 2./

Applying the method to thermal studies on light-emitting diodes we were able to detect:

- contact and junction failures
- the temperature of the p-n junction with an accuracy of about several tenth ^{o}C
- warming curves of LED-s
- the exact temperature maps.

Fig. 1 and 2 shows a microphotograph and a complete temperature map of an LED, respectively.

The use of the method in LED - ageing studies helped us to solve some degradation problems. Furthermore nematic liquid crystal thermography may well be beneficial for the thermal mapping of high power devices, e.b. Gunn-effect diodes[3]; MESFETS.

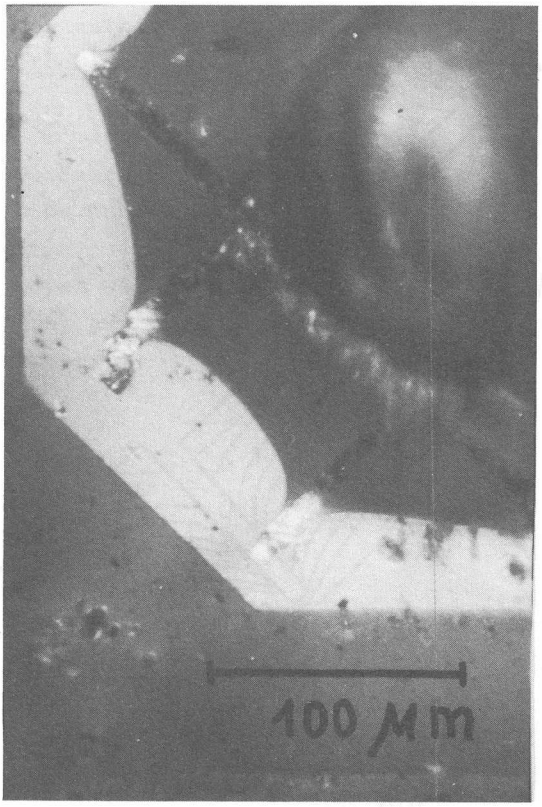

Fig. 1. Original photomicrograph of a LED with octagonal dissipation area. The isotherm corresponding to 31.9°C is the boundary of the nematic-isotropic regions. Using a polarized incident light beam the isotropic region is the dark one. The evaporated Au-contacts can also be seen. Due to the higher current density /dissipation/ near the contacts, the surface is at higher temperature there.

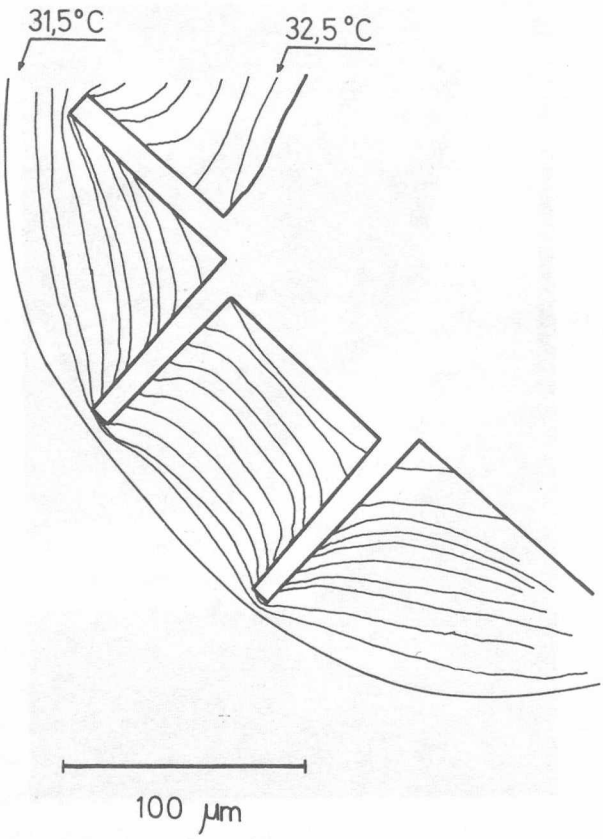

Fig. 2. Complete temperature map of the same LED as shown in Fig. 1 constructed from eleven similar photographs. For the sake of clarity only the outermost and innermost isothermals are marked with their temperature values. The temperature difference between two consecutive lines is 0.1°C.

1. C.E. Stephens and F.N. Sinnadusai, A surface temperature limit detector using nematic liquid crystals with an application to microcircuits, J.Phys.E.: Scient. Instr. 7, 641 /1974/

2. G. Aszódi, J. Szabon, I. Jánossy and V. Székely, Solid St. Electron, to be published

3. G. Aszódi, paper will be presented at the IIIrd Symposium on Thermography and Thermogrammetry 13-17 february 1981, Budapest, Hungary

THE STUDY OF DEEP LEVELS AND THEIR INFLUENCE ON THE DEGRADATION PROPERTIES OF LED'S

G. Ferenczi, G. Aszódi, L. Dózsa, M. Somogyi and T. Tóth

The study of radiative and non-radiative recombination centers in semiconductor light sources is of uppermost importance for a research effort directed

a/ to increase the quantum efficiency

b/ to decrease the degradation rate of the devices.

We have found that this task is best approached by combining minority carrier life-time results with electroluminescence and DLTS data.

In the following a brief summary of our results on VPE GaP is given:

I. During forward current stressing a deep electron trap, called T_6 appears in the DLTS spectra. The trap concentration increases proportionally with the degradation rate and with rate of decrease of the minority carrier life-time. In fact a single non-radiative trap model based on these observations explains completely the measured light output degradation. As to the origin of this trap we conclude that recombination enhanced dislocation motion creates a cloud of vacancies which acts as non-radiative recombination center. To our knowledge this is the first quantitative study which connects the degradation to a directly observed recombination center[1] .

II. The most common electron trap in nitrogen doped GaP was studied in detail. We established that the trap concentration depends nearly linearly on the shallow donor concentration and quadratically on the nitrogen concentration. At high driving current-levels recombination enhanced dissociation of this trap was observed with simultaneous formation of new nearest neighbour radiative nitrogen pairs /derived from electroluminescence/. We suggest that this trap is in fact an interstitial nitrogen pair on a phosphorous site. A manifold of further data suggest this identification[2].

III. We observed that the majority of electron traps in GaAsP and in GaP are characterized by non-exponential capture and emission time constants. The possible consequences of this non-exponentiality were investigated /the usual effects as electric field dependence, edge region effects, high concentration, Coulomb interaction of neighbouring sites etc. was considered and excluded/:

a/ Trap parameters as concentration, capture cross section, activation energy established from DLTS measurements in the conventional way are grossly incorrect. In fact trap concentration up to a factor of 5 are underestimated, activation energies about a factor of 5 are overestimated. Capture cross section data are simply irrelevant. All these are due to the fact that DLTS inherently approximate with a single exponential time constant.

b/ A microscopic model was found to explain this non-exponentiality. It was shown that the collective excitation of the lattice by a captured carrier relaxes logarithmically in time /infrared dispersion/. This new lattice relaxation model explains non-exponentiality and persistent photoconductivity much better than the multiphonon emission model[3].

1. G. Ferenczi, Degradation induced formation of extended defects in GaP:N LED's, to be published

2. G. Ferenczi, P. Krispin and M. Somogyi, to be published

3. G. Ferenczi, F. Beleznay and L. Dózsa, to be published

DEVELOPMENT AND APPLICATIONS OF A DEEP LEVEL SPECTROMETER

G. Ferenczi, F. Tóth[+], P. Horváth[+], J. Boda

As a result of three years research and development effort we developed a Deep Level Spectrometer[1] for studying localized states in semiconductor materials and devices.

Our equipment is a custom built semi-automatic implementation for Deep Level Transient Spectroscopy, a method introduced by D.V. Lang in 1974.

The basic design targets were the followings:

- To increase sensitivity near to the theoretical detection limit.
- To limit operating frequency at 1 MHz since experimental samples with worse than ideal series resistance are not measurable at higher frequencies.
- Wide detectable emission time constant interval.
- The spectrometer should be compact and self-contained unit, i.e. no auxiliary equipments are to be used.
- Operational simplicity and short scan times.

To achieve these goals, i.e. to transform a basic research method into a routine characterisation technique we had to introduce several innovating ideas:

- Repetition rate independent phase setting: The use of lock-in amplifier for signal averageing is justified by the superior noise reduction of a lock-in amplifier compared to other signal averageing techniques. Lock-ins are, however, very sensitive to overload. To avoid this, the bias pulse period should be gated off. In previously published solutions this gate off is constant resulting in inaccurate DLTS amplitudes and activation energies.

+ Central Research Institute for Physics

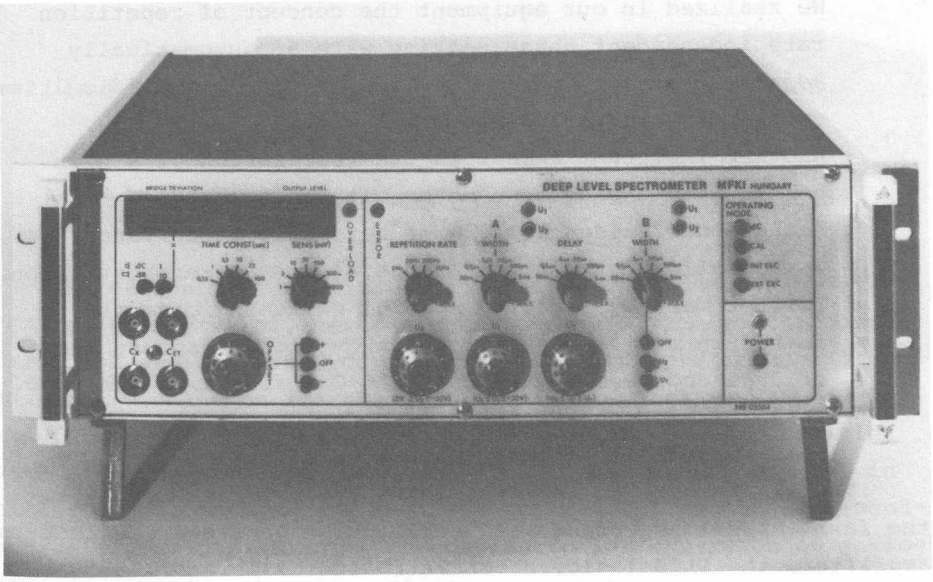
DEEP LEVEL SPECTROMETER MFKI HUNGARY

Fig. 1.

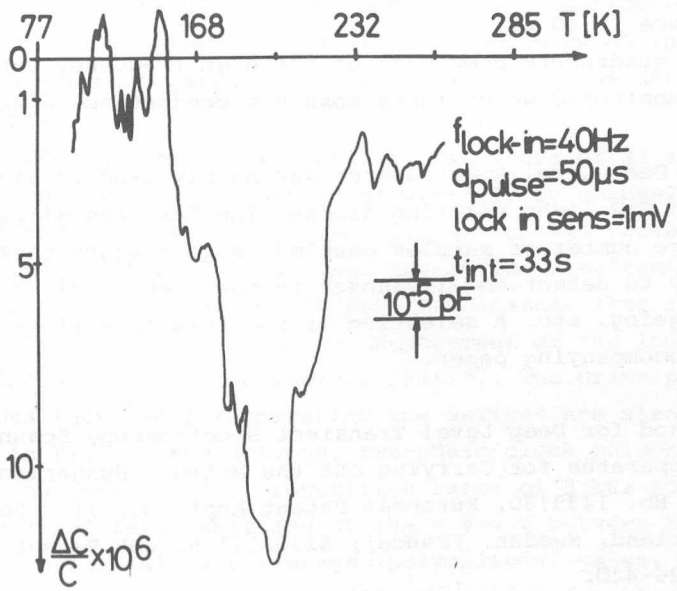
77
168
232
285 T [K]
0
1
5
10
$f_{lock-in}$=40Hz
d_{pulse}=50µs
lock in sens=1mV
t_{int}=33s
10^{-5} pF
$\frac{\Delta C}{C} \times 10^6$

Fig. 2.

We realized in our equipment the concept of repetition rate independent phase setting with an automatically adjusted gate off period which overcomes all difficulties encountered in the previous solutions.

- Another important aspect is the realization of a high sensitivity capacitance meter with fast response time. Using a new bridge design and automatic capacitance compensation to keep the bridge always at zero deviation, further more by applying special switching circuits to introduce excitation pulses, an overload response time of 5 μs and sensitivity up to $\Delta C/C \geq 5 \times 10^{-7}$ was achieved. These parameters are about an order of magnitude better than the similar figures published so far.

The final unit, called Deep Level Spectrometer contains the fast capacitance bridge, a double pulse generator, a lock-in amplifier, the DLTS logic, a concentration calibrator, triger source for external excitation, automatic capacitance compensator and power supply for the cryostat /Fig. 1/. The sensitivity of the Spectrometer is illustrated on Fig. 2. The sample capacitance in 10 pF.

The quadrature component of the high frequency capacitance is also monitored which makes possible conductance spectroscopy as well.

The Deep Level Spectrometer was mainly used to study deep levels in GaP light emitting diodes. The fast and simple way to scan large number of samples enabled us to measure these diodes routinely to detect small changes in the deep level spectra during ageing, etc. A selection of the results will be presented in the accompanying paper.

1. A Method for Deep Level Transient Spectroscopy Scanning and Apparatus for Carrying out the Method. Hungarian Patent Appl. No. 1439/80, European Patent Appl. No. /for BGFR,UR, Netherland, Sweden, France/; 81302531.9, GDR Patent Appl. No. 226-420.

DEVELOPMENT AND APPLICATION OF CHARGE COUPLED DEVICE /CCD/ DELAY LINES

G.Forgács, S.Biró, M.Németh-Sallay, I.Cseh, G.Stubnya

After one decade of their invention, charge coupled devices /CCD's/ can certainly be considered as one of the most important family of semiconductor devices. The research project our group has been working on for the last couple of years was aimed at the investigation of fabrication and application possibilities of MOS CCD delay lines. Such delay lines can widely be used in analog signal processing, e.g. for accurate, frequency-independent delay, multiplexing, time compression or expansion of analog signals, for reverberation effects, voice scrambling, tone generation and other applications in audio equipments etc. as well as in a variety of filtering applications.

Improving our technology, we designed and fabricated 64-stage CCD delay lines with overlapping polycrystalline silicon and aluminum gates. The block diagram of the device is shown in Fig.1.

This CCD consists of two parallel registers of 32 stages each. The input signal is sampled alternately by channels A and B, and thus 64 consecutive samples, or "charge packets", can be stored and transferred along the device simultaneously.

Both p- and c-channel CCD's were fabricated. /The latter in co-operation with Semiconductor Department of the Industrial Research Institute for Electronics, "HIKI"/. The drive pulses and voltages required for operating the devices are also indicated in Fig. 1. For driving, two-phase clock pulses of 10 V amplitude were used at repetition rates of 5 kHz to 1.5 MHz with an external level shifting of ΔV_ϕ = 4-6 V between the adjacent transfer /Al/ and storage /polysilicon/ gates. The effective sampling rate, f_m, is twice the clock frequency and the delay which can be obtained employing one CCD is

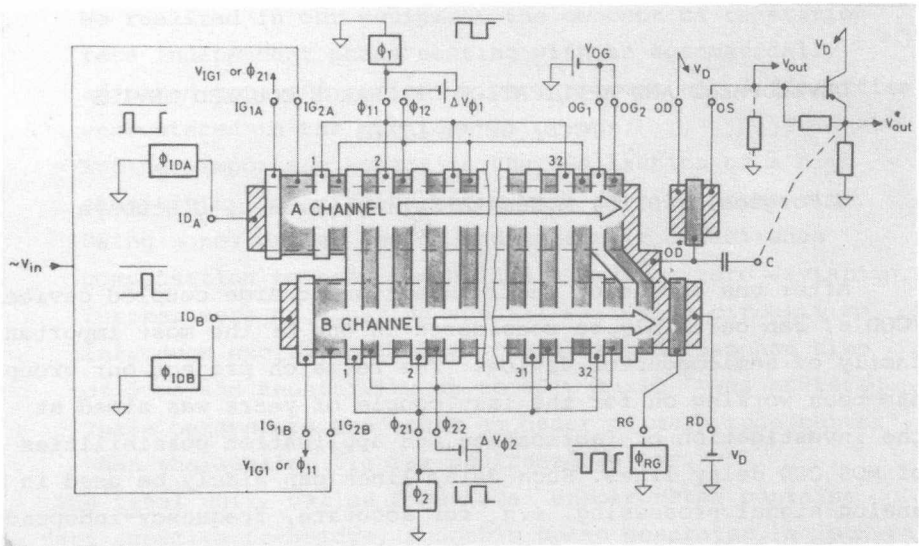

Fig. 1. The block diagram of the 64-stage CCD /The white and shaded stripes represent the aluminum and polysilicon gates, respectively, and the hatched areas are the diffused charge injection and output parts./

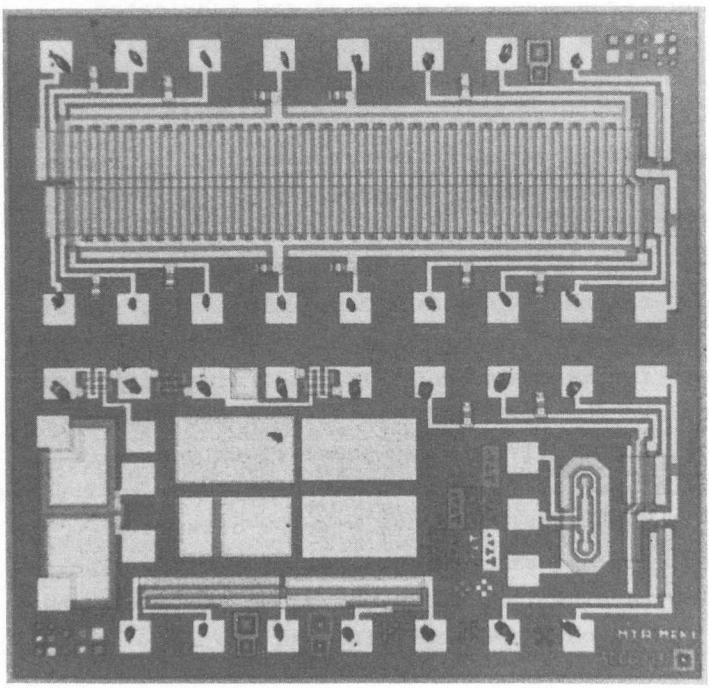

Fig. 2. Photomicrograph of the CCD chip

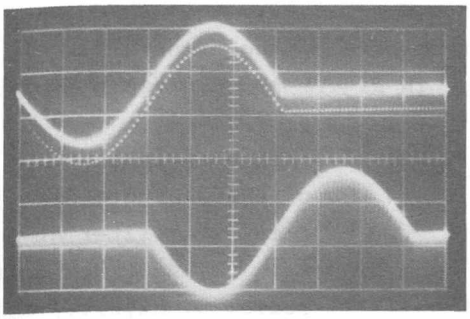

Fig. 3. Delaying of an analog signal by CCD. /Upper trace: : input signal, lower trace: output, horizontal scale: 2 ms/div./

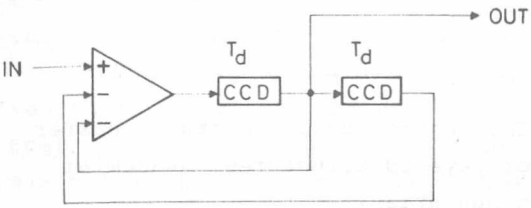

Fig. 4. Block diagram of the second--order recursive filter

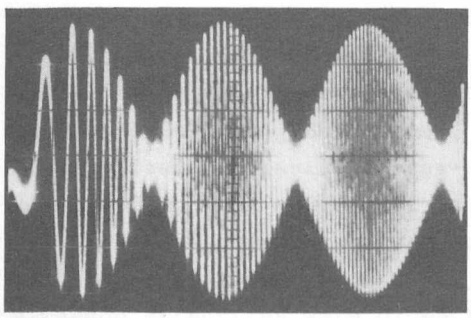

Fig. 5. Frequency response of the transversal filter at f_m = 32 kHz /Horizontal scale: 300 Hz/cm/

$T_d = 64/f_m$ = 6.4 msec to 21 μsec. Fig. 2 is the photomicrograph of a CCD chip containing also some test devices in its lower half.

An illustration of the analog delay operation is shown in Fig. 3. Using the fabricated CCD's, first-order transversal and second-order recursive filters have been built. The block diagram of the recursive filter, the resonant frequencies of

which are $f_o = (2N+1)f_m/128$, where N = 0,1,2,..., is shown in Fig. 4. The observed frequency responses of the transversal and recursive filters can be seen in Fig. 5 and 6, respectively.

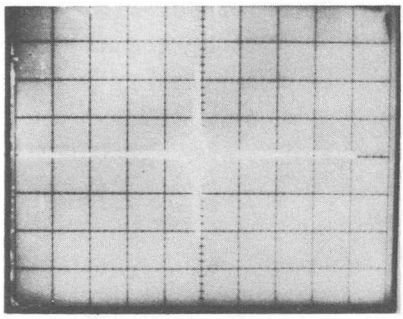

Fig. 6. Frequency response of the second-order recursive filter at f_m = 32 kHz. /Horizontal scale: 57 Hz/div./

1. I. Szép and G. Forgács, Charge Storage and Charge Transfer in Insulator-Semiconductor Layered Structures, Akadémiai Kiadó, Budapest, 1980 /in Hungarian/

INVESTIGATION OF GaAsSb AND GaAlAsSb STRUCTURES

T. Görög, E. Lendvay

The aim of this work was to investigate the equilibrium processes of LPE in GaAsSb and GaAlAsSb systems and to determine the respective growth parameters. Heteroepitaxial structures of $GaAs_{1-x}Sb_x$ and $Al_yGa_{1-y}As_{1-x}Sb_x$ layers were grown onto /100/ GaAs substrates. The gallium rich-side of the pseudobinary phase diagram has been investigated in detail. The specimen composition were chosen in the band-gap region, which is of interest for optical communication.

The ternary and quaternary layers were grown in a conventional horizontal LPE system, using multiple bin grafite boat with slider as described[1]. The grafite boat contained six melts. As source materials 6N Gallium, /Hung. Aluminium Work, Ajka/, 5N5 Sb, and 6N Al /Aluterv-FKI, Budapest/ and policrystalline GaAs /synthetised from elements in our Institute/ were used.

The lattice constans for the binary components are 0.5653 nm for GaAs and 0.6096 for GaSb. In order to achieve a good lattice match between the GaAs and $GaAs_{1-x}Sb_x$ as well as the $Al_yGa_{1-y}As_{1-x}Sb_x$ layers, a few epitaxial layers have to be deposited increasing X step-by-step from low values of $x = 0.002$ up to $X = 0.03$ for GaAsSb and $X = 0.03$-0.04; $Y = 0.22$-0.26 composition ranges for AlGaAsSb heterostructures.

In these experiments up to six layers of GaAsSb and AlGaAsSb structures were grown from saturated Ga solutions. After the saturation the epitaxial growth was performed either from supersaturated melt /isoterm LPE/ or the usual constant cooling method, with $1^{o}C$/min cooling rate[2]. The atomic ratio of As in the melts $/X^{l}_{As}/$ was varied over the range 0.012-0.037, while the aluminium concentration $/X^{l}_{Al}/$ was in the range 0.0020-0.0025. The melts were prepared with different Ga to Sb weight ratio. It varied between 1.05 and 32.3.

The growth temperature was between 780-745^{o}C.

Using isotherm LPE ternary and quaternary layers with mirror like surfaces were grown. For these layers, X-ray microprobe analysis showed that the composition was homogeneous when the layers were grown above a particular T_{cr} = 745^{o}C /critical temperature/. This means that during LPE process no macroscopic segregation takes place above T_{cr}. The same results can be assumed in both the ternary and the quaternary epitaxial structures.

The concentration profile of the different components in the layers was determined by wavelength dispersive X-ray scan measurement with digital data processing.

The solid composition was measured both at the surface and at the cleaved crossection of the sample. Optical absorption and low temperature photoluminescence were also measured. The excitation source was an argon ion laser operating at 488 nm. The radiation from the sample was analysed with a high resolution spectrometer. The type and the carrier concentration across the $GaAs_{1-x}Sb_x$ layers were obtained by electrochemical profile measurement, using Post Office Profile Plotter /Synchrist Ltd/.

Undoped $GaAs_{1-x}Sb_x$ layers showed p type conduction having 10^{-2} ohmcm, $n_p = 5.10^{17}$-2.10^{18} cm^{-3} and a room temperature hole mobility of 260-280 $cm^2V^{-1}s^{-1}$. Using tellurium and germanium as doping materials, we could grow n or p type layers in the 5.10^{16}-1.10^{18} cm^{-3} concentration range. By using n and p doping materials in the consecutive LPE sources, heterostructures containing p-n junction have been grown. In some cases the active layer /GaSb, or GaAlSb/ thickness was less than one micron, and the p-n junction showed good I-V characteristics.

1. E. Lendvay, T. Görög and L.A. Tóth, LPE growth of GaAsSb and AlGaAsSb, to be published in Gallium arsenide and related Compounds 1980.

2. E. Lendvay, T. Görög and L.A. Tóth, LPE growth of $GaAs_{1-x}Sb_x$ to be published in J. Cryst. Growth.

VAPOUR PHASE GROWTH OF TIN DOPED GaAs EPITAXIAL LAYERS

I. Gyuró, T. Görög

Different homoepitaxial GaAs structures are used as basic materials for microwave devices. To grow suitable homoepitaxial layers in our Institute we have developed a vapour phase epitaxial system. During our work both the electrical and the crystallographycal properties of the layers had to be taken care of. Layer structures of different thicknesses and concentration profiles have been prepared in some case with a buffer layers. In our project we had to develop a doping technology, which enabled us to vary the value of the charge carrier concentration. Our technology allowed us to achieve a good reproducibility of the sample series and to grow layer structures of uniform electrical and other physical parameters. The equipment used in the experiments has been published[1,2].

Tin was added to the source as doping material, since it has advantageous diffusion properties for device applications.

The source which contained 6N Ga /Aluminium Works, Ajka/, was R.F. heated in vacuum at 750^{o}C after which it was measured into a quartz boat of high purity /Spectrosil, Hereaus GmbH/. The boat was placed into the reactor tube and heated at 820^{o}C in pure hydrogen atmosphere /Linde AG, West-Germany/. After the oxide layer was removed from the tin /5N5 United Mineral Chemical Corp./ by chemical etching, the required quantity of the metal was added to the source, taking care that no oxygen could enter the system. The source was homogenized and saturated with arsenic at 820^{o}C. This way the system was ready for growth. During our experiments three sources of different Tin concentrations have been made /Table 1/.

This doping method made the modification of the reactor system unnecessary and enabled us to grow layer of required carrier concentration by using different tin containing sources.

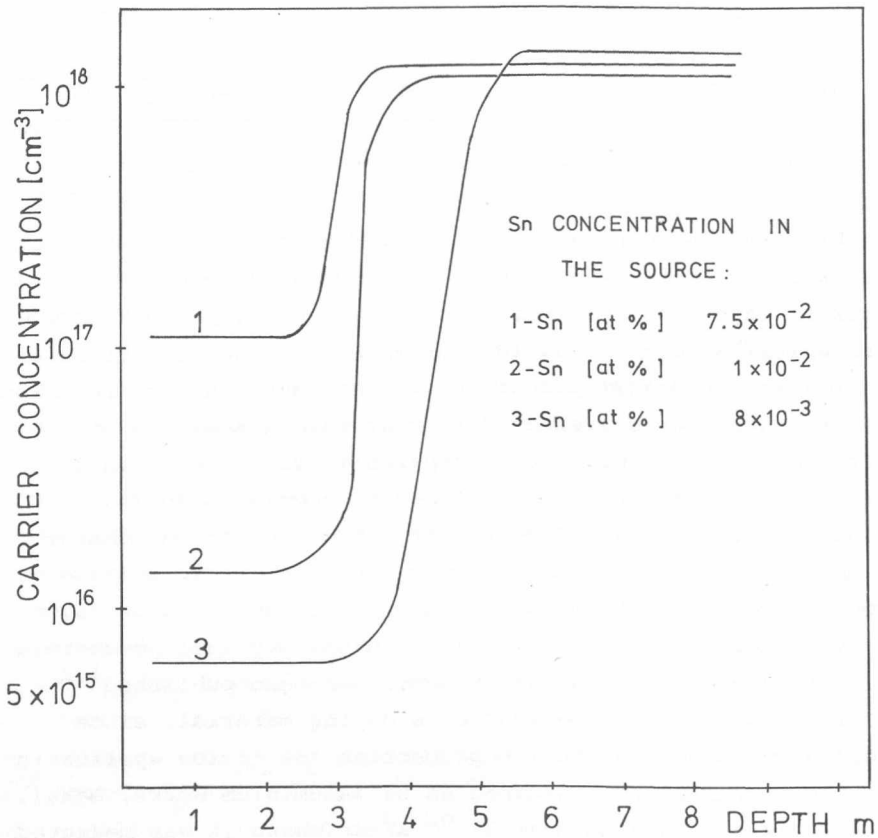

Fig. 1.

The typical growth parameters were:

- source temperature /T_s/ 820 °C
- growth temperature /T_g/ 786 °C
- $AsCl_3$ mole fraction 6.41×10^{-3}
- flow rate of H_2 in main stream: 200 cm^3/sec
  bypass: 100 cm^3/sec.

According to our results the homogeneity of the charge carrier concentration in the grown layers, the transition of the substrate-epilayer, and the quality of the surfaces are suitable for device fabrication /Fig. 1/.

Table 1. summarizes the obtained results which resulted from measuring the samples having the same growth parameters. It shows that reproducible growth can be carried out in our system.

Table 1.

1	2	3	4	1	2	3	4
7.5×10^{-2}	459	1.1×10^{17}	2.8	1×10^{-2}	428	1.4×10^{16}	3.2
"	460	1×10^{17}	2.6	"	429	1.3×10^{16}	3.1
"	461	1.5×10^{17}	3.2	"	444	1.8×10^{16}	3.2
"	462	2.8×10^{17}	3.2	"	445	2.5×10^{16}	3.0
"	463	2.8×10^{17}	3.6	8×10^{-3}	483	6×10^{15}	3.0
"	464	1.8×10^{17}	3.8	"	484	9×10^{15}	3.6
"	465	1.4×10^{17}	1.1	"	485	5.6×10^{15}	4.0
"	466	1.4×10^{17}	1.2				
"	467	1.2×10^{17}	1.4				

1 - Sn concentration in the source /at%/
2 - Number of samples
3 - Charge carrier concentration /cm^{-3}/ measured by Post Office Profile Plotter
4 - Layer thickness /μm/

Carrier concentrations of epitaxial layers grown with tin doped sources.

1. T. Görög and E. Lendvay, Epitaxial growth of $A^{III}B^{V}$ semiconductors from vapour phase, Acta Phys. Hung. 44 13 /1978/

2. T. Görög and I. Gyuró, High purity GaAs layers grown by vapour phase transport in the MFKI Yearbook '78, pp. 50-51, /1978/

3. R. Sankaran, Vapor phase epitaxial growth of Sn-doped GaAs, J. of Electrochemical Society 126 797 /1979/

TECHNOLOGICAL EXPERIMENTS IN SPACE

M. Hársy, T. Görög, E. Lendvay, I. Gyuró

The first Hungarian-Soviet space flight, as a part of Hungary's contribution to the Intercosmos Program, took place in 1980. Of the numerous scientific projects carried out in Salyut-6, the "Eötvös" experiment /named after the famous Hungarian physicist/ aimed to study the growth of semiconductor crystals in near zero gravitational field. The stainless steel cartridges were supplied by Central Research Institute for Physics. The experimental set-up was prepared in our Institute.

As the resistance furnace available on board had given temperature profiles and pulling facilities, the experiment was resctricted to definite dimensions and to strict safety measures as well.

The experimental materials were loaded in vacuum-sealed quartz ampoules which were later enclosed into heat resistant steel containers and kept in place with asbestos-wool stuffings. /Each container had to pass a rigorous vibrational test./

The Eötvös Program covered the growth of three inter-metallic semiconductors: GaAs, InSb and GaSb.

In case of GaAs the study of chromium distribution in the matrix material was planned. It is known that, in ordinary conditions, the chromium concentration along the growth direction shows a fluctuation due to the solubility and density inhomogeneities in the solidifying molten material. The space experiment was based on the Travelling Solvent Method. Between a single crystalline and a polycrystalline GaAs ingot there was a piece of gallium-chromium-GaAs mixture placed which, due to the increasing temperature gradient, moved in the direction of the polycrystalline material, while the chromium containing GaAs grew onto the single crystalline interface /Fig. 1/. Data evaluation is still in progress.

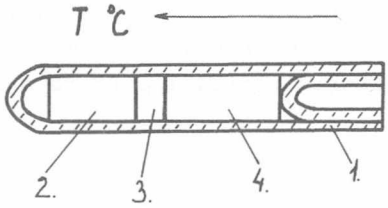

Fig. 1. GaAs growth
1. quartz tube and stopper
2. GaAs polycrystal
3. Ga-Cr-GaAs alloy
4. GaAs single crystal

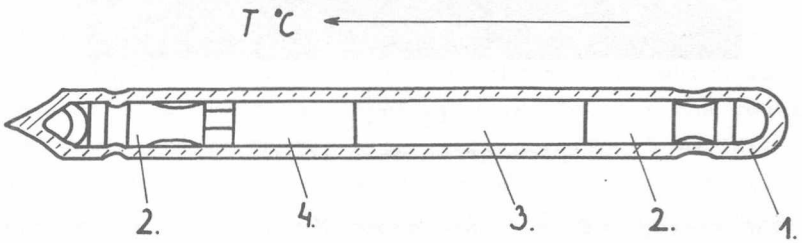

Fig. 2. InSb growth
1. quartz
2. graphite spacers
3. InSb single crystal
4. InSb polycrystal

The crystallization of both InSb and GaSb took place in a modified Bridgman arrangement. Fig. 2 shows the schematic setup of the InSb experiment.

Although the study of samples is far from being completed, some remarkable results have been already found:

In space the molten material in the tube formed a cylindrical rod ending in hemispheres. The surface tension and the adhesion, however, are not enough to press the melt against

the ampoule properly. Therefore the solidification is quite free of wall effects. Much fewer seeds and much larger crystals developed than in usual gravitational circumstances.

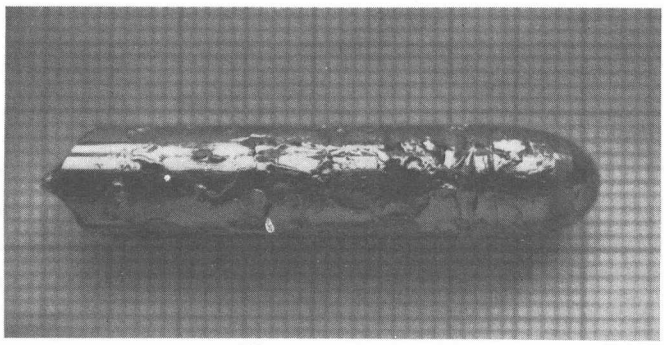

Fig. 3.
Space grown GaSb ingot

The surface of the space grown ingot is not smooth but shows a ridged structure /Fig. 3/, due to the fluid flow in the melt caused by the extending solid material and the subsequently uneven heat transport in the system.

According to the first measurements the space grown crystals have extremely low dislocation densities.

EXPERIMENTAL INVESTIGATIONS ON HIGH FREQUENCY GUNN DIODES

K. Kazi, I. Mojzes

In the previous Yearbooks we briefly reported on our activities concerning the development of Gunn diodes for X-band. These devices have been used mainly for process control purposes and in intrusion alarm and motion detection systems. Device users were supplied with low cost, easy-to-use, custom designed Gunn oscillators for X-band with low power consumption.

The optimal use of the frequency plan requires the application of the higher frequency devices and oscillators characterized generally by smaller geometrical dimensions, which is very advantageous from practical point of view. To meet the requirements of device users on the high frequency /up to 40 GHz/ Gunn devices, we have developed a Gunn diode and an oscillator family constructed according to the "building block" system.

The high frequency Gunn diodes and the oscillators we have developed are aimed to serve as a low power high frequency signal source.

The Gunn diodes were made from n^+-n wafers grown by vapor-phase epitaxy. The wafer was coated with AuGeNi contact layer and the structure was formed by photolitography. For the heat treatment of the contact and for the bonding we have used a new method[1]. More details of the diode fabrication and characterization will be published elsewhere.

Fig. 1 shows the cavity construction which was used to test the diodes.

The tuning of the cavity can be carried out by changing the length of the cavity /coarse tuning/ and by a tuning screw /fine tuning/. The length of the cavity can be controlled with an accuracy of ±0.05 mm and the variation of the length is more than $\lambda_g/2$. The waveguide band coverage of our cavities was from 10 to 34 GHz /R100, R140, R220, R320/.

The measurements were carried out at 14, 17, 26, 34 GHz by using a microwave spectrum analyser C4-27.

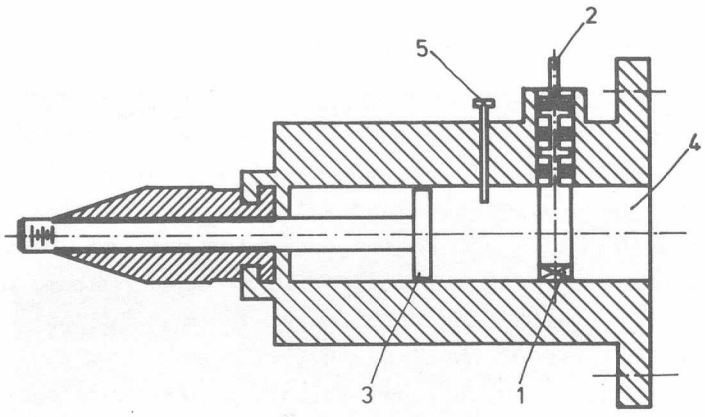

Fig. 1. The cavity construction

1 - Gunn diode
2 - DC bias and wavetrap
3 - Short circuit
4 - Cavity resonator
5 - Tuning screw

Typical experimental results are shown in Fig. 2. and 3.

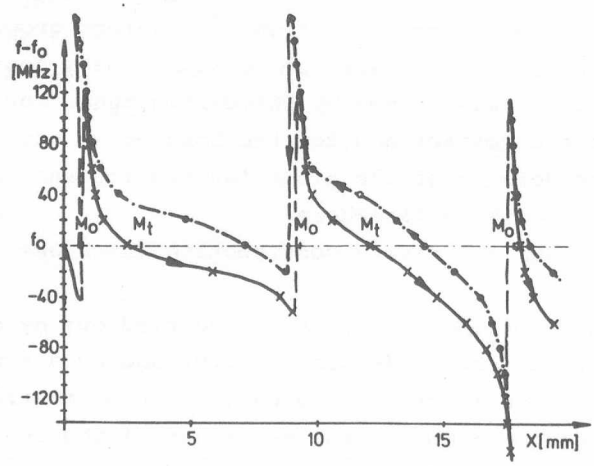

Fig. 2. The variation of the frequency vs the length of the cavity

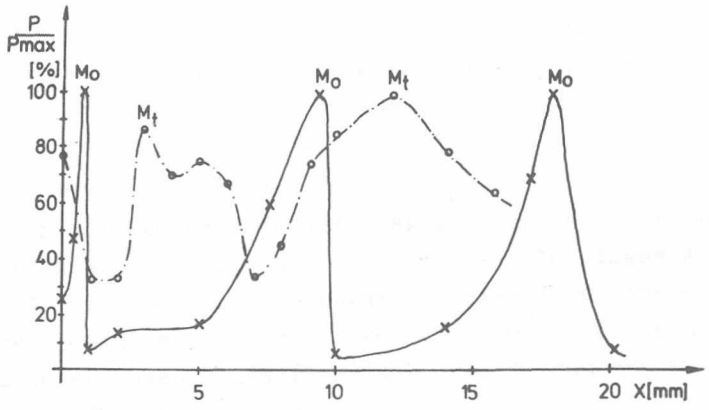

Fig. 3. The change of the microwave power vs the cavity length
--- at the fixed position of the tuning screw
-.- at the optimal tuning

The microwave power was found to decrease at higher frequencies due to the loss in the cartridge used in this work. Results presented in the Figs. 2 and 3 show that by the changing of the cavity length and the position of the tuning screw the optimum of the cavity-diode interaction can be found. At this position the microwave power is relatively high and the frequency variation is low.

Further experiments and calculations are in progress.

1. Hungarian patent registration N^{O} 173621.

PHYSICS AND CHARACTERIZATION OF UV-EPROMS

A. Lőrinczy, Yu Ponomarenko

The first Hungarian 2048-bit EPROM was manufactured in 1979 as a result of the fruitful cooperation between our Institute and the Industrial Research Institute for Electronics "HIKI", whose p-channel PSG-MOS technology has been used in developing the memory device with floating gate chargeable by avalanche injection and eraseable by ultraviolet light.

Specific features of these memories created some new demands on the technological parameters, so the technology had to be properly adjusted. For this purpose various types of floating gate MOS transistors had been fabricated at HIKI, investigated at our Institute and the most important technological parameters were determined.

At the outset basic mechanisms such as the charging of the floating gate by avalanche injection, the charge retention on the floating gate, and the charge removal from the floating gate by UV light, and also phenomena related to these mechanisms have been investigated. Effects of surface fields and oxide trapped charge on the breakdown voltage of planar silicon p-n junction, charge trapping in oxide layer caused by avalanche injection of hot electrons and the UV photoemission of electrons have also been studied.

As the next step in the development of EPROM, 1-bit and 64-bit models were fabricated with the aim of studing the selecting, decoding and reading circuitry connected to the floating gate transistor.

One of the most critical questions that had to be cleared up was the unintentional programming of the memory caused by low voltages applied during reading. This process makes quite an opposite demand on the value of the junction curvature /or its depth/ than the programming efficiency does. That is why the diffusion depth has been properly corrected.

The memory retention has been investigated at elevated temperatures to accelerate the charge loss. Having been completed on single transistors this study was a very sensitive tool for the determination of the oxide quality.

The reliability studies of 2048-bit EPROM consist of operating life test and EPROM retention test. The former is intended for the checking of the unintentional programming and is accomplished at high /125^{o}C/ and low /-10^{o}C/ temperatures with dinamically operated non-programmed EPROMs for 160 hours. During the retention test EPROMs are fully programmed and baked at 125^{o}C /plastic package/ or at 155^{o}C /ceramic package/ for 160 hours as well.

Based on the results of these investigations the devices which have been manufactured at HIKI correspond to the international standard. The work here is continued on 8-kbit n-channel EPROM.

INVESTIGATION OF METAL CONTACTS TO $A^{III}B^{V}$ COMPOUND SEMICONDUCTORS

I. Mojzes, D. Szigethy, T. Sebestyén[+], G. Gergely

Ohmic and rectifying metal contacts to GaAs are extensively used in microwave semiconductor devices, such as Gunn diodes, Schottky diodes and field-effect transistors. During the technological steps the metal/semiconductor systems are exposed to heat treatments and the volatile components can evaporate through the thin metal or oxide layers. This evaporation was used to investigate the mechanism of formation of metal-semiconductor contacts[1]. Using in-situ mass spectrometric studies during the alloying process of contacts on GaAs and GaP samples the evaporation of the volatile component /As_2 and P_2 resp./ was determined. The volatile component loss and its dependence on the temperature of the heat treatment were strongly affected by the composition of the contact layer on the semiconductor. Fig. 1 shows some typical results for the most commonly used contact systems. Our investigations show that the addition of gallium greatly reduces the arsenic loss and completely eliminates the peak/s/ in the arsenic yield-temperature curves[1]. The effect is demonstrated in Fig. 2. It should be noted that in all cases the main evaporating species are As_2 /or P_2/ molecules. The evaporation rates of As, As_4 and Ga, as detected by our Riber QML-51 quadrupole mass spectrometer joined on a liquid-nitrogen cooled chamber, were not comparable to that of As_2.

Several metal contact systems containing gallium were used to study metallurgical and electrical effects by using a molecular beam during the alloying of the contacts on GaAs epitaxial layers[2].

+ Central Research Institute for the Development of Services

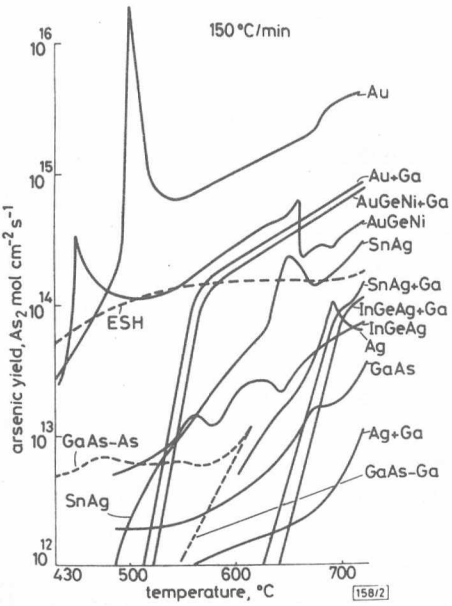

Fig. 1. Arsenic yield from several metal contacts with and without Ga. For comparison, background yields are also shown for empty sample holder /curve ESH/ in a chamber without cooling, for a pure GaAs surface measured by us /curve GaAs/ and by Arthur for Ga--stabilised /curve GaAs - Ga/ and As--stabilised /curve GaAs-As/ surfaces of GaAs samples.

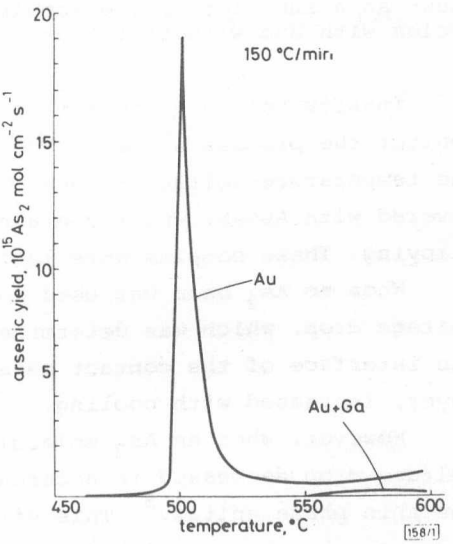

Fig. 2. Dependence of arsenic loss intensity on temperature for pure Au and Au+Ga layer during heating at 150 °C/min

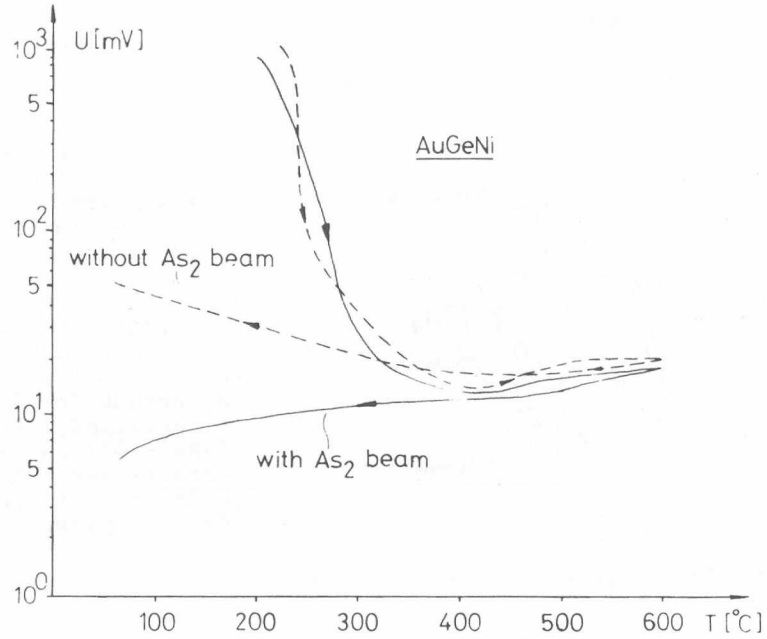

Fig. 3. The voltage /U/ which appears across the GaAs sample with contacts made of 580 nm $AuGe_{eut}$+90 nm Ni+150 nm Au is shown as a function of the sample temperature /T/ for heat cycles with and without the use of As_2 molecular beam

In-situ voltage-temperature measurements were used to monitor the processes during the heat treatment[3,4]. Fig. 3 shows the temperature-voltage values of some characteristic samples covered with AuGeNi which contained no gallium prior to alloying. These samples were later heat treated.

When no As_2 beam was used during the heat treatment the voltage drop, which was determined mainly by the resistance at the interface of the contact metal system and the epitaxial layer, increased with cooling.

However, when an As_2 molecular beam was applied, the voltage drop decreased in accordance with the principles of the thin phase epitaxy[5]. This effect was still more pronounced when samples covered with AuGeNi+Ga were used.

The behaviour, the technology and the mechanism of the formation of ohmic and rectifying contacts on $A^{III}B^{V}$ compound semiconductors are not yet understood in detail. Further experiments, such as on the diffusion of the components, thermal dissolution in the presence of thin metal layers, are in progress.

1. T. Sebestyén, I. Mojzes and D. Szigethy, Use of Ga in metal--GaAs contacts to eliminate large As loss peaks, El.Lett. 16, 504 /1980/

2. I. Mojzes, T. Sebestyén, P.B. Barna, G. Gergely and D. Szigethy, Gallium plus metal contacts to gallium arsenide alloyed in arsenic molecular beam, Thin Solid Films, 61, 27 /1980/

3. I. Mojzes, Formation of AuGe contacts to n-GaAs, phys.stat. sol. /a/ 47, K183 /1980/

4. I. Mojzes, Electrical modelling of ohmic contacts formation on metal-n-GaAs systems, Acta Phys. Hung. 48, 131 /1980/

5. T. Sebestyén, Thin phase epitaxy of III-V compound semiconductors, Acta Phys. Hung. 47, 51 /1980/

CHARGE MOTION IN THERMAL SiO_2 AS INFLUENCED BY PROCESS VARIABLES

M. Németh-Sallay, R. Szabó, I. C. Szép

We have reported previously[1,2] that a peak can be found on MOS capacitors in the thermostimulated current spectra /TSC/ at 260 K, which is characterized by an activation energy of 0.35 eV. The height of this current peak could be reduced by vacuum heat-treatment and also by ether-vapour treatment[3] while the presence even of trace amount of water-vapour increased it /Fig. 1/. These changes in the current peak and the value of activation energy allowed us to suppose, that the motion of a hydrogen-bearing species, most likely H^+ ions, were responsible for this effect.

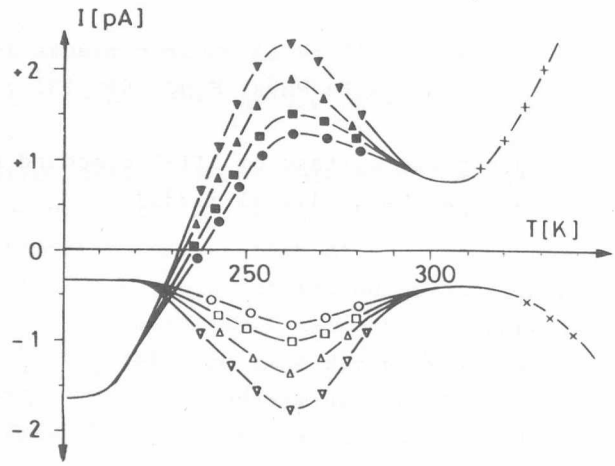

Fig. 1. The effect of various treatments on the TSC curves of MOS capacitors for both dry and wet oxides: ●○, MOS samples vacuum heat treated and treated with ether vapour /25°C/; ■□, vacuum heat-treated samples; ▲△, the untreated MOS structures; ▼▽, samples treated with water vapour /25°C/; x +, the initial part of the Na^+ curve; ○□△▽×, measured at V_C = OV and V_G=-9V; ●■▲▼+, measured at V_C=OV and V_G=-9V. β was 0.5 Ks^{-1} in all cases.

Subsequent investigations showed, that for the appearance of the TSC peak, the main role is due to the interaction between the SiO_2 surface layer and water-vapour. The thickness of the active surface layer is about 30-40 nm and it is formed during the process of oxide growth[4].

It was also found that removing the surface layer of SiO_2 by an oxide etchant, the height of the current peak diminishes nearly exponentially with depth, which means, that the ability of surface oxide to react with water-vapour also decreases. /Fig. 2/.

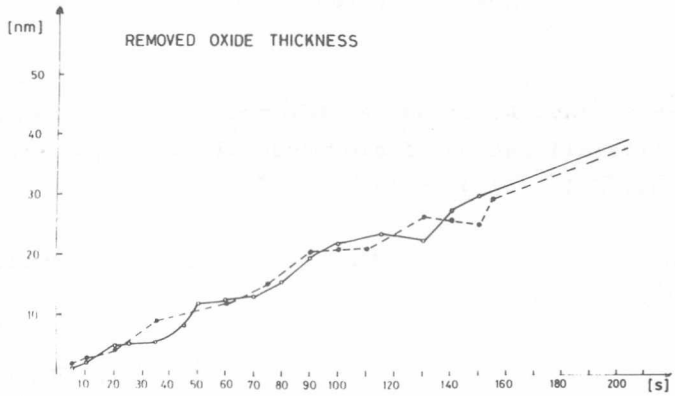

Fig. 2. shows the etching rate of the surface oxide layer measured by ellipsometry on heat-treated /●/ and as grown /○/ dry oxide layers. As can be seen in the first 30-40 nm of the surface oxide layer periodic structural changes appear, which is in a good agreement with the TSC measurements.

At the same time when using plasma-etching for the removal of the 30-40 nm oxide layer, the TSC peak does not disappear. However a new peak appears as a result of the plasma discharge, even when a surface layer was removed previously by chemical etching. Apparently, the plasma process produces an active surface in contrary to the chemical etching.

When reoxidizing the chemically etched /30-40 nm/ surface, the TSC peak appeared at an oxide thickness less than the previously removed oxide thickness. In forming the active surface layer the oxidation process and its mechanism evidently play a role.

1. M. Németh-Sallay, R. Szabó, I.C. Szép and P. Tüttő, Charge motion in ether-treated silicon MOS structures, in Proc. ESSDERC, 1979, Münich, p. 155.

2. M. Németh-Sallay, R. Szabó, I.C. Szép and P. Tüttő, Charge motion in silicon MOS structures, Thin Solid Films, 70 37 /1980/

3. M. Németh-Sallay, Á. Barna, A. Lőrinczy and I.C. Szép, Induced crystallization of amorphous silicon dioxide, Phys. Stat. Sol. /a/ 43 K 135 /1977/

4. R. Szabó, Investigation of MIS structures by TSC method, Ph. D. Thesis, Budapest, 1980.

N DOPING DURING LPE GROWTH OF DOUBLE /AlGa/P - GaP HETEROJUNCTION STRUCTURES

J. Pfeifer, É. Radácsi, L. Csontos, Ju.P. Jakovlev[+]

The properties of the ternary compound $Ga_{1-x}Al_xP$ and layered structures involving $Ga_{1-x}Al_xP$-GaP-$GaAs_{1-x}P$ heterojunctions are of interest for optoelectronic applications. The mixed crystal $Ga_{1-x}Al_xP$ can be well employed in heterostructures as confinement layer with GaP due to its wider band-gap and smaller refractive index. The wide band-gap of AlP provides a possibility of obtaining deep green light emission. A high level of the nitrogen isoelectronic dopant in direct and indirect $GaAs_{1-x}P_x$ showed stimulated emission using optical pumping.

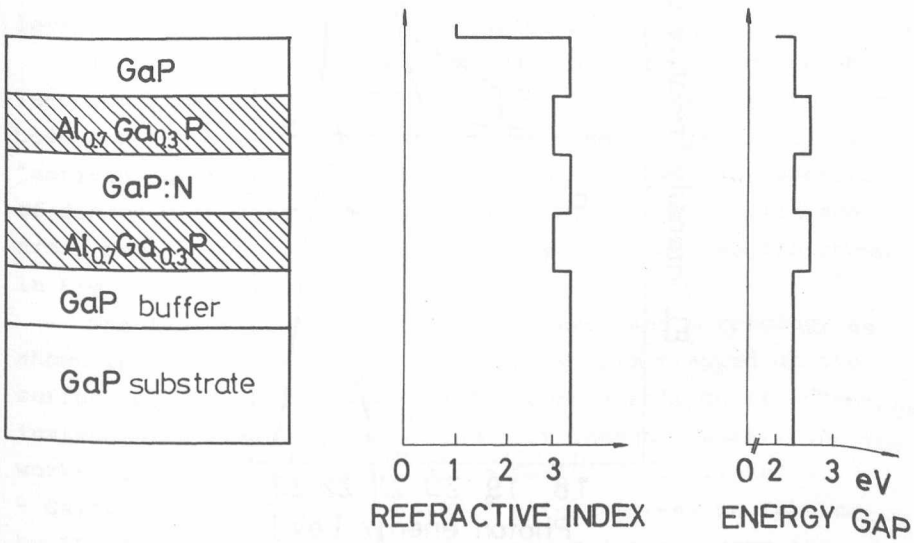

Fig. 1. Schematic drawing of double heterojunction /GaAl/P - GaP p-n structure. The middle /"active"/ layer is doped with nitrogen

[+] A.F. Joffe Physical-Technical Institute, Leningrad

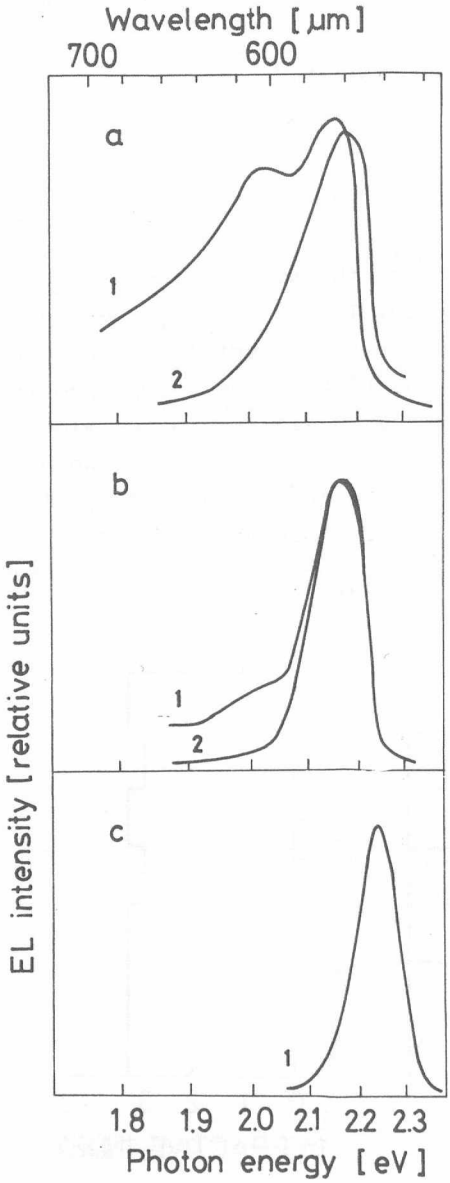

Fig. 2. EL spectra of GaP p-n junctions at room temperature a. GaP:Si grown on /GaAl/P; b. GaP:Si grown on GaP; c. GaP without Si contamination. Dependence on applied current: 1. I = 2 Acm^{-2}; 2. I = 200 Acm^{-2}.

For the investigation of the electroluminescence of GaP and $GaAs_{1-x}P$ at a high level of direct current injection structures containing p-n junction and $Ga_{1-x}Al_xP$ confining layers were grown /Fig. 1/. If we compare the requirements with the /GaAl/As system we find a number of differences, such as: the generally higher growth temperature, a higher segregation coefficient for aluminium, and, if nitrogen has to be incorporated, difficulties caused by the formation of AlN due to the reaction between Al and NH_3.

The high temperature of the epitaxy causes a higher chemical reactivity of the boat material and furnace tube with the melts and with the gaseous ambient. Silicon contamination of the grown layers /Fig. 2/[1,2,3] was found using a graphite melt container with a quartz inner tube. Ga melts containing Al interacted through the graphite wall with the quartz material. In these experiments the residual donor level was so high that it could not be overcompensated in the process of LPE. Carbon contamination on the other hand causes a residual acceptor level, which could be overcompensated by doping with tellurium.

In the experimental work we were able to introduce NH_3 into the growing system. Fig. 3 shows the scheme of the LPE boat and the cooling programm. N was incorporated in the middle "active" layer. Fig. 4 shows the electroluminescent spectra of diodes with and without N doping. Aluminium profile and cross section of different double-heterostructures are shown in Fig. 5. and Fig. 6.

The improvement in thickness control and morphology as shown in Fig. 6. is due to a thin melt film trapped on the surface of the substrate. We have found a melt cover advantageous instead of a clean wiping during melt change. Summarizing the work: we have demonstrated that a GaP"n" - /GaAl/P"n" - - Ga/AsP/:N - /GaAl/P"p" - GaP"p" structure can be fabricated by LPE in one process doping from the melts and from the geseous phase respectively.

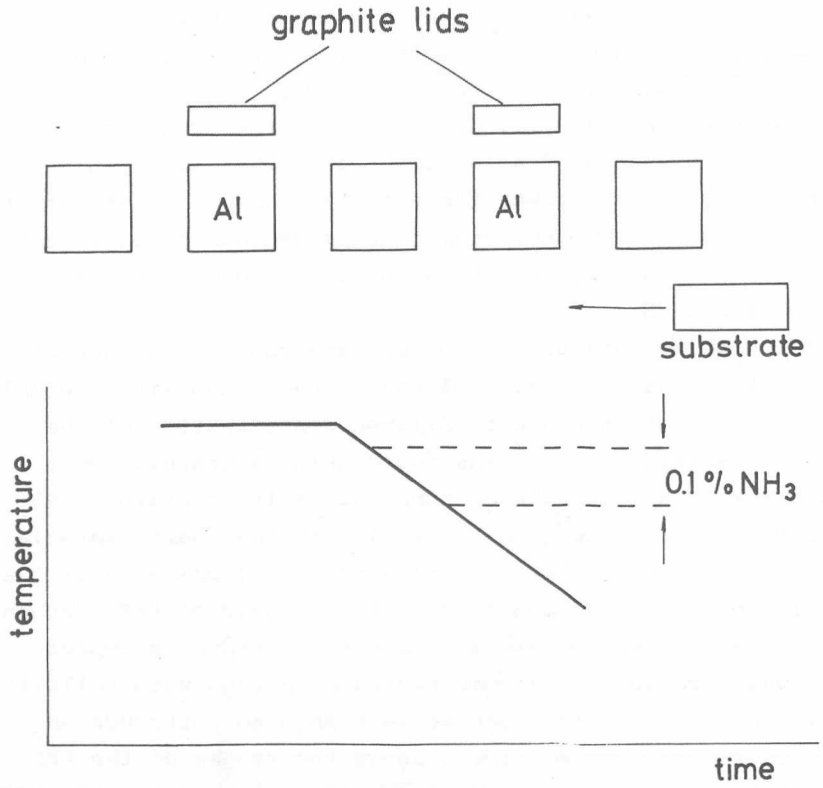

Fig. 3. The scheme of the LPE boat and cooling program for a one step growth of N doped /GaAl/P-GaP p-n junction structures

In the experimental work we were able to introduce NH_3 into the growing system. Fig. 3 shows the scheme of the LPE boat and the cooling programm. N was incorporated in the middle "active" layer. Fig. 4 shows the electroluminescent spectra of diodes with and without N doping. Aluminium profile and cross section of different double-heterostructures are shown in Fig. 5. and Fig. 6.

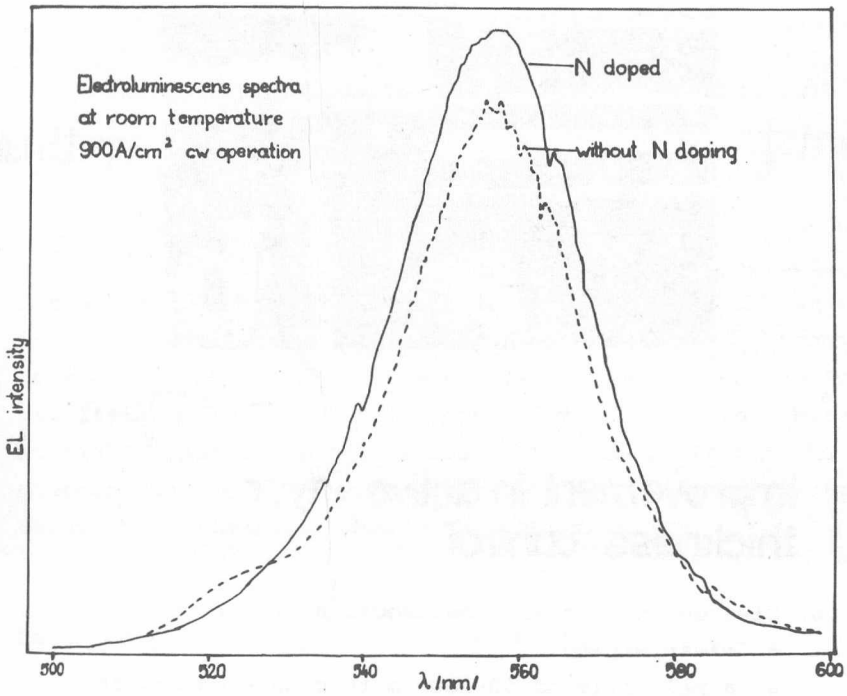

Fig. 4. EL spectra of diodes at room temperature

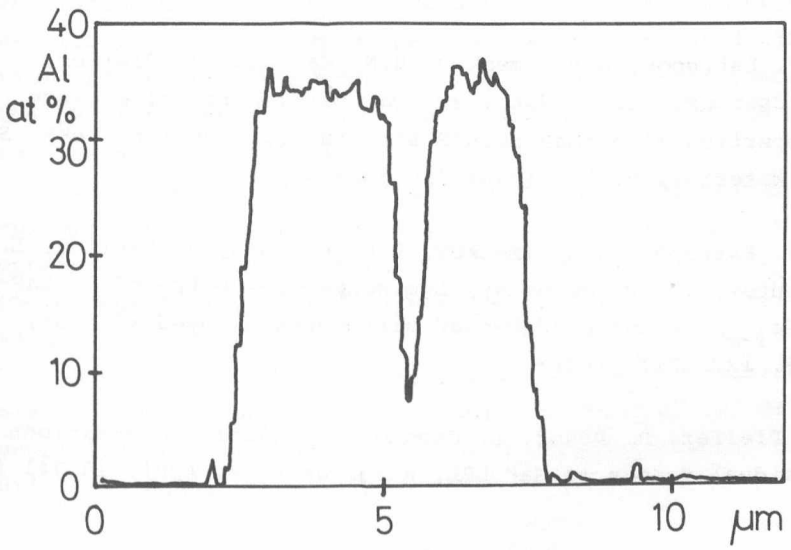

Fig. 5. Concentration of Al across a typical layer structure as determined by electronprobe microanalysis

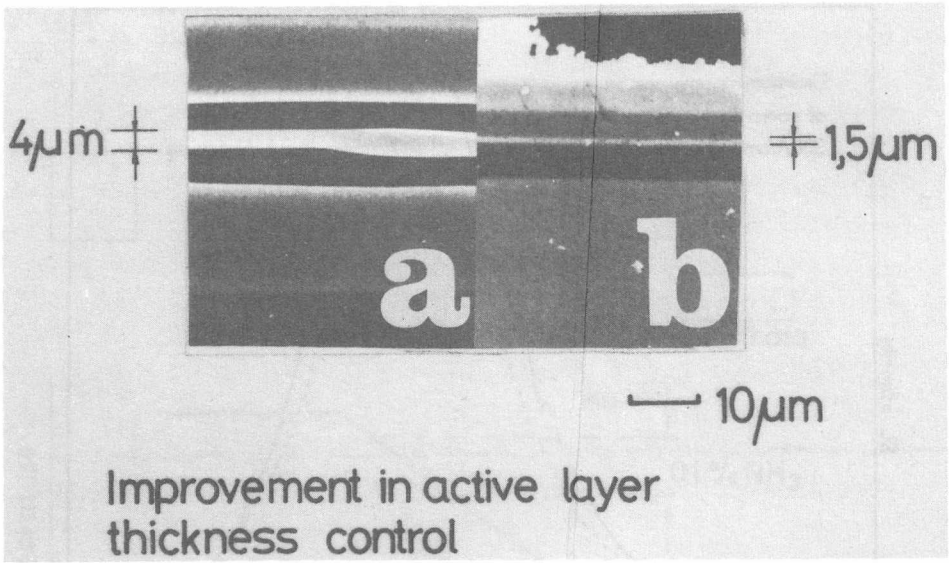

Fig. 6. Cleaved and etched cross section of structures
a. clean wiping
b. a melt-film of 50-100 m thickness covers the substrate during the change of melt

1. V.V. Estropov, A.N. Imenkov, B.N. Kalinin, J. Pfeifer, L. Csontos, Ju. P. Jakovlev, On the electroluminescence properties of p-nGaP-nGaAlP structures, Elektron. Tekh. Ser. 6. Materialy p. 51 /1978/ /in Russian/

2. V.V. Estropov, A.N. Imenkov, B.N. Kalinin, J. Pfeifer, L. Csontos, Ju. P. Jakovlev, Luminescence spectra of p-nGaP--nGa$_{1-x}$Al$_x$P and p-nGaP-nGaP structures alloyed with Si, FTP, 12, 1017 /1978/

3. J. Pfeifer, B. Pődör, L. Csontos, N. Nádor, Observations on residual donors in GaP LPE, Revue de Phys. Appl. 13 741 /1978/

DEVELOPMENT OF PbS and $PbS_{1-x}Se_x$ TYPE IR DETECTORS

V. Rakovics, T. Görög, G. Hoffmann, J. Balázs

Lead sulphide is well known as a versatile photoconductor for use in the visible and near infrared regions of the spectrum. At 25°C, PbS responds to radiation in the wavelength region from 0.4 μm to 3.3 μm, while at lower temperatures the long wavelength limit of response moves further into the infrared. At -196°C there is usable response to 4.3 μm. In our Institute photoconductive PbS layers were deposited on glass substrate, using the following exchange chemical reaction

$$Pb(CH_3COO)_2 + (NH_2)_2CS \xrightarrow{\text{Alkaline}} PbS/film/ + CH_2N_2 + 2H^+ + 2CH_3COO^-$$

The influence of deposition conditions on the film structure and its photoconductive properties was investigated. The reaction rate was stabilized by controlling the deposition temperature, the pH of the solution and the relative concentration of the reactants in the solution.

When used as additives to the conventional thiourea--plumbite solution the oxidising compounds in aqueous solution enhance the photoconductivity of the deposited layers. The photoconductivity of the layers can be further increased by vacuum heat treatment.

The film structures were characterized by scanning electron microscopy. Fig. 1. shows the pictures of different sensitized PbS layers in order of decreasing ammount of oxidising agent.

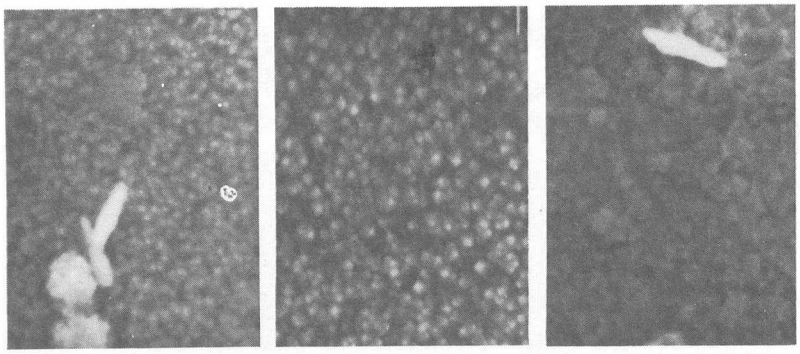

1/a 1/b 1/c

Fig. 1. The SEM picture of PbS layers. The films shown on 1a., 1b and 1c were deposited from solutions containing 2, 0.2 and 0.02 g/l oxidising agent respectively. Magnification: 10 000x

Table 1.

Type of detectors	Sensitive area	Resist-ance	Respon-sitivity at 25°C	Time constant	λ_{max}	Maximum bias voltage
	[mm.mm]	[Kohm]	[V/W] 2.0 µm	[µs]	[µm]	[V]
PbS * PCP 1	10x10	600-3000	$1\text{-}4x10^4$	80-200	2.0	500
PbS **PCE 1	2.5x2.5	500-1500	$0.5\text{-}2x10^5$	60-100	2.3	100
PbS ***PCE 2	2.5x2.5	100-400	$2\text{-}8x10^4$	10-50	2.6	100

* without encapsulation

** encapsulation with glass window

*** encapsulation with Si window

For the preparation of photoconductive cells we used evaporated gold electrodes, to which the leads were soldered with indium.

A single acrylate protective layer was applied against atmospheric damages.

Representative technical data of three different detectors developed in our Institute are summarized in Table 1.

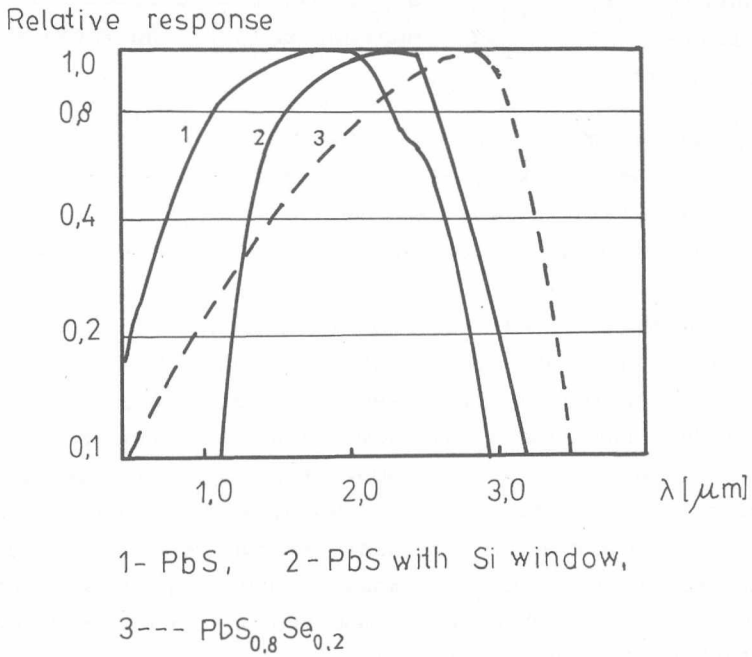

Fig. 2. Spectral response at room temperature

The deposition of $PbS_{1-x}Se_x$ by adding sodium selenosulphate to the thiourea-plumbite solution proved to be effective in shifting the limit of spectral response towards the longer wavelength, and also in decreasing the time constant. The relative spectral response of two type PbS and the $PbS_{0.8}Se_{0.2}$ are sown in the Fig. 2.

1. J.N. Humphrey, Optimum utilization of lead sulfide infrared detectors under diverse operating conditions, Appl. Optics, 4, 665 /1965/

2. N.C. Sharma et.al ., Electroless deposition of semiconductor films, Thin Solid Films, 60, 55 /1979/

3. J. Balázs, V. Rakovics, G. Hoffmann and T. Görög, On the measurement of time constant of PbS photoconductors, to be published in Proc. CIE Symposion on Light and Radiation Measurement'81.

NEW RESULTS OF MNOS RESEARCH AND IC DEVELOPMENT

G.Stubnya, P.Tüttő, Zs.J.Horváth, M.Németh-Sallay,
R.Szabó, J.Balázs, I.Cseh

Since 1979 we have investigated the IC compatibility of MNOS transistors and related technology. The investigation of oxidation technology has proved that the only reliable oxidation technique to produce thin /$\sim$2 nm/ "memory" SiO_2 films is the chemical oxidation method.

We found that an optimal annealing temperature, time and gas ambient could result in a favourable position and width of the memory window of MNOS devices. This technologically important fact is in strong correlation with the number and distribution of Si-H, N-H and dangling silicon bonds within the Si_3N_4 film.

Using proper annealing we succeeded in setting the reading voltage to -5 V, an optimal value for IC purposes.

The next problem was to fabricate MNOS transistors containing both memory and non memory gates /with about 50 nm SiO_2/ and to investigate the reliability of our thermal oxidation technique producing electrically active MOS elements. The threshold voltage of the stepped oxide and other MOS transistors produced by our technology were -2 to -3 V which was satisfactory. On the basis of these results we started to fabricate and investigate MOS and MNOS transistors having dimensions complying with IC fabrication requirements.

The results of different electrical measurements (CV hysteresis, memory retention and degradation) on these IC size transistors demonstrated the capability of our technology to produce integrated memory cells.

In cooperation with the engineers of HIKI, we developed a test memory IC, which consist of a totally decoded 64 bit memory cell with MNOS transistors, a 1 bit totally decoded memory cell, and different testing capacitors and transistors. Fig. 1. is a photomicrograph of this test memory IC.

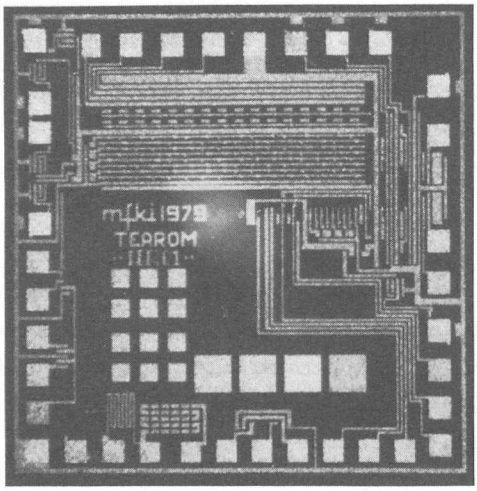

Fig. 1.

Part of the investigation of the IC has been performed on an automatic measuring instrument developed by HIKI /ICOMAT/, and partly on an automatic testing instrument developed by us.

The electrical measurement of the 1-bit memory IC showed that the yield of our technology was about 40-50%.

Parallel with the device development, we have investigated the memory hysteresis, I-V characteristics, charge motion and the surface state density at the $Si-SiO_2$ interface in MNOS structures.

We have also studied the effect of annealing circumstances on the hydrogen movement and etching properties of Si_3N_4 films.

MICROWAVE SCHOTTKY BARRIER MIXER DIODES FOR STRIPLINE APPLICATION

B. Szentpáli, Á. Tichy-Rács

In the YEARBOCK '78 the first results of the development of microwave Schottky diodes were described. The diodes encapsulated in coaxial cartriges /type S4/ were tested in the mixer unit of a receiver.

In order to meet the demands of the modern microwave telecommunication engineering a new form of encapsulation of the mixer diodes /foreseen for stripline circuits/ was constructed, the so called LID /Leadless Inverted Device/ /Fig. 1/. As the tuning possibilities of the stripline circuits are very poor, compared with the well tunable waveguide systems, special emphasis must be laid on the uniformity of the diode impedance.

Another advantage of the LID structure manifest itself in simplifying the preparation of greater coaxial devices. Instead of having to contact the chip with a long wire small in diameter, the complete LID diode may be installed. Such a device has a lower reactance and a high uniformity when used as a detector or a mixer in a waveguide equipment.

The parameters characterizing the mixer diodes are:

- the "ideality factor" in the exponent of the forward I-V characteristic n. n = 1.08 ... 1.12, i.e. the video resistance of the diode has a value of

$$R_V = \frac{28 \ldots 30 \text{ mV}}{I}$$

where I is the forward current,

- the reverse breakdown voltage is greater then 3 V,
- the junction capacitance of the 10 μm diameter diode is 0.05 pF,
- the stray capacitance is 0.14 pF,

- the series inductance is about 1 nH,
- the value of the series resistance is typically 3 ohm.

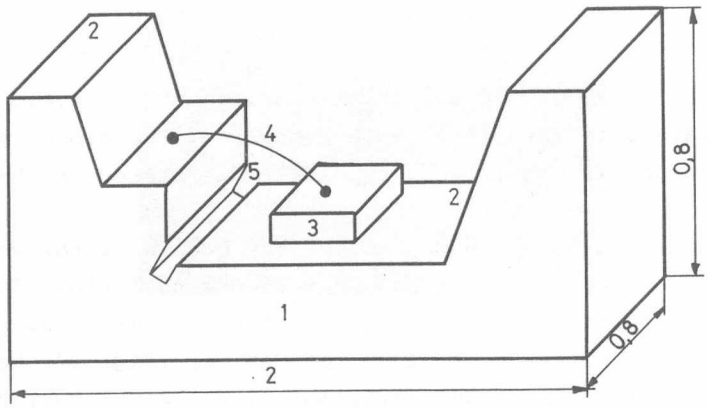

Fig. 1. The LID outline.
1 - ceramic body, 2 - metallization, 3 -chip, 4 - Au wire
/All dimensions in mm/

The noise of the GaAs LID Schottky diodes was tested in a specially built receiver similar in circumstances and bandwith to those of the GTT 70 system with a 7 GHz local oscillator. The mean noise figures were typically at about 5.5 dB.

INVESTIGATION OF MNOS STRUCTURES BY C-V METHODS

P. Tüttő

In our research work on MNOS memory devices to get reliable devices of good quality it was necessary to investigate the properties of the $Si-SiO_2$ interface and in general the capacitance voltage behaviour of the MNOS structures.

From the analysis of the C-V characteristics it was found that the generally used evaluation methods must be rejected since they supplied contradictory results for the surface potential and for the fast interface-state density in MNOS memory capacitors[1].

For getting reliable information on the interface and the insulator properties we have developed a new method to measure the quasi-static and the high-frequency C-V characteristics simultaneously, thus eliminating most of the uncertainties caused by the internal instability of the memory structures[2].

By utilizing the information redundancy of the C-V characteristics we have developed a method to evaluate the quasi-static and the high-frequency C-V curves. This new method allows us to calculate the interface-state density and the internal polarization of the insulator as a function of the surface potential and the electric field strength respectively[2].

In evaluation of the characteristics we have to calculate at first the accurate value of the insulator capacitance. However in the case of instable insulator /that is in MNOS memory structures as well/ it is not possible to fit the measured and the theoretical curves, especially in the case of very thin insulator layers / <10 nm/.

We have suggested a simple experimental method to obtain the insulator capacitance which, in spite of the electrical ininstabilities, prooved to be useful down to the nitride film thickness values[1] of 4 nm .

The evaluation of the C-V curves by the new methods showed that there exist a fast reversible polarization process in the Si_3N_4 layer at low values of the electric field strength, which differs from the normal memory charging and discharging process. To explain this type of polarization we had to suppose that beside the trapped memory charge carriers there exist certain amount of nontrapped charge carriers, with a density of about 10^{11} cm^{-2}, which can move almost free in a rather inhomogeneous built in electric field. The motion of these species extends over a large part of the nitride layer /10-50 nm/.

In an earlier work we investigated the in-depth distribution of Si-H and N-H bonds by MIR method and found significant non-uniformities[3]. We have also investigated the effect of this non-uniformity on the electric properties of the nitride layers. By measuring MNOS capacitors prepared on angularly etched nitride layer we have got that there is a fluctuating built-in charge above the SiO_2 layer[4]. The local density of this charge varies between $\pm 10^{19}$ cm^{-3} resulting in fluctuating built-in electric field strength /between $\pm 10^{6}$ Vcm^{-1}/. From point of view of the memory effect it is important, that the fluctuating built-in charge results in potential valleys which considerably improves the charge retention. When the deposition technique produces nitride films with homogeneous distribution of the hydrogen bonds without intentionally introduced inhomogeneities /potential valleys/ good memory properties cannot be achieved.

Analyzing the interface-state density evaluation it was found, that the presence of any instabilities strongly affects the virtual surface-state density values. Using our model which takes into account the insulator polarization almost an order of magnitude less and probable more reliable interface-state density values could be evaluated in memory MNOS structures. It was characteristic in our MNOS structures that beside the continuous interface-state spectrum we have found a discrete level of very fast surface-states at about E_C = 150 meV. These states were fast enough to follow the high-frequency signal that is the usual evaluation methods could not observe them.

1. P. Tüttő, J. Balázs and Zs.J. Horváth, Surface-state density evaluation problems in MNOS structures, to be published in Proc. INFOS 81.

2. P. Tüttő and J. Balázs, Insulator polarization effect in quasi-static and high-frequency C/V/ curves, to be published

3. G. Stubnya, I.C. Szép, G. Hoffman, Zs.J. Horváth and P. Tüttő, Distribution and role of N-H and Si-H bonds in MNOS structures, Revue de Physique Appliquée, 13 679 /1978/

4. P. Tüttő, G. Stubnya and Zs.J. Horváth, Depth inhomogeneity of CVD Si_3N_4 layers, to be published

METAL RESEARCH DIVISION

METAL RESEARCH IN PROGRESS 1979-1980

L. Bartha

The research in the department is characterized by a synthesis of the fundamental and applied research in physics, chemistry and metallurgy to develop new technological procedures and on-line inspection systems based on new ideas. Our efforts are devoted to the following major fields of the science in engineering:

/I/ General fundamental problems of the powder metallurgy and peculiar problems in the powder metallurgy of the refractory metals.

/II/ On-line inspection and control systems for steel mills.

In these two fields we are involved also in basic problems urging a theoretical solution at first. Such problems are:

- development of a percolation treatment for the formation of an interconnected skeleton in the early stages of the powder metallurgical technology and the destruction of the interconnected porosity in the late stages of the sintering.
  The percolation model proved to be a good tool for planning successful experiments studying pressed powder behaviour and sintering.
- mechanisms and kinetics for the formation of metal grains upon oxide reduction. Two important parameters in powder metallurgy, the metal powder morphology and the size distribution can be very much influenced during the oxide reduction. The study of some non-stochiometric compounds wich develop transitionally in the reduction of the oxides of some refractory metals help to clarify structural problems of solid state chemistry.
- internal oxidation and reduction in dilute alloys. This work helped to explain the role of some dopants in refractory metals and resulted in a new method for the determination of the oxygen solubility in tungsten.

- peculiar problems of working and annealing of metals with closed and open porosity. The main results were some new aspects for the prevention of dangerous atmospheric effects during porous metal treatment.
- Research for clarifying the driving forces of liquid phase activated sintering. Driving forces, like stress, chemical potencial, grain size and temperature gradient were quantitatively determined and initiating effects were found which may influence the direction of material transport and of grain growth.
- basic aspects of the shape defects in steel sheets and engineering methods to avoid these defects by the control of the rolling mills. A new continuous non-destructive testing method has been developed and successfully applied in steel mills in the production of high quality sheets.
- electroanalytical methods for control of chemical processes.

The research staff dealing among others with the above mentioned topics consists of 30 graduated members most of them with PhD or other academic degrees, and cooperates both with Hungarian and foreign institutes and also with industrial firms in order to have the possible highest working efficiency.

The following selection of extended abstracts gives a general view on our most interesting results of the last two years.

ANOMALOUS TWO-LEVEL SYSTEMS AND THE SPECIFIC HEAT OF VITREOUS SILICA

T. Geszti

Below a few K all glassy substances show a specific heat roughly linear in temperature, which is absent in the crystalline state. This is explained in terms of tunneling two-level systems[1,2]: atoms or atomic groups which are able to pass from one equilibrium position to another by means of phonon-assisted tunneling. Besides heat capacity, these two-level systems /TLS/ appear in a number of other phenomena, in particular in sound absorption. The model of tunneling TLS is characterized by the distribution function of a tunneling matrix element Γ. This distribution has a lower cutoff Γ_{min}, corresponding to the thickest potential barrier between the two equilibrium positions. An important prediction of the model - very hard to check experimentally - is that those TLS with a low Γ are very slow in responding to external changes, which causes a time-dependence of the specific heat.

Soon after the beginning of the story[1,2] it turned out that the concentration of TLS needed to explain the specific heat of a particular glass, viz. vitreous silica, is by a factor of ten larger than the concentration seen in sound absorption. To explain the discrepancy, Black and Halperin[3,4] introduced the notion of "anomalous TLS", to mean such TLS which contribute to the specific heat, but - for some unknown reason - fail to absorb the ultrasound. This model was so far unsuccessful, since no set of parameters was able to describe the whole set of experimental observations.

In the present work[5] we suggest that "anomalous TLS" are characterized by a value of their Γ_{min} as high as 0.48 K /in temperature units/, a possibility so far not investigated. The above numerical value has been extracted from a recent measurement of time-dependent specific heat[6], in which a fast-relaxing contribution could be separated. Making use of the fact that

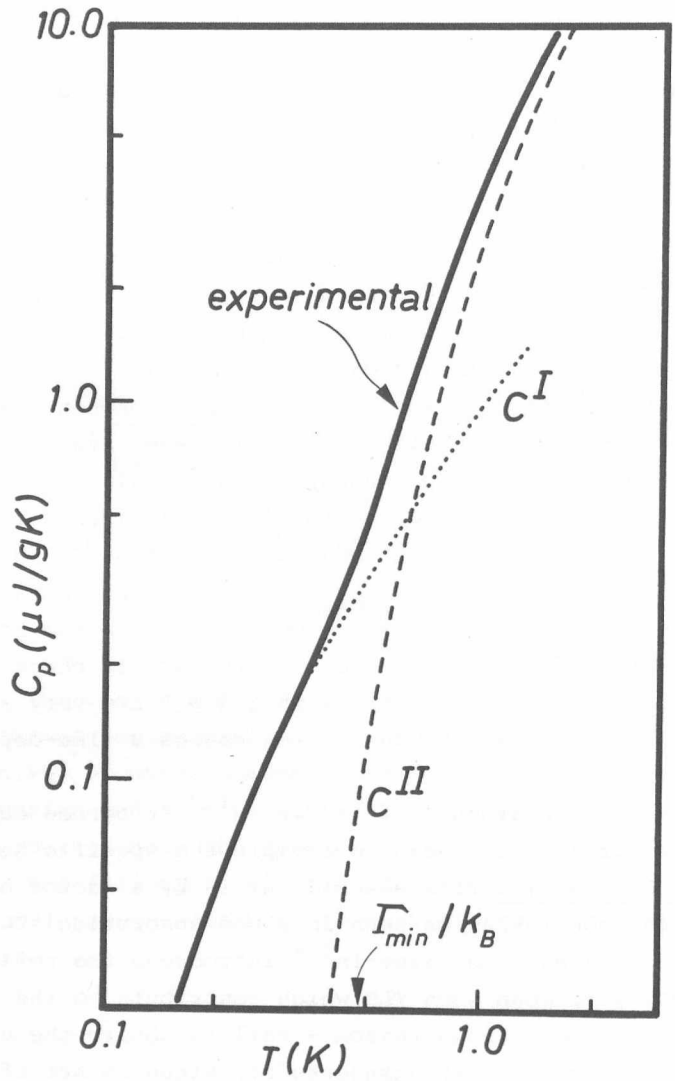

Figure 1.
Short-time specific heat of vitreous silica "suprasil W". Experimental data are extracted mainly from Ref. 6. C^I and C^{II}: contributions of two steps in the distribution of Γ /for details see Ref. 5/.

Γ_{min} is a threshold /or "gap"/ below which no TLS excitation energy of the given species of TLS is possible[7], the anomalously high value of Γ_{min} explains both the absence of ultrasonic absorption /the frequency corresponding to the threshold is 10 GHz, attainable only in Brillouin scattering/, and the fastness of relaxation. The temperature dependence of the fast specific heat is calculated in very good agreement with the experiment /Fig. 1./.

1. P.W. Anderson, B. I. Halperin and C.M. Varma, Anomalous low-temperature thermal properties of glasses and spin glasses, Philos. Mag. 25, 1 /1972/

2. W.A. Phillips, Tunneling states in amorphous solids, J. Low Temp. Phys. 7, 351 /1972/

3. J.L. Black and B.I. Halperin, Spectral diffusion, phonon echoes, and saturation recovery in glasses at low temperatures, Phys. Rev. B 16, 2879 /1977/

4. J.L. Black, Relationship between the time-dependent specific heat and the ultrasonic properties of glasses at low temperatures, Phys. Rev. B 17, 2740 /1978/

5. T. Geszti, to be published

6. M.T. Loponen, R.C. Dynes, V. Narayanamurti and J.P. Garno, Observation of time-dependent specific heat in amorphous SiO_2, Phys. Rev. Lett. 45, 457 /1980/

7. J.C. Lasjaunias, R. Maynard and M. Vandorpe, Existence of a gap in the low-energy density of states of vitreous silica, J. Phys. /Paris/ C6, 973 /1978/

THE INFLUENCE OF OXYGEN ON POTASSIUM BUBBLES IN TUNGSTEN

P. Harmat, J. Major, I. Gaál

To follow up the kinetics of the volume change of the potassium bubbles high temperature dilatometric studies were carried out on thin doped tungsten wires. The driving force for the volume change is the difference between the Laplace pressure ($2\gamma/r$) and the potassium pressure. The basic kinetical steps in the bubble volume change are the absorption or emission of vacancies at the bubble surface, the corresponding generation and annihilation of vacancies at dislocations and the transport connecting these two processes. The dislocation climb originating from the vacancy transport is very essential, since this very process transforms the volume change of the bubbles into a macroscopic volume change. (For an isotropic dislocation network the relative length change of the specimen is one third of the relative volume change.)

The length changes of a specimen related to changes in the bubble volume freeze in even at moderate cooling rates. In this way if every length is determined at a given low temperature, the length change, brought about by a certain high temperature annealing step, will be simply equal to the difference in the sample length before and after annealing. In the present work the kinetics of the bubble volume change was followed up by this "cool down and measure" mode of operation[1].

The frozen in length changes following various changes in the temperature are "reversible". (The stationary lengths established correspond to the appropriate equilibrium volume of the bubbles.) To achieve full reversibility it was of primary importance to hold the oxygen partial pressure at a constant level.

According to Figure 1 changes in the oxygen partial pressure give rise to length changes even at a constant temperature, if the temperature is relatively low, but such an effect is

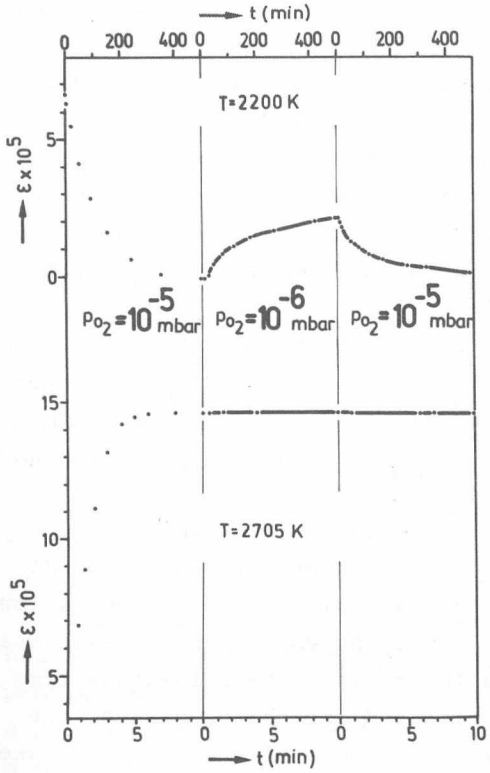

Fig. 1.

Influence of the oxygen partial pressure on the sample length. The sign of the effect at 2200 K is unexpected, since the sample shrinks upon oxygen uptake.

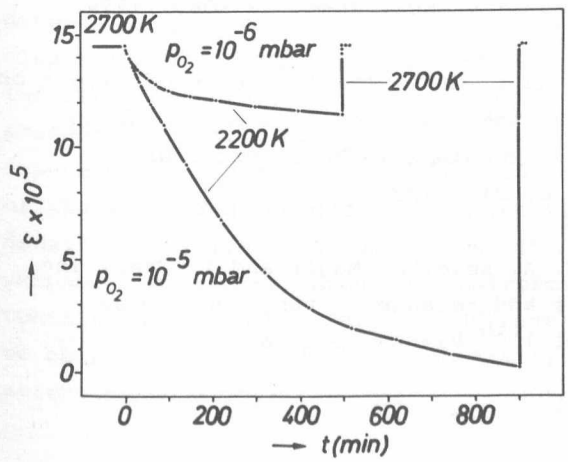

Fig. 2.

Both the extent of the effect and the relaxation time depend on the oxygen partial pressure at 2200 K.

absent, if the temperature is high enough. The shrinkage upon oxygen uptake has to be ascribed to the internal oxidation of the potassium in the bubbles, since the volume decrease upon oxidation is a peculiarity of the alkali metals. This peculiarity is due to the fact that the alkali oxides are ionically bound and the ionic radii of the alkali metals are much smaller than the corresponding metallic radii. The volume change upon oxidation of potassium in the bubbles is characterized by the ratio: V_{K_2} (liquid)/$2V_K$(bubble) = 0.25.

When samples, which have been equilibrated at 2700 K, are annealed at 2200 K, both the rate and the extent of the effect depend on the oxygen partial pressure (Fig. 2.). At 10^{-6} mbar the shrinkage is due to the thermal shrinkage of potassium and the relaxation time can be favorably compared with the relaxation time predicted for the bubble shrinkage via the vacancy mechanism put forward in the theory of sintering. At $P_{O_2} = 10^{-5}$ mbar, the small size part of the bubble population undergoes internal oxidation, hence the shrinkage is relatively large. The relaxation time is longer than the relaxation time characteristic for vacancy controlled shrinkage, because the kinetics is determined mainly by the rate of the oxygen uptake[2,3].

1. P. Harmat and J. Major, A high-temperature dilatometer for thin wires, J. Physics E: J. Sci. Inst. 12 1067 /1979/

2. P. Harmat, J. Major and I. Gaal, The influence of oxygen on the volume and growth kinetics of potassium bubbles in tungsten, Interfacial Phenomena in Metallurgy, NPL, Teddington Abstracts p. 34. /1980/

3. P. Harmat, L. Lipták, A. Kele, J. Major and I. Gaal, The rate of oxygen uptake and release in tungsten, to be published in Proc. of 10^{th} Plansee Seminar.

EFFECT OF GAS PHASE ON SINTERING POROSITY

O. Horacsek

Due to the attractive interaction between gas-filled bubbles and dislocations[1], at high temperatures and low stresses bubbles are more effective in blocking the motion of dislocations than solid inclusions. Thus, bubble strengthened alloys are preferred materials for high temperature applications where under small loading excellent resistance to creep deformation is required. The presence of a bubble forming additive makes however the alloy sensitive to microstructural instability leading to local or overall swelling. Since a sintered compact containing swelled regions is liable to break in the early stage of working, optimalisation and control of the residual sintering porosity has a particular technological and economical importance. This problem was studied in the last year. The results have been discussed in detail for KSiAl-doped tungsten[2], which may be summarized as follows.

On the basis of recent results obtained on nuclear materials, we have attempted to describe quantitatively how the final density of a sintered compact is influenced by the content and dispersion of a bubble forming additive. Our investigations indicate that the same amount of a bubble forming additive present in a solid can occupy various equilibrium pore volumes depending on its dispersion. Therefore, the chemical composition of the alloy and the degree of dispersion determines a theoretical densification limit. Assuming that the residual porosity of the compact can be attributed to a uniformly sized pore network containing the bubble forming additive at equilibrium pressure, we obtain for the densification limit, ρ_{max} of a bubble strengthened alloy:

$$\rho_{max} = \rho_o - \frac{\rho_o^2 \, cRTr}{2A\,\gamma}$$

where ρ_o = theoretical density of the matrix metal, c = the concentration /by weight/ of the bubble forming additive, R = gas constant, T = sintering temperature /K/, r = bubble radius, A = atomic weight of the bubble forming additive, γ = surface energy per unit area.

For example, in the case of KSiAl-doped tungsten, the bubble forming material is elementary potassium[3]. According to the equation, Fig. 1 shows the correlation between calculated densification limit and degree of dispersion for

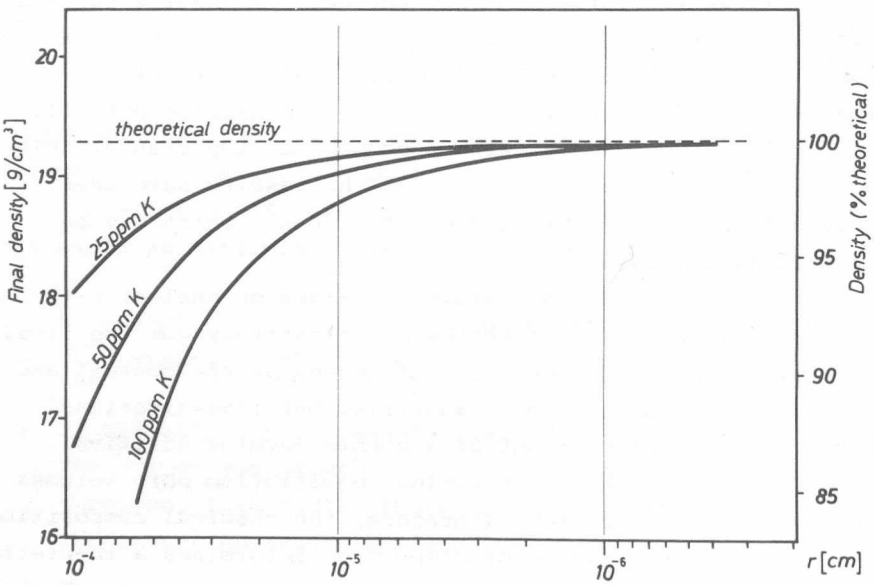

Fig. 1.

various K-contents. The diagram reflects clearly, that, the finer is the dispersion of a given amount of the potassium--additive, the higher is the final density which can be

achieved at equilibrium bubble size. Consequently, bubble coarsening taking place during sintering operation, is always accompanied by a swelling process /desintering/, which may lead in extreme cases even to bursting.

The swelling tendency of bubble strengthened alloys may be explained by internal instability which develops at a critical pore radius and internal pressure. In the case of doped tungsten, Fig. 2 illustrates the conditions for internal instabilities calculated for various potassium contents. Since potassium atoms are insoluble in tungsten and they cannot diffuse away

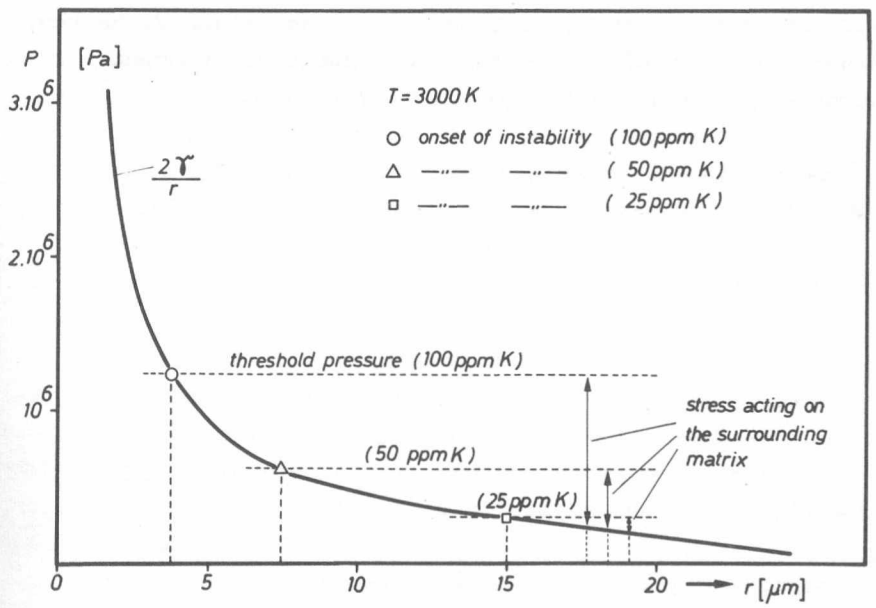

Fig. 2.

from the surroundings of an expanding pore, the amount of potassium inside the pore steadily increases proportional to r^3. Thus, the internal pressure becomes independent of the pore size, and a threshold pressure level $p_p = \rho_o cRT/A$ can be presumed, below which the internal pressure in a growing pore cannot decrease. The surface tension, $2\gamma/r$, decreases however with

increasing r. If a critical point will be reached and the surface tension is insufficient to balance the internal pressure, continuous and unlimited swelling is possible.

1. R.W. Weeks, S.R. Pati, M.F. Ashby and P. Barrand, The elastic interaction between a stright dislocation and a bubble or a particle, Acta Met. 17 1403 /1969/

2. O. Horacsek and L. Bartha, Sintering swelling in bubble strengthened tungsten, to be published in Proc. 10th Plansee-Seminar /1981/

3. H.G. Sell, D.F. Stein, R. Stickler, A. Joshi and E. Berkey, "Identification of bubble-forming impurities in doped tungsten", J. Inst. Met. 100 275 /1972/

MAGNIFESZ FLATNESS MEASURING SYSTEM

P. Ivanov, J. Gráner, D. Zsámbók[+]

Thin metal sheets always have shape defects which influence their usability. Our institute together with the Dunai Vasmü started to work in 1976 on discovering the reasons of the formations of the defects in order to minimalise them. The result of this work was the MAGNIFESZ equipment family.

We have found that the main reason of shape defects is that during cold rolling the plastic deformation changes in both directions perpendicular to the rolling direction. The inhomogeneity results partly in residual stresses, and partly it distorts the shape of the sheet, i.e. wave formation takes place. Cold rolling happens always under external stress, and in such case the shape defects, i.e. the waves are generally not visible. Therefore the resulting inner stress-distribution describes the inhomogeneities of the plastic deformation and of the shape defects which will be visible after rolling.

We have developed and patented[1] a method and an instrument for the determination of the stress-distribution of ferromagnetic strips /e.g. of soft carbon-steel/. We have built the MAGNIFESZ DK electronic unit and the magnetoinductive measuring heads typ. MD. The equipment was used in the cold rolling mill of the Dunai Vasmü[2].

On the basis of industrial and laboratory experiments a further equipment was developed which consisted of the DKL 59 TT electronic unit and of the MD 6R measuring heads. The new system has been applied under industrial conditions for the continuous determination of the visible and invisible shape defects during cold rolling and secondary cold reduction and on the basis of the signals shown on a display /Fig. 1./ the rolling was controlled in order to have a strip of minimum defect.

+ Duna Ironworks

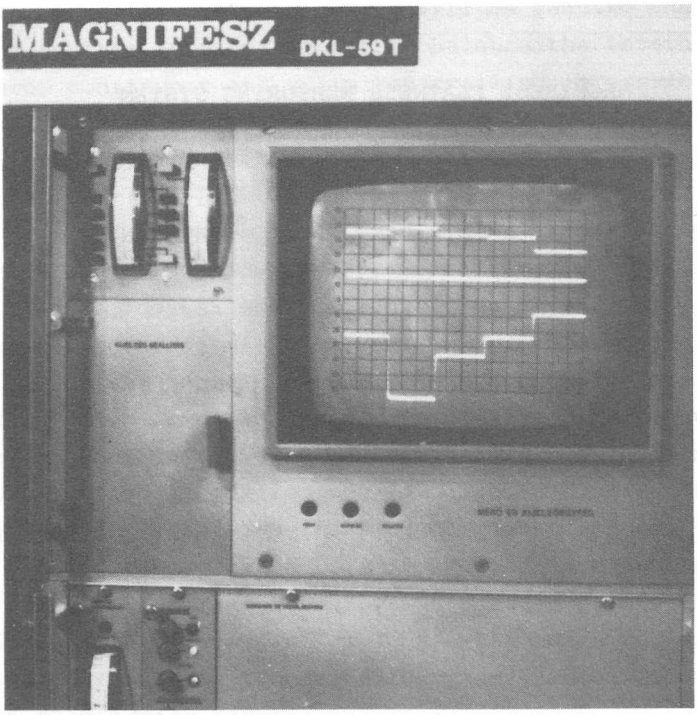

Fig. 1.

The equipment has been part of the regular production control for several months already in the rolling mill of the Dunai Vasmü. For a considerable change of quality all rolling mill--stands of the line should be equipped with the device in order to control every step of deformation. Some changes in the rolling technology might be also needed.

The patent rights for the production have been sold for the Metallurgical Engineering Co /KGyV/, Budapest. The first device abroad works in the cold rolling mill of the Steel Mill Bochum, FRG[3].

1. Hungarian pat. No. 174.945

2. P. Ivanov et. al., On-line magnetic shape meter for steel strips, in MFKI '78 Yearbook, 44-45 /1978/

3. Contechnik GmbH, Modernes ungarisches Planheitsmessgerät für Kaltwalzwerke, Stahl u. Eisen 100 /1980/ Nr. 24. 1478/79.

ON THE OXYGEN UPTAKE OF K-Al-Si DOPED TUNGSTEN

A. Kele

The rate of oxygen uptake can be monitored via the internal oxidation only at relatively high temperature /$T \geq 0.55\ T_m$/, where the mobility of the less noble /substitutional/ solute is high enough[1]. The oxygen uptake may be, however, appreciable even at temperatures, where the migration of the substitutionals is frozen in, since the mobility of the oxygen interstitial is high also at intermediate temperatures /$0.5\ T_m \geq T \geq 0.4\ T_m$/. In this case the oxygen uptake may lead to dissolved oxygen concentrations, which correspond to supersaturation with respect to the formation of oxides from the dissolved less noble trace elements in a broad temperature region. This supersaturation may cause a temporary internal oxidation at higher temperatures, at which there is no stationary oxide formation at the actual oxygen pressure. In this way the low temperature oxygen uptake can also be demonstrated by means of internal oxidation.

Fig. 1. demonstrates these phenomena on a typical example. In the first step aluminium was brought into solid solution, then, at 1900 K, the sample was charged with oxygen, and in the third step a temporary internal oxidation was revealed in a reducing atmosphere. /The precipitation of the oxide particles reduces the excess resistivity./

The essential point of this new method of oxygen monitoring is that it gives hints for the state of bonding also in the case of low temperature oxygen uptake. The moral of the present experiment in this context is as follows. From the extent of the temporary internal oxidation we might get a lower limit for the total oxygen uptake, by taking into account the stoichiometry of the oxides formed and the resistivity contribution of the dissolved aluminium[1]. /In the given example this lower limit was 10 at ppm./ Quench experiments[2] prove that at 1900 K the oxygen uptake leads only to a very low dissolved oxygen concentration /e.g. < 1 at ppm/. It is well documented however

that dissolved oxygen may form interstitial-substitutional atom pairs with various less noble metallic solutes. The M-O pairs are not necessarily revealed by the quench experiments, since the pair formation decreases the low temperature mobility of oxygen. The resistivity contribution of the M-O pairs was, however, in the present case negligible: the resistivity remains virtually constant during the oxygen uptake /Fig. 1/. The resistivity contribution of oxygen in M-O pairs is roughly the same as in the truly dissolved state, and so the concentration of the M-O pairs was probably less than 0.1 at ppm.

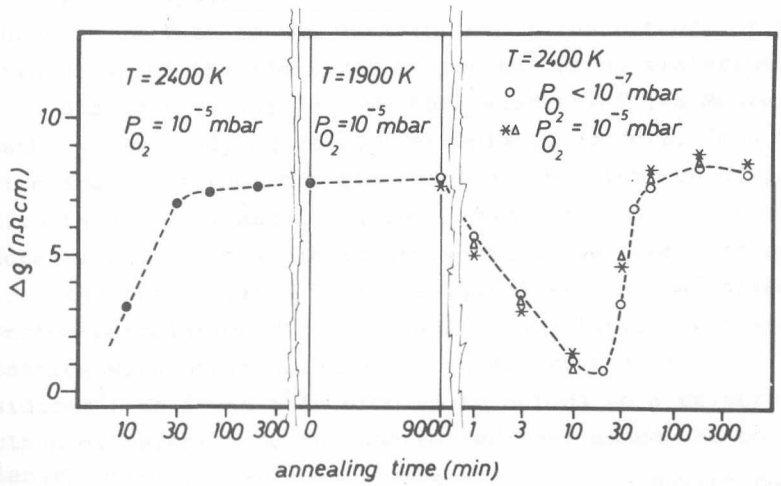

Fig. 1. Annealing schedule for the demonstration of the "low" temperature oxygen uptake by means of a temporary internal oxidation at a "high" temperature

The low amount of dissolved and pair bound oxygen urges new experiments to solve the question concerning the mechanism of oxygen storage during low temperature oxygen uptake. Besides the free surfaces acting as possible condidates for

the oxygen storage are potassium bubbles. /Thermomechanical data suggest: in our temperature range, oxygen can be dissolved in liquid potassium./

1. A. Kele, M. Menyhárd, L. Uray and I. Gaál, State of Bonding and Distribution of the Impurities in K-Al-Si Doped Tungsten, Planseeberichte für Pulvermetallurgie, 26 3 /1978/

2. P. Harmat, L. Lipták, A. Kele, J. Major and I. Gaál, The rate of oxygen uptake and release in tungsten, to be published in Proc. of the 10th Plansee-Seminar, /1981/

MONTE CARLO STUDIES IN PERCOLATION THEORY

J. Kertész and T. Vicsek

Sintering can be regarded as a process during which mechanical bonds appear between the originally separated powder particles. First relatively small numbers of grains join in a cluster, but at a definite threshold density of randomly distributed bonds a very large "infinite" cluster appears - the powder becomes a solid. This geometrical /percolation/ picture can also be applied to the interpretation of microcrack structures as well as to the description of the network of voids through which the additives evaporate during sintering.

During the last year we have elaborated two Monte Carlo methods for studying various percolation models: i/ a finite-size scaling method for time saving determination of percolation thresholds, and ii/ a real space renormalization procedure making it possible to study continuous percolation.

i/ The first system we investigated was the so called directed percolation model, in which percolation on a square lattice with bonds directed along an external field is considered[1]. We found this problem to belong to a universality class different from the undirected one, since the correlation length critical exponent ν /describing the singular behaviour of the clusters near the threshold/ we obtained, was about 25% larger than the standard value.

Next we proposed a method[2] based on finite-size scaling of samples with various length to width ratios for the determination of percolation critical probabilities p_c. Using this method /which demands less computing time, gives accurate results and does not use any assumption on the value of ν/ for the honeycomb site problem, $p_c = 0.6973 \pm 0.0008$ was found, discarding a current conjecture by Wu on critical probabilities of Potts' models.

ii/ Since the critical properties of various lattices have been found to be independent of the lattice geometry /universality/, it is usually supposed that the lattice-off lattice universality also holds. To justify this assumption we studied a system consisting of overlapping discs of equal radii with randomly distributed centers on a plain[3]. It was shown that a Monte Carlo renormalization technique could be employed for direct renormalization of a system on a continuum. We found the critical area fraction covered by the discs $s_c = 0.688 \pm 0.005$ and the correlation length critical exponent $\nu = 1.33 \pm 0.07$. The latter result supports the regular lattice-off lattice universality, since the average of the ν values obtained for the lattice models is $\nu = 1.33 \pm 0.01$. As an interesting fact we mention, that ν does not depend even on the distribution of the discs radii; we obtained the same ν, as above, for the model from overlapping discs of various radii too.

1. J. Kertész and T. Vicsek, Orientated bond percolation, J. Phys. C. 13 L343 /1980/

2. T. Vicsek and J. Kertész, Finite size scaling study of percolation on the honeycomb lattice with various length to width ratios, Phys. Lett. to be published

3. T. Vicsek and J. Kertész, Monta Carlo renormalisation-group approach to percolation on a continuum: test of universality, J. Phys. to be published

LOW TEMPERATURE ALLOYING BY MEANS OF ACTIVATED RECRYSTALLIZATION

L. Kozma, J. Lábár

Recrystallization of heavily drawn tungsten is accelerated upon annealing if iron and platinum group elements are added. The aim of this work was to investigate the role of nickel in the low temperature grain growth in tungsten.

Pieces of tungsten wires were coated with nickel and recrystallized in hydrogene atmosphere in the temperature range of 1400-2000 K. In the doped and undoped commercial tungsten used in our investigations grain growth does not take place at such temperatures with a noticeable rate. However, if nickel was present a well defined recrystallization front advanced from the periphery towards the center. The grains behind the front were of equiaxial shape while the non-recrystallized region retained its original fibre structure.

Considering the mechanism of the grain growth suggested for the liquid phase sintering of the W-Ni system[1], we assumed that the grain growth in this solid system was also chemically induced, i.e. the driving force of the grain growth was due to the formation of a W-Ni solid solution.

Electron microprobe analysis proved that the grains contained nickel while the fibrous center was free of the activator. The nickel content was uniform in the recrystallized grains, the actual concentration being dependent only on the annealing temperature Fig. 1.

The fitting of the experimental data to the solubility line calculated by means of the optimization program[2] on the basis of thermodynamical data[3] suggests that the Ni content of the W grains is the equilibrium concentration in some cases and it does not differ considerably from that of the solubility in the others.

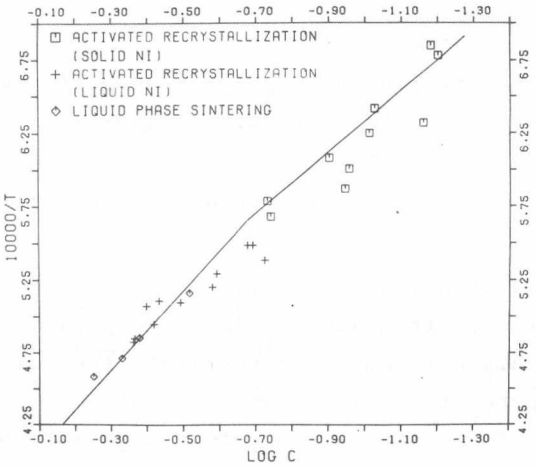

Fig. 1.
W-rich part of the W-Ni phase diagram

While diffusional alloying proceeds only at high homologous temperatures /in the case of tungsten above 0.7 T_m/, the activated recrystallization takes place at low homologous temperatures / $< 0.5\ T_m$/ resulting in a homogeneous alloy.

1. L. Kozma, W.J. Huppmann, L. Bartha and P. Mezei, Initiation of directional grain growth during liquid-phase sintering of tungsten and nickel, Powder Met., 24, 7 /1981/

2. P. Dörner, E-Th. Henig, H. Krieg, H.L. Lukas and G. Petrow: Optimization and calculation of the binary system Al-Si, CALPHAD, 4 241 /1980/

3. L. Kaufman and H. Nesor, Coupled phase diagram and thermochemical data for transition metal binary systems, CALPHAD, 2 55 /1978/

A REDOX SENSOR FOR DETERMINING HYDROGEN PEROXIDE

I. Szilassy, K. Vadasdi

Many electrode sensors have been suggested for measuring hydrogen peroxide concentrations. Mostly they are based on the decomposition of hydrogen peroxide in a membrane impregnated with different catalyzators and measuring the evolved oxygen with oxygen electrodes[1,2].

These electrodes show several disadvantages, e.g.

- slow response time, usually 4-5 min, therefore they are unsuitable for control purposes in dynamic systems
- cannot be used in acidic /<2 pH/ media
- preparation and fitting to oxygen electrodes are cumbersome.

The Fe^{3+}-H_2O_2 catalytic reaction has been studied with a Pt/Hg_2Cl_2 redox electrode couple in acidic media. The emf. of the electrodes v.s. $C_{H_2O_2}$ were measured at different iron concentrations. Stable emf. values can be obtained within short periods /10-30 sec./ in wide hydrogen peroxide and iron concentration intervals, suggesting that stationary Fe^{2+}/Fe^{3+} ratios are reached /Fig. 1/.

Applying steady-state approximation the emf. v.s. $C_{H_2O_2}$ curves can be explained with the reaction mechanism given by Barb et al.[3,4].

On the basis of these measurements a simple method has been developed for determining hydrogen peroxide in the range 10^{0}-10^{-4} M through the measurement of Fe^{2+}/Fe^{3+} ratios in an acidic medium[5].

The interference of chelating and other oxidizing species can be eliminated by a suitable calibration.

The method can be used for determining free hydrogen peroxide in "buffered" solutions as well and has been used for studying different metal-peroxo species.

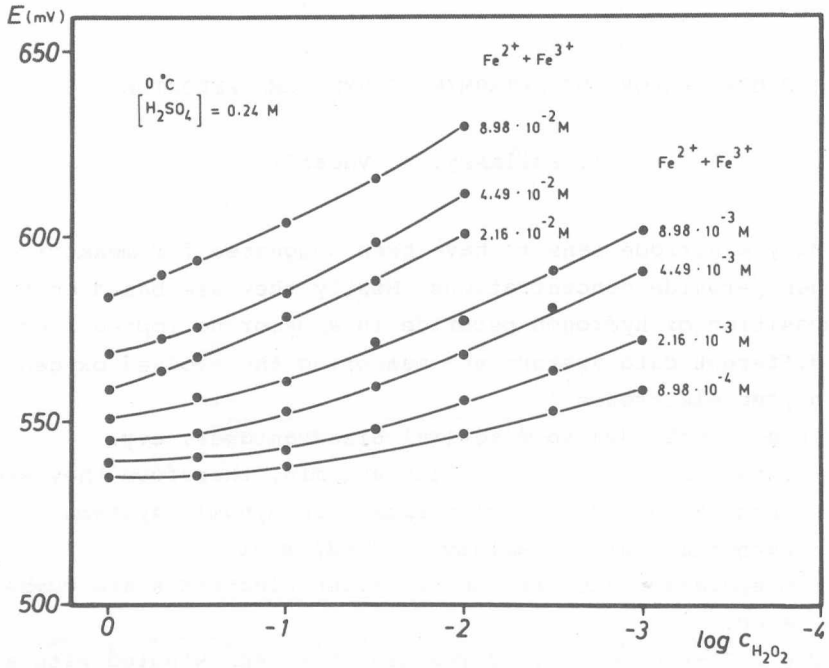

Fig. 1.

1. S.J. Updike et. al., Catalyst Electrode Specific for Peroxide, Anal. Chem. 47 1457 /1975/

2. M. Alizawa, et. al., Specific Biochemical Sensor for Hydrogen Peroxide, Anal. Chim. Acta 69 431 /1974/

3. W.G. Barb, et. al., Reactions of Ferrous and Ferric Ions with Hydrogen Peroxide, Trans. Faraday Soc. 47 462 /1951/

4. C. Walling, et. al., Oxygen Evolution as a Critical Test of Mechanism in the Ferric-Ion Catalyzed Decomposition of Hydrogen Peroxide, Int. J. of Chem. Kinetics IX. 595 /1977/

5. I. Szilassy and K. Vadasdi, A Redox Sensor for Determining Hydrogen Peroxide, SAC 80 Fifth Int. Conf. on Anal. Chem. 1980.

GRAIN BOUNDARIES AND FLOW STRESS IN TUNGSTEN

A.Szőkefalvi-Nagy, G.Radnóczi, L.Lipták, J.Major, I.Gaal

Published work is rather limited in the field of microstructures and mechanical properties achieved by relatively large deformations /$\varepsilon > 2$/, although it is already evident that also qualitatively new phenomena appear in this strain region[1]. Most of the detailed studies of the high strain behaviour has been carried out at a low homologous temperature /0.15 T_m/ on BCC iron alloys[2,3]. Thus it is of some importance to carry out similar studies on an other BCC metal, tungsten, the actual drawing of which takes place at a relatively high homologous temperature /0.3 T_m/.

In heavily drawn commercial tungsten the fibre boundaries involve high misorientations[4]. This means that the fibre structure is an ordinary grain structure consisting of elongated grains with a very fine diameter /< 1 μm/.

In heavily drawn and partially annealed tungsten a linear relationship has been found between the excess electrical resistivity and the flow stress in a broad range of the annealing and working conditions /Figs. 1 and 2/. Since there is an empirical linear relationship between the excess resistivity and the grain boundary area per unit volume /i.e. the reciprocal of the "fibre size"/[4] it means that a Hall-Petch type relationship is valid with an exponent of -1 instead of the usual -1/2. This result can be rationalized in the framework of the Langford-Cohen model. This interpretation suggests that the hardening of the tungsten during drawing and its softening during annealing is due to the refinement and the coarsening of the fibres, respectively. Transmission electron micrographs call, however, for a revision of this simple picture, since the contrast changes at the fibre boundaries upon deformation and annealing reveal important changes in the structure of the dislocation network attached to the grain boundaries. These so called extrinsic grain boundary dislocations seem to give an

important contribution to the stage IV recovery of the resistivity and the yield stress[5,6].

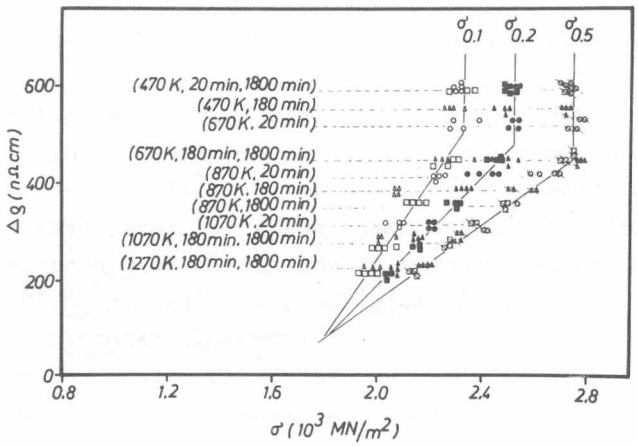

Fig. 1. Δρ-σ annealing diagram for heavily drawn K-Al-Si doped tungsten

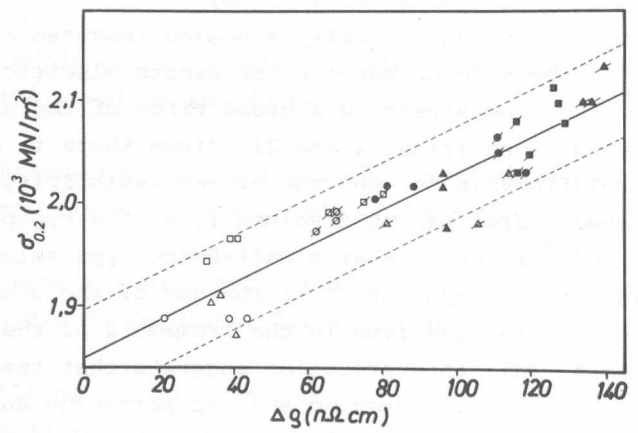

Fig. 2. Δρ-σ plot for wires drawn to various diameters /○: 151 μm, △: 139 μm, □: 130 μm, ◇: 121 μm, ⊿: 112 μm, ◪: 105 μm, ●: 98 μm, ▲: 94 μm, ■: 87 μm, ◭: 87 μm, ◮: 83 μm, ◼: 83 μm/ at 1070 K and annealed at 1270 K for 1 hour. /Δρ=ρ-ρ* and ρ* is a residual resistivity corresponding to 275 nΩcm/.

1. H. Mecking, Deformation of polycrystals, in Strength of Metals and Alloys /Eds. P. Haasen, V. Gerold, G. Kostorz/ Aachen ICSMA 5. p. 1573 /1979/

2. G. Langford and M. Cohen, Strain hardening of iron by severe plastic deformation, Trans. ASM, 62 623 /1969/

3. G. Langford and M. Cohen, Microstructural analysis by high voltage electron diffraction of severely drawn iron wires. Met. Trans. 6A 901 /1975/

4. A. Barna, I. Gaal, O. Geszti-Herkner, G. Radnóczi and L. Uray, The fibre structure of K-Al-Si doped tungsten wires, High Temp.-High Press. 10 197 /1978/

5. A. Szőkefalvi-Nagy, G. Radnóczi, A. Kele and I. Gaal, The structure of torsion-deformed tungsten wires, in Recrystallization /Eds. N. Hansen, A.R. Jones, T. Leffers/ Proc. of the 1st Risø International Symposium on Metallurgy and Materials Science p. 269 /1980/

6. A. Szőkefalvi-Nagy, G. Radnóczi, L. Lipták, J. Major and I. Gaal, Grain boundaries and flow stress in tungsten, to be published in Proc. of the 10th Plansee Seminar /1981/

APPLICATION OF THE FLAMELESS ATOMIC ABSORPTION METHOD

P. Tekula-Buxbaum

For testing raw and auxiliary materials the semiconductor industry needs new analytical methods of increasing sensitivity and accuracy.

The atomic absorption method with electrothermal atomization /flameless atomic absorption/ is one of the most sensitive analytical tools at present.

A flameless atomic absorption method was developed for the determination of certain elements /K, Na, Mg, Ca, Cu, Fe/ in high purity water and chemicals /sulphuric acid, nitric acid - Merck, Suprapure; hydrogen peroxide - Carlo Erba, Electronic Grade/ used in the semiconductor industry.

Time and temperature programmes were optimized for the elements in question in some given matrices using a Pye Unicam SP 192 Atomic Absorption Spectrophotometer, an SP 9-01 Digital Flameless Atomizer and coated PROFIL-type graphite tubes.

In case of some elements /Na, K, Ca, Fe/ present in higher concentrations in the environment difficulties were encountered keeping the highest sensitivity and accuracy given in the literature.

Results obtained for high purity water as a matrix are summarized in the Table 1.

A significant advantage associated with the flameless atomic absorption technique is that there is no need for any preliminary concentration steps when determining elements present in very low concentrations in high purity materials.

In the future we should like to improve the detection limits of the elements and extend the number of matrices beeing analysed.

Table 1.

Element	Atomization		Range of measurement		Min. quantities measured	
	Time [s]	Heat [°C]	absolute amount [pg]	concentration related to the matrix [µg/l]	absolute amount [pg]	concentration related to the matrix [µg/l]
Na	5.0	2260	20-400	1-20	20	1
K	5.0	2260	20-400	1-20	20	1
Mg	3.5	2900	10- 60	0.5- 3	10	0.5
Ca	6.0	2850	100-800	10-80	100	10
Cu	5.0	2730	20-200	1-10	20	1
Fe	5.0	2730	50-200	2.5-10	50	2.5

RESISTOMETRIC STUDY OF THE SINTER-NECKS

L. Uray, I. Skopal, I. Gaal

In the early stages of sintering powder grains form an interconnected skeleton, which may be characterized by the average neck-size and the number of necks per grain. In the present work it shall be pointed out that numerical estimates for both the average neck-size and the average number of necks per grain can be deduced from the temperature dependence of the resistivity and its effective value at room temperature. Let us realize that although the current flows through a tortuous path in the skeleton, this path will be independent of the temperature, if all the relevant necks have the same size. The resistance ratio, $R(T)/R_o$, will be equal to the resistance ratio of the average neck. If the dominant mechanism of the electron scattering is the scattering at the free surface of the neck, the average neck diameter can be deduced from $R(T)/R_o$ by means of Wexler's model calculations[1]. (Direct observations support the results of the model.) The large effective resistivity can be ascribed to the fact that the average number of necks per grain was less than the number of neighbours in a close packed powder bed. A quantitative estimate for the average number of necks per grain can be obtained by means of the bond percolation model[2]. As the sintering proceeds, both the size of the necks and their average number per grain increases[3] (Table 1).

Figure 1. Shows the temperature dependence of the resistance of tungsten in various stages of sintering /a/. The effective resistivity as a function of the apparent density is given in /b/. The numbers refer to various stages of the processing: 1,2 unwashed, baked, 3 washed, baked, 4 presintered, 5 sintered, 6 zone melted single crystal. R_o and ρ_W^o are the room temperature resistance of the sample, and the ideal resistivity of tungsten at room temperature, respectively.

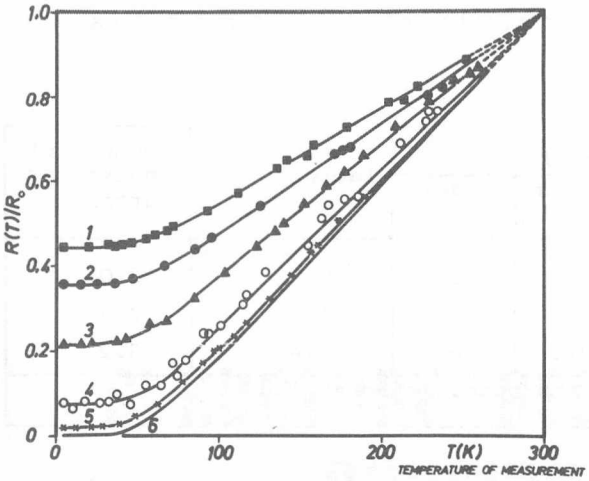

Fig. 1. /a/ The temperature dependence of the resistance of tungsten in various stages of sintering

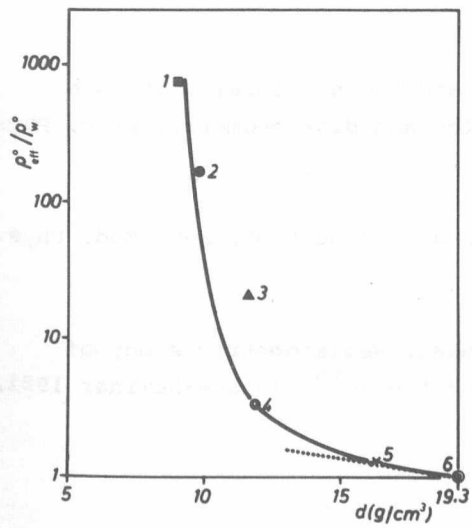

Fig. 1. /b/ The effective resistivity as a function of the apparent density

Table 1. Derived characteristics of the sintered bodies.

rod	neck diameter μm	ρ_{eff}/ρ_W^o		tortuosity factor	number of necks per grain
		measured	model		
1	0.11	750	26	29	2.0
2	0.16	163	15	11	2.3
3	0.33	20.4	6	3.4	3.2
/For rods 4-6 the model is not valid/					

/The average grain size was 2 μm. The word "model" refers to the effective resistivity of an ideal cubic lattice, in which the adjacent lattice points are connected by a resistance, corresponding to the neck resistance deduced from the Wexler model. The maximum number of necks per grain is six in this model./

1. G. Wexler, The size effect and the non-local Boltzmann transport equation in orifice and disk geometry, Proc. Phys. Soc. 89 927 /1966/

2. S. Kirkpatrick, Percolation and Conduction, Rev. Mod. Phys. 45 574 /1973/

3. L. Uray, I. Skopal and I. Gaal, Resistometric study of sinter-necks, Proceedings of the 10th Plansee-Seminar 1981, Vol 1, pp. 167-177.

STRUCTURE RESEARCH DIVISION

STRUCTURE RESEARCH IN 1979-80

L. Zsoldos

Our work in the field of structure research was connected, as earlier, both to semiconductor and metal research in the traditional fields as micro- and surface analysis, thin film physics, phase transformations and lattice defects. The selected short papers of this volume give a general survey of our activity, not including, however, all the results. Therefore, in this short introduction we try to give a brief summary of some of these results too.

In cooperation with the Inst. for Solid State Phys. and Electromicroscopy in Halle /GDR/ the wavelength dispersive TEM microanalysis of defects causing microplasma breakdown in the active zones of MOS devices showed enhanced oxygen concentration in "cloudly" polycrystalline Si precipitates /3×10^{-16} g oxygen within a diameter of 0.6 μm/[1].

As an other application of microanalysis the study of the role of Si in sintering of Pt catalysts should be mentioned here[2].

The structural changes of NiCr thin film resistors during trimming with current pulses were investigated by "in situ" TEM and it was shown that the resistivity changes are caused by phase transitions rather than by oxidation.[3] Transmission electron microscopy was successfully used also for the study of formation and structure of thin films[4,5,6] of a-Ni-P, a-Ge-Mo and Se.

In scanning electron microscopy the range of methods applied has been expanded considerably /eg. standardless quantitative analysis/ and the realization of the computer controlled SEM opened new possibilities for application.

SEM diagnostics of semiconductor devices revealed the origin of several defects /eg. transistor bondig degradation due to the presence of Cl/ as well as layout faults in LSI circuits.

Mass spectrometry of solids was applied to semiconductor research. A simple SIMS system was developed, using a RIBER QML 51 quadrupole mass spectrometer. SIMS studies on ether treated SiO_2 layers revealed the depletion of hydroxil ions by this treatment[7].

In situ mass spectrometric studies during the alloying process of contacts on GaAs diodes determined the evaporation of As_2[7,8]. The latter was strongly affected by the contact composition. The treatment by an As_2 molecular beam improved the electrical properties of contacts. The in situ mass spectrometric and electrical measurements during the contacting process enabled its optimization.

Some properties of misfit dislocations in Si were studied in cooperation with the Inst. of Semiconductor Physics in Novosibirsk, and the theoretical estimation of the two critical thicknesses of the strained layer was verified experimentally.

To the measurement of strain distribution in epitaxial diffused etc. layers double crystal diffractometry was applied, and a topographic method was developed for such measurements on bent crystals[9].

1. M. Pasemann, Á. Barna, P. Werner and H.I. Hagel, Electron optical identification of precipitations in silicon semiconductor devices, Kristall und Technik, 14, 553 /1979/

2. Á. Barna, P.B. Barna, L. Tóth, Z. Paál and P. Tétényi, Electron microscopic studies of platinum catalysts Abstracts, 9th Hungarian Conf. on ELMI, Szeged, 1979

3. M. Lomniczy, Á. Barna and P.B. Barna, Effect of current trimming on the structure of Ni-Cr thin films, Abstracts, 9th Hungarian Conf. on ELMI, Szeged, 1979

4. T. Bagi, Z. Hegedüs, E. Tóth-Kádár, I. Nagy and P.B. Barna, Formation mechanism of amorphous Ni-P thin films, Acta Phys. Hung. 49 /1-3/ 181 /1980/

5. A. Belu, A. Dévényi, R. Manaila, L. Miu, C. Rusu, Á. Barna, P.B. Barna, G. Radnóczi and L. Tóth, Structure and electrical properties of amorphous Ge-Mo films, Acta Phys. Hung. 11 /1-3/, 207 /1980/

6. P.B. Barna, L. Tóth, B. Petrestis and R. Rinkunas, The effect of ion current density in the molecular beam on the structure and properties of Se films /in Russian/ Acta Phys. Hung. 48, 315 /1980/

7. G. Gergely, I. Mojzes, T. Sebestyén, D. Szigethy and M. Riedel, Mass spectrometric study of semiconductor layer structures, Acta Phys. Hung. 49 /1-3/, 199 /1980/

8. G. Gergely, I. Mojzes, T. Sebestyén and D. Szigethy, Mass spectrometric study of the decomposition and evaporation of semiconductor surfaces, Proc. of the Surface Analysis 79 Conference, Karlovy Vary, 1979

9. L. Zsoldos, Determination of strain distribution in surface layers of bent crystals by double-crystal X-ray topography Coll. Abstr., X. Hung. Diffr. Conf., Balatonaliga 1980, p. A21.

IMPURITY CONTROLLED CRYSTAL GROWTH IN Al THIN FILMS

P.B. Barna, F.M. Reicha,+ J. Barcza

In our recent studies we found the surface chemical interactions taking place between the surface of the growing film and the species of residual gases to control the incorporation of impurities into the films[1]. In the case of the aluminium and oxygen system a correlation between the crystal face anisotropy in the surface microchemical activity[2] and the crystal face anisotropy in the crystal growth has been proved. According to our model proposed for the explanation of anisotropic impurity incorporation, "active" foreign species not penetrating into the surface layer of a crystal face of given Miller indices /e.g. into ⟨111⟩ type faces in the case of the Al/oxygen system/ are accumulated by the moving growth steps and develop local surface covering layers. The growth of crystals is limited in these directions and the crystal "habit" is destroyed by this way /Fig. 1/. On other surfaces on which the given foreign species can penetrate into the surface layer, the accumulation of foreign species does not take place /e.g. on the ⟨100⟩ type faces of Al/oxygen system/. These phenomena result in the selection of crystals with respect to both their gorwth conditions and coalescence according to their orientation.

Our results are a contribution to the better understanding of the formation of hillocks /Fig. 2/ and whiskers /Fig. 3/ in Al thin films depending on the partial pressure of oxygen as well as the accumulation of foreign species /impurity of doping materials/ to the grain surfaces and/or boundaries of monocrystalline and polycrystalline metal or semiconducting films[3,4,5]. Also the influence of the environment or the doping level on the structure and growth morphology of the crystals of various orientations and on the properties of films can be explained in this way.

+ Ph.D student from university of Mansoura, Egypt

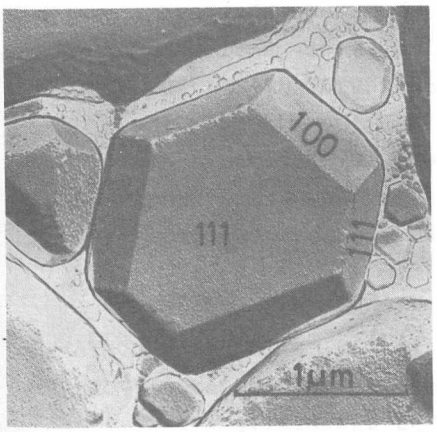

Fig. 1. Preferential truncation of an Al crystal at the edges between ⟨111⟩ faces. Al film deposited onto mica at 500°C, deposition rate 1 nm/s, P_{oxygen} 10^{-5} Pa.

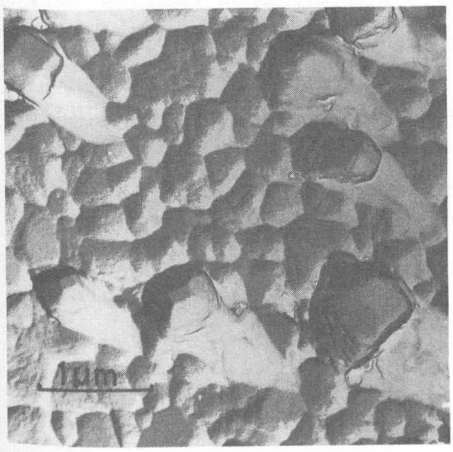

Fig. 2. Growth hillocks in 1 µm thick Al film deposited onto a glass substrate at 300°C. Deposition rate 2 nm/s, P_{oxygen} 10^{-4} Pa.

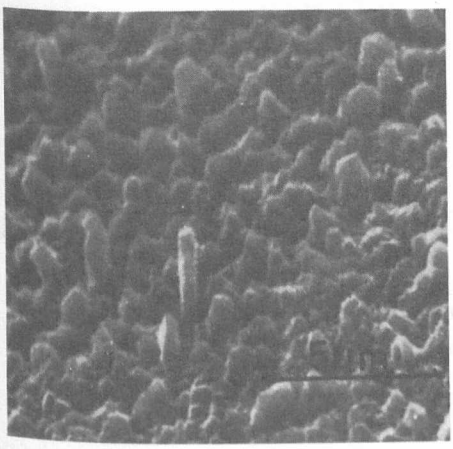

Fig. 3. Growth whiskers in a 1 µm Al film deposited onto glass substrate at 300°C. Deposition rate 2 nm/s, P_{oxygen} 5.10^{-3} Pa.

1. P.B. Barna and Z. Paál, Surface chemical phenomena influencing the growth of thin films, Proc. ELFT-ÖGW Vacuum Conf. 1979, Győr, Acta Phys. Hung. 49 77 /1980/

2. M. Michel, J. Castaldi, C. Allasia, C. Jourdan and J. Derrien, Initial interactions of oxygen with aluminium single crystal faces: a LEED, AES and work function study, Surface Sci., 95 309 /1980/

3. Á. Barna, P.B. Barna, G. Radnóczi, F.M. Reicha and L. Tóth, Formation of aluminium thin films in the presence of oxygen and nickel, Phys. Stat. Sol. a, 55 427 /1979/

4. F.M. Reicha and P.B. Barna, On the mechanism of hillocks formation in vapour deposited thin films, Proc. ELFT-ÖGW Vacuum Conf. 1979 Győr, Acta Phys. Hung. 49 237 /1980/

5. P.B. Barna and F.M. Reicha, The effect of oxygen uptake of crystallographic faces on the growth and coalescence of crystals in Al films, Proc. 8th Intern. Vacuum Congress Sept. 22-26, 1980. Cannes /France/, Vol. 1, p. 165.

STRUCTURAL CHANGES ACCOMPANYING REPEATED DEHYDRATION--HYDRATION PROCESSES IN APT.$4H_2O$/$[NH_4]_{10}H_2W_{12}O_{42}\cdot 4H_2O$/

M. Farkas-Jahnke, T. Grósz, E. Benes, K. Vadasdi

The effect of repeated heat treatment on the structure and composition of APT.$4H_2O$/$[NH_4]_{10}H_2W_{12}O_{42}\cdot 4H_2O$/ was investigated by X-ray technique and weight-loss measurements respectively in the temperature region of technological interest, i.e. between room temperature and 150°C. X-ray patterns were taken in a high temperature Guinier-Lenné powder camera with CuK_α radiation on air. During the first heating process two structure changes were detected occuring near 60°C and 85°C respectively, being almost reversible when cooling down the samples to room temperature again. More detailed investigations reveal however some minor changes in the room temperature line system, corresponding to a slight deformation of the monoclinic unit cell.

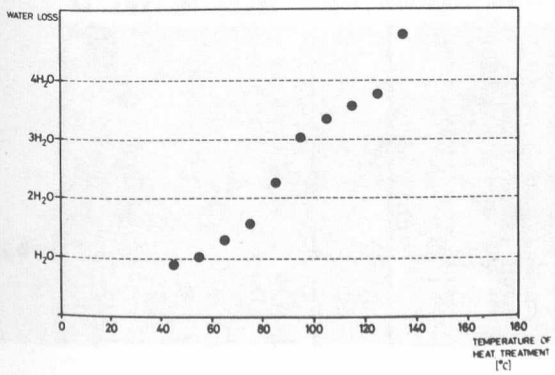

Fig. 1. Weight loss of 10 g APT.$4H_2O$ sample after heat treatment at 45-135°C for 2 hours

Parallel to the structure investigations weight-loss measurements ere carried out on 10 g of the material heated in air at 45, 55, 65, 75, 85, 95, 105, 115 and 135°C respectively for 2 hours. After each heat treatment the powder sample was quenched and the weight-loss was measured at room

temperature at 45% humidity. From the percentage of weight-loss, the number of water molecules leaving the sample from each paratungstate ion could be calculated /Fig. 1/.

Repetition of the heating process results in the splitting of the first structural transition /near 60°C for the first heating/ into two distinct changes occuring near 35°C and 60°C respectively. This separation - splitting of the first structural change into two steps - remains when repeating the heating--cooling cycle several times.

The transition occuring at higher temperatures /near 85°C/ was not influenced by the heating cycles /Fig. 2/.

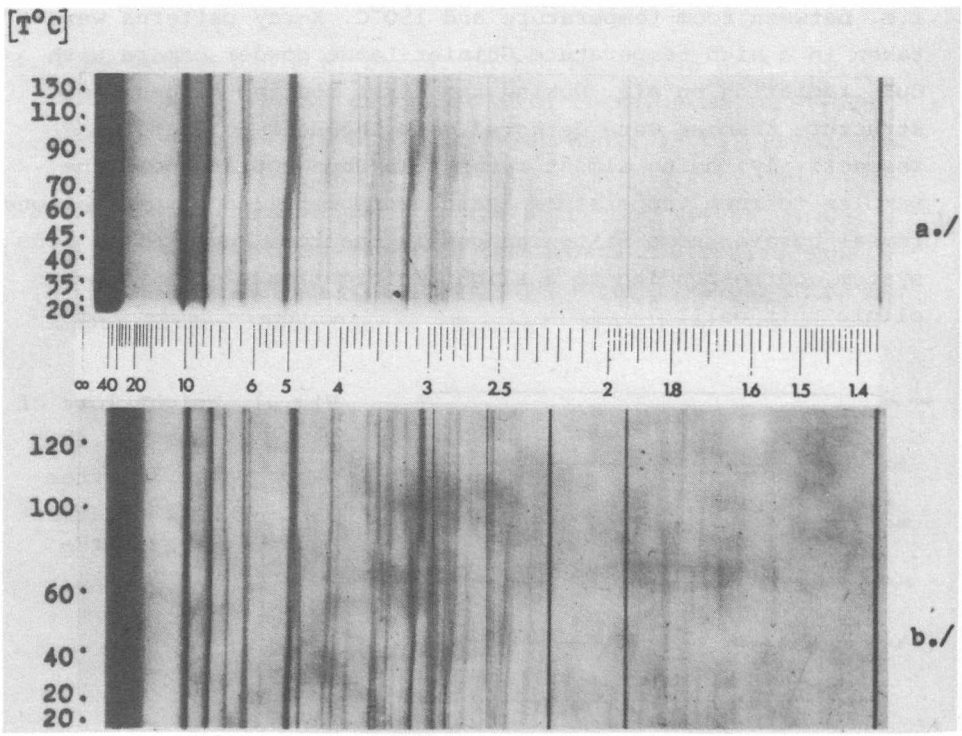

Fig. 2. Guinier-Lenné patterns taken during the a/ first b/ second heating cycle of APT.$4H_2O$

After the second heating cycle the room temperature line system shows some further changes, but after the third cycle

neither the position nor the intensity of the lines did alter any more. All the resulting structures preserve the monoclinic character of the parent lattice apart from little changes in the lattice parameters. A possible mechanism of the changes in the crystal structure can be the following: The crystal structure of APT.$4H_2O$ is built up of $\left[H_2W_{12}O_{42}\right]^{10-}$ paratungstate complex ions connected by H_2O-s and NH_4-s. The most significant changes are the increase of the lattice parameter a together with the decrease of lattice parameter b. This can be explained by small rotation of the paratungstate complex ions around the c axis.

Repeating the heating-cooling cycles on the sample the structural changes are accompanied by a definite decrease of the particle size. This effect has to be taken into account in the drying technology.

1. H. D'Amour and R. Allmann, Die Kristallstruktur des Ammonium-parawolframat-tetrahydrats /$NH_4/_{10}\left[H_2W_{12}O_{42}\right].4H_2O$, Z. Kristallographie 136 23 /1972/

2. M. Farkas-Jahnke, T. Grósz, E. Benes and K. Vadasdi, Reversible chemical changes in the APT.$4H_2O$ /$NH_4/_{10}\left[H_2W_{12}O_{42}\right].4H_2O$ during heat treatment, Fifth European Crystallographic Meeting, Copenhagen 1979, Collected Abstracts 327.

3. M. Farkas-Jahnke, T. Grósz, E. Benes and K. Vadasdi, Structural changes accompanying repeated dehydration--hydration processes in APT.$4H_2O$ /$NH_4/_{10}\left[H_2W_{12}O_{42}\right].4H_2O$/ X. Hungarian Diffraction Conference, Balatonaliga, 1980, Collected Abstracts A60.

QUANTITATIVE AES IN THE FRACTOGRAPHY OF STEEL AND TUNGSTEN

G. Gergely

AES fractography[1] of thin overlayers and second phases produced by segregation enables the determination of some trace impurities affecting the mechanical properties of metals, e.g. in steel, S, P, Sb etc.[2]. In a similar way impurities /e.g. oxide/ or doping elements /e.g. K/ can determine the fracture path in tungsten[3].

Some important factors as:

- The backscattering excitation of Auger electrons by the substrate[4],
- The reflection of Auger electrons on the substrate[4,5],
- The real attenuation of Auger electrons by the overlayer[4,5]

are not accounted for when evaluating Auger spectra obtained on fracture surfaces with the commounly used Palmberg sensitivity factors[1].

Furthermore, the temperature of fracture proved to be very important in tool steel[2] and tungsten as well, producing surface diffusion of potassium[3].

The contamination of the fresh fracture surface by residual gases was eliminated by applying a sublimation pump cooled by streaming liquid nitrogen[5], working in the 10^{-8} Pa pressure range.

The backscattering factor and reflection by the substrate were evaluated using eq. /1/ for a thin overlayer:

$$r_{BAo} = 1 + \frac{e}{\sigma I_r}\left[\int_{E_i}^{E_r} \sigma N/E/dE + N_r/E_A/\right] \qquad /1/$$

denoting by $N/E/$ the backscattering spectrum[4,5], by σ the ionization cross section and by $N_r/E_A/$ the reflection coefficient of

an Auger peak. The integral in eq. /1/ differs from Gallon's formula[4] by a factor of 2 being valid for the backscattering factor r_{BA} of the substrate Auger electrons. In Fig. 1 r_{BA} and the inelastic reflection coefficient r_B /based on our measurements[4]/ are plotted versus Z atomic number. Auger spectra of a thin overlayer with $\theta \leq 1$ coverage are evaluated with a modified formula of Marchut and McMahon[1] with the above mentioned corrections using experimental results available. In eq. /2/ I_o and I_s stand for the Auger peak heights of the overlayer and the substrate, resp., while P_o and P_s denote their Auger yield factors[7]:

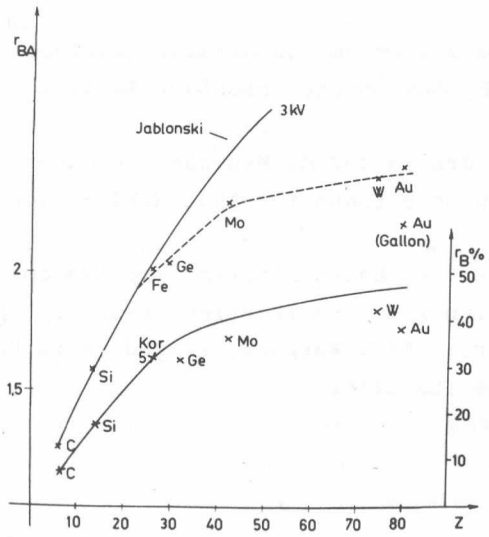

Figure 1.

$$\frac{I_o}{I_s} = \frac{P_o r_{BAo}\,\theta(1-k_s)}{P_s r_{BA}(1-\theta+\theta k_o)} \qquad /2/$$

$$k_s = \exp\left(-\frac{1}{0.74 L_s}\right)$$

k_s is the attenuation of the substrate with L_s escape depth of Auger electrons. k_o denotes their attenuation by the overlayer. In all cases $k_o > k_s$ was found. Data on the Auger yield factors, L_s and k_o for various substrates and adatoms are presented in[1,4,5].

1. G. Gergely, Some problems of quantitative AES in fractography, Acta Phys. Hung. 49 87 /1980/

2. K. Romhányi, Zs. Szász Csih, G. Gergely and M. Menyhárd, Auger spectrometric studies on fracture surfaces of tool steel, Kristall und Technik 15 471 /1980/

3. M. Menyhárd, Potassium on the fracture surface of tungsten wires studied by AES, Surf. Interface Anal. 1 175 /1979/

4. G. Gergely, B. Gruzza and M. Menyhárd, Backscattering spectra of medium energy electrons for AES, MFKI'80 Yearbook, p....

5. G. Gergely, Electron backscattering spectra for quantitative AES in fractography and segregation, Proc. 5th Seminar Surf. Phys. 23-27 April 1980, Karpacz, Poland, Acta Univ. Wratislawiensis /in print/

BACKSCATTERING SPECTRA OF MEDIUM ENERGY ELECTRONS FOR AES

G. Gergely, B. Gruzza[x], M. Menyhárd

Backscattering excitation of Auger electrons is important in the case of quantitative AES. The backscattering factor[1] is mainly determined by the distribution N(E) of secondary and backscattered electrons. Another important advantage of the knowledge of the N(E) spectrum is to enable the background subtraction in the counting mode of SAM or LMS and in the DC methods[2] of AES. Electron backscattering spectra were determined on graphite, Si, stainless steel, Ge, Mo, W and Au atomically clean polycrystalline samples. Spectra were measured under normal incidence excitation in the medium energy range: E_p = 0.7 - 3.1 keV using a Riber OPC 103 CMA analyser operated in the DC mode[2]. The sensitivity level of the detector system was kept carefully constant supplying quantitative results on the spectra and the percentage N_e of elastically reflected electrons, as well. The main experimental results are summarized in Figs. 1-2 representing N(E) spectra for E_p = 2.2 and 3.1 keV, resp. Fig. 3 shows a typical fine structure around the elastic peak with the plasmon loss peaks of Si, supplying some information on the elastic reflection N_e and the loss processes as well.

In Fig. 4 N_e is plotted versus the atomic number Z for E_p = 2.2 and 3.1 keV.

The N(E)spectra and N_e are strongly affected by E_p and Z. The Auger backscattering factor and the inelastic reflection coefficient of the samples were evaluated using the N(E)spectra.

Results were published in detail[3,4], compiling also comprehensive literature on electron backscattering.

[x]Laboratoire de Microscopie et Diffraction Électronique, Université d'Aix-Marseille III., France

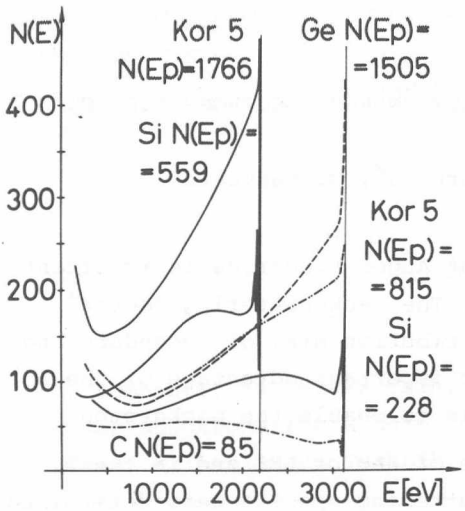

Fig. 1.

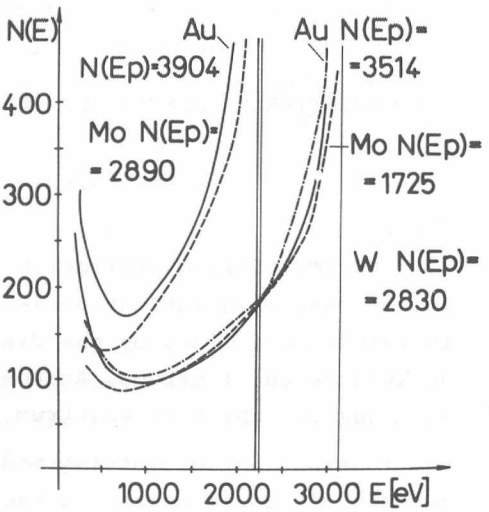

Fig. 2.

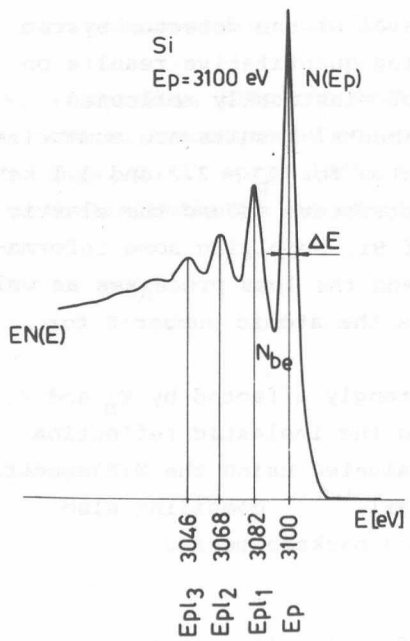

Fig. 3.

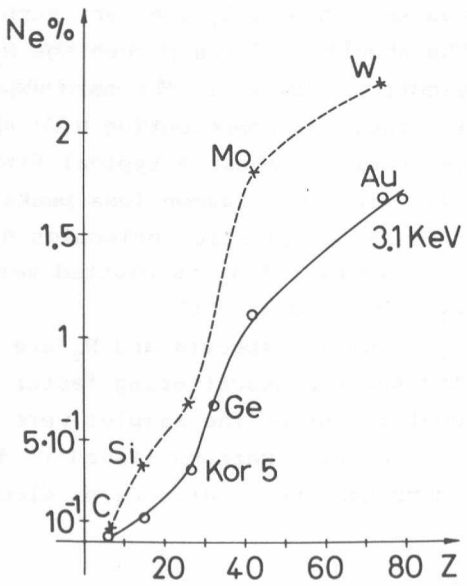

Fig. 4.

1. A. Jablonski, Backscattering effects in Auger electron spectroscopy : A review, Surf. Interface Anal. 1, 122-31 /1979/

2. Bui Minh Duc, C. Jardin, J.P. Gauthier and P. Michel, A low-energy electron spectrometer using concentric hemispheres and a grid retarding field, J. Phys. E.: Sci. Instrum. 12 43-46 /1979/

3. G. Gergely, B. Gruzza and M. Menyhárd, Backscattering spectra for quantitative AES of thin overlayers, in Proc. 4th ICSS and ECOSS 3. 22-26 Sept. 1980, Cannes, Suppl. Le Vide, les Couches Minces No. 201, 1392-5 /1980/

4. G. Gergely, B. Gruzza and M. Menyhárd, Backscattering spectra of medium energy electrons, Acta Phys. Hung. 48, 337 /1980/

INVESTIGATION OF GRAIN BOUNDARIES BY SCANNING ELECTRON MICROSCOPY

F. Koltai and G. Radnóczi

The efficiency of SEM in materials science is much increased when crystallographic information can also be obtained. Electron channelling patterns /ECP/, first observed by Coates[1] on GaAs single crystals and interpreted by Booker et al.[2] can be used for this purpose. We have applied this method to tungsten wires and GaSb ingots. Tungsten wires of 0.5 mm diameter were investigated after heat treatment at 2500 K for 3 minutes[5]. To obtain flat surfaces a longitudinal section was prepared using an abrasive disc. The deformed surface layers were dissolved by electrolytic etching in 2% NaOH and then electrolytically polished in the same solution at smaller currents.

Secondary electron images /SEI/ of the longitudinal sections of wires and ECP-s of each grain were recorded /Fig. 1, 2/. For the evaluation of the ECP a computer program was generated. Using the distances between the centre of the pattern and three identified Kikuchi lines or poles as input data, the Miller indices of the optical axis in the coordinate system of the crystal were calculated. The rotation of the crystal about the optical axis can be determined from the angle of an ECP line with a fixed direction. In this way the orientation of a grain became known.

For 23 grains the angles between the wire axis and the nearest $\langle 110 \rangle$ direction were calculated. The standard deviation of the $\langle 110 \rangle$ directions around the wire axis is 2.2°. Comparing our results with TEM measurements[3] on as received wires we can conclude, that the angle deviation of the $\langle 110 \rangle$ directions covers a broader range after heat treatment. The angle and axis of rotation transferring the coordinate system of one grain to that of neighbouring one were calculated. Comparing the obtained data with the coincidence site lattice /CSL/ model[4] we observed that from 54 boundaries the CSL relationship is statisfied only in four cases when allowing 4° deviation. Another four boundaries are small angle ones /$\theta \leq 4^{\circ}$/. Accordingly CSL

misorientations do not occur more often than expected from a random distribution of misorientations. The presence of small angle boundaries is a consequence of the texture. The rest of the boundaries can be considered as random.

The examined GaSb crystals were grown by the Bridgman method[6]. Quartz ampoules of 8 and 28 mm diameter about 60 mm length and 1 2 resp., were filled with polycrystalline GaSb. The ampoules were heated to 718°C, slightly above the melting temperature. The lowering rate was 0.3, 3.6 and 18 mm/hour. The ingots were cut into halves and etched in $HCl:H_2O_2:H_2O$/1:1:2/ to reveal their grain structure.

Moving from grain to grain perpendicularly to the growth direction across the boules, the number of low and wide angle grain boundaries was determined /Table 1/. We may conclude, that both the diameter of the ampoule and the lowering rate influences the grain size in the applied intervals. The effect of the ampoule diameter seems to be stronger as can be seen in the case of specimen 4 in Table 1.

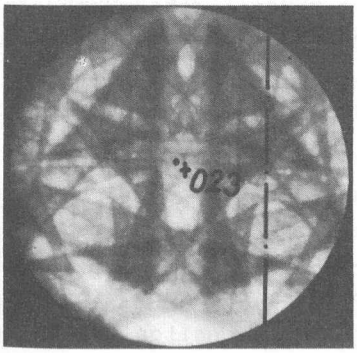

Fig. 1 ECP from a W grain of nearly /023/ orientation. The exact orientation is: /1,55,84/. The line shows the wire axis direction.

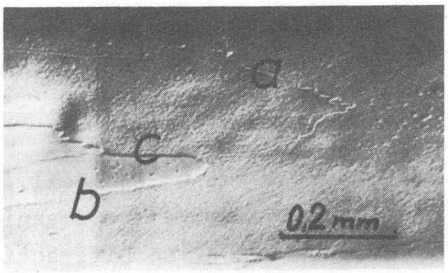

Fig. 2 SEM image of a W wire. The rotation axis and the angle pairs of some grain boundaries:
a/ 47,56,68 , 2.36°
b/ 29,46,84 , 119.6°
c/ 7,35,93 , 131.6°

Table 1. Growth parameters of GaSb ingots and the density of grain boundaries along a diameter of the ingots

Sample	Ampoule dia. /mm/	Lowering rate (mm/hr)	No. of boundaries/cm		
			wide angle	low angle	total
1	8	0.3	4	6	10
2	8	18	10	20	30
3	28	18	8	16	24
4	28	3.6	0-1	7	7-8

1. D. Coates, Kikuchi-like reflection patterns obtained with the scanning electron microscope, Phil. Mag. 16, 1179 /1967/

2. G.R. Booker et al., Some comments on the interpretation of the "Kikuchi-like reflection patterns" observed by scanning electron microscopy, Phil. Mag. 16, 1185 /1967/

3. D.B. Snow, The recrystallization of heavily-drawn doped tungsten wire, Met. Trans. 7A, 783 /1976/

4. P.H. Pumphrey and K.M. Bowkett, Axis/angle pair descriptions of coincidence site lattice grain boundaries, Scripta Met. 5, 365 /1971/

5. F. Koltai and G. Radnóczi, Investigation of grain orientation in tungsten wires by scanning electron microscopy, in Proc. of 10th Hungarian Diffraction Conf., Balatonaliga, A85 /1980/

6. M. Hársy, T. Görög, E. Lendvay and F. Koltai, Direct synthesis and crystallization of GaSb, to be published in J. of Cryst. Growth.

AUTOMATIC X-RAY ANALYSER BASED ON AN EEDS-II SYSTEM

J. Lábár

With the appearance of semiconductor detectors and microprocessors, the energy dispersive analyser systems /EDS/ have widely spread as quick and comfortable tools for composition determination. Their microcomputer, firmware and floppy disk offer a lot of convenient service and make the data acquisition and reduction possible. Most of the firms selling such systems /including ORTEC, the manufacturer of our EEDS-II analyser/ designed their equipment for manual operation, i.e. firmware routines making the data acquisition and partial data reduction can only be activated by mechanical push buttons. Moreover, no possibility has been offered for the users to establish a connection between these routines and the microcomputer responsible for the data storage and the full data reduction. This "split-minded" system is inadequate for automation because it needs human handling of push buttons to initiat each step of the analysis and to switch from the microcomputer to the analyser mode of the system.

In a laboratory established for industrial problems a lot of similar samples must be analysed under similar circumstances. /E.g. homogeneity test, composition profiles, serial measurements for comparing technologies and their steps, etc./ The demand for automation arises, because otherwise the measurements require the continuous presence of an operator due to the need of frequent push button operation.

Our present development, the so called LEARN mode, added to a commercial energy dispersive X-ray analyser of the type EEDS-II is compatitive with all the similar systems on the international market. The introduction of this new facility provided us with an automatic analyser offering the following benefits.

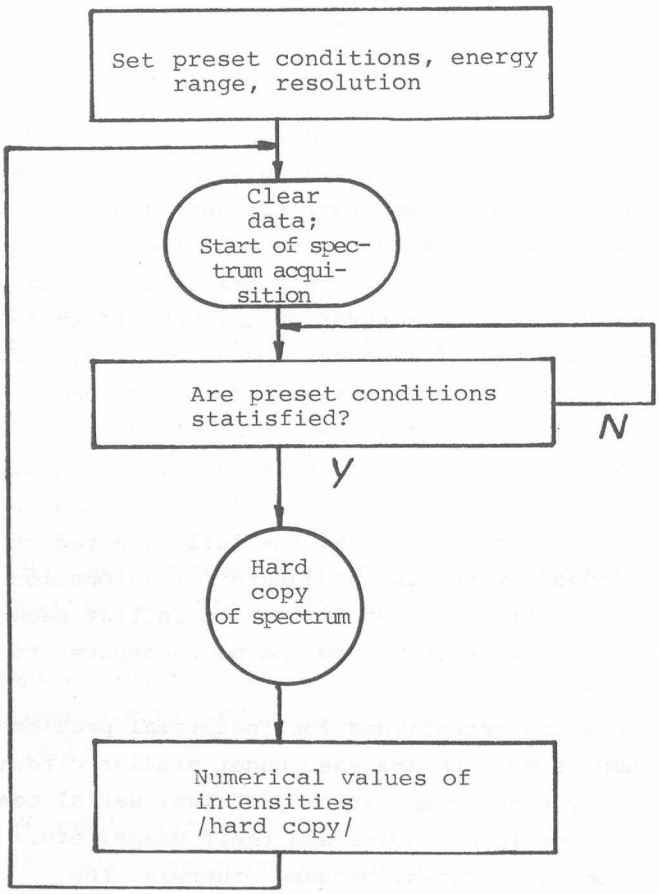

Fig. 1.

An example for "LEARNED" algorithm. The numbers show how many manual push buttons were necessary in the "old" system

1. Algorithms with an unlimited number of steps can be defined for automatic execution. The steps of the algorithms are those firmware routines which before could only be activated by push buttons. /See Fig. 1./
2. These algorithms can be executed by programs written in a high level programming language /ORACL/, and can be an integral part of an ORACL program.
3. The algorithms can be saved on a floppy disk in similar manner as programs, so there is no need for redefining the same procedure each time when a similar problem occurs.

Summarizing the essence of our development: serial analysis can be automatized, the operator's only duty is to define the procedure of measurement for the computer and the remaining part of the analysis does not need highly qualified assistance. The automatism is flexible and can be modified within minutes.

This LEARN mode, with the intermediate step of developing the computer control of the scanning electron microscope[1], has made it possible to realize a fully automatic energy dispersive X-ray analyser.

1 J. Lábár and A. Vladár, this volume p 115.

COMPUTER CONTROLLED SCANNING ELECTRON MICROSCOPE /SEM/

J. Lábár and A. Vladár

With the automation of our X-ray analyser system it became possible to realize an automatic EDS microprobe. The only intermediate step required was to develop the computer control of the JSM-35 SEM. A digital scan generator /DSG/ has been constructed for the JSM-35 by the engineers H. Borody and P. Sárvári. The innovation discussed here refers to the interface between this DSG and the microcomputer and to the development of a controlling software.

Our aim was to minimize the time and costs and not to interfere with the inner parts of the computer, therefore we based our interface on the utilization of existing signals, which have not been utilized up to now. The new software can be divided into two logical packages. One of them provides the beam control if the coordinates of the destination points are given, the other one makes the allocation of the destination points easy, quick and exact.

This computer control is able to determine the number of image points in one line /and thus the distance between them/, and to make the beam step and/or reset both in the X and the Y direction. At the same time we can blank the beam, that is of importance when examining, electron sensitive materials. It makes it possible to analyse points along an arbitrary pattern, which can be necessary e.g. in the case of a second phase analysis, a homogenity test and the investigation of composition profiles.

The points to be measured can be assigned by the keyboard of the computer as well. For this purpose we had to redefine the keyboard of course. With the help of four buttons of the keyboard the electron beam of the SEM can be moved, while its position can be seen as a bright spot on the screen of a storage display. There are max. 3 rates of speed of movement depending on the number of points in a line determined at the start.

When the points is in the right position one push button makes the microcomputer remember the coordinates of the point. The number of points to be analysed do not have to be known in advance.

The number of points in a line may be in the range of 4-2048. /The limitation originates from the stability of the SEM and the construction of the DSG./ The beam control takes place within max. 0.05 sec, as the frequency of the computer output signals is 40 kHz in this case.

The modification of the hardware in order to show the selected point position together with a "live" TV picture is in progress.

The LEARN mode[1] together with the computer control of the SEM /as described here/ provides the possibility of a fully automatic EDS analysis.

1 J. Lábár, this volume, p 112.

AES STUDIES ON THE FRACTURE SURFACE OF DOPED TUNGSTEN

M. Menyhárd

Though tungsten is, similarly to the other bcc metals, susceptible to brittleness it is ductile enough for drawing and coiling using an appropriate technology. In order to be able to improve the technology the physics of the fracture must be studied. The aim of our AES investigations is to explain some failures of the wires. It was shown in our previous works[1,2] that fracturing the doped tungsten wires in the temperature region of 100-300 K a/ the fracture path runs through potassium rich regions b/ the potassium spreads along the surface from the three dimensional potassium second phases revealed by the fracture. Studying the time necessary for this spreading, it turned out that in samples, with a diameter larger than 0.9 mm, in addition to the usually excepted three dimensional potassium second phases also quasi-two-dimensional second phases appeared[3,4]

The row of bubbles necessary for the good creep behaviour can not be produced, however, by the quasi-two-dimensional second phases. On the other hand it is very likely that the brittleness of the wire can be partly attributed to these potassium second phases. We must add, however, that the role of the potassium in the fracture is reduced considerably if the temperature is higher than 500 K. It is well accepted that the oxygen contamination of the tungsten causes brittleness. To elucidate the role of the oxygen some model experiments were carried out. The wires were flashed in air by a current impulse. On the fracture surface of the wires, prepared in this way, considerable oxygen contamination was observed. The distribution of the oxygen and potassium along the radius of the wire is shown in Fig. 1.

This result can be interpreted as follows: grain boundary or/and microcrack corrosion took place during flashing and the fracture nucleated on the oxidised regions and run along it.

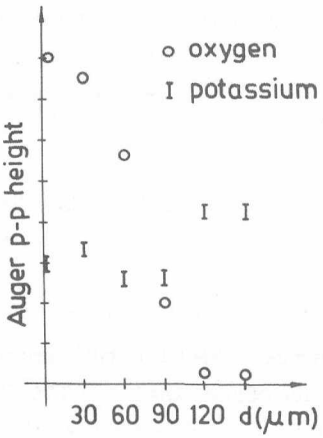

Figure 1. The Auger peak-to peak height of the oxygen and potassium v.s. the distance measured from the edge of the wire

On the fracture surface of "as received" commercial wires susceptible to brittleness large potassium and oxygen inhomogeneties were found, as shown in Fig. 2.

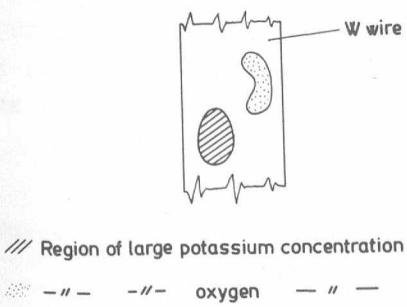

Figure 2. The scheme of the oxygen and potassium inhomogenities present on the longitudinal fracture surface of wires susceptible to brittleness

The fracture can nucleate on these inhomogenities, as our model experiment shows, that is these oxygen and potassium inhomogenities are responsible for the brittleness. The potassium inhomogenities are very likely due to the quasi-two--dimensional potassium second phases. The oxygen inhomogenities are caused by inproper sintering. In certain cases oxygen contamination was found by our AES studies on the fracture surface of the sintered rods showing that the reduction was not complete.

This oxygen will not be removed from the sample during the manufacturing of the wire; thus the oxygen inhomogenities found on the longitudinal fracture surface of the wire are present already in the sintered rods.

1. M. Menyhárd, Investigation of tungsten wires by AES, Proc. of Surface Analysis 79 /Karlovy Vary, 1979, ed. D. Stulik/ Vol. 2 38/1

2. M. Menyhárd, Potassium on the fracture surface of tungsten wires studied by AES, Surf. and Interface Anal. 1 175 /1979/

3. A. Kele and M. Menyhárd, On the fracture of doped tungsten, Acta Phys. Hung. 49 127 /1980/

4. M. Menyhárd, On the detection of small inclusions by AES, in Proc. ECOSS 3 1388 /Cannes, 1980/

CORRECTION FOR X-RAY ABSORPTION IN THIN FILM MICROANALYSIS

I. Pozsgai

The absorption of X-rays in multicomponent thin films has to be taken into account when a measured characteristic line is selectively absorbed by one of the film components. The question has been theoretically treated by Philibert and Tixier[1] and this paper describes a further development of their work. Our investigations refer to self-supporting thin films with a mass thickness $/\rho D \leq 170 \mu g/cm^2/$ equal to or somewhat more than that of films transparent for electrons in a transmission electron microscope /TEM/ at 100 kV. The correction accounting for X-ray absorption requires the knowledge of the chemical composition and the mass thickness of the analyzed "point", both are provided by our quantitative method of analysis[2-5]. The measured X-ray intensities from an n-component thin film can be written as follows:

$$I_i = k_i c_i \rho D f_i \qquad /i = 1,2,\ldots,n/ \qquad (1)$$

where c_i - concentration of the component "i"

ρD - local mass thickness of the analyzed "point"

k_i - $I_{i(standard)}/\rho D_{i(standard)}$

f_i - factors accounting for the X-ray absorption in the specimen

$$f_i = \frac{\int_0^{\rho D} \varphi/\rho z, \rho D/ \exp\left[-/\mu/\rho/_i \rho z \operatorname{cosec}/\theta/\right] d/\rho z/}{\int_0^{\rho D} \varphi/\rho z, \rho D/ \, d \, /\rho z/} \qquad (2)$$

If the depth distribution function of the X-ray generation for thin films $/\varphi/\rho z, \rho D/$ / is constant, f_i can be expressed in the following way:

$$f_i = 1 - (\mu/\rho)_i \cdot \operatorname{cosec}(\theta) . \rho D/2 \qquad (3)$$

where $(\mu/\rho)_i$ - mass absorption coefficient of the specimen for the measured line of the i-th component

θ - take-off angle of the X-rays

The mass absorption coefficient of the specimen can be expressed[6]:

$$(\mu/\rho)_i = \sum_j c_j (\mu/\rho)_i^j \qquad (4)$$

where $(\mu/\rho)_i^j$ - mass absorption coefficient of the component "j" for the measured line of the component "i".

In our iterative approach to account for the X-ray absorption the values ρD and c_i can be calculated from the X-ray intensities and the integrated electron transmission which are measured both on the specimen and on standards[2-5]. The first approximation of ρD and c_i are obtained assuming $f_i = 1$. In the next step f_i can be determined from eqs. (3) and (4) inserting the first approximation of ρD and c_i. Then substituting for f_i in eq. (1) a further refinement of ρD and c_i becomes possible. The efficiency of such a correction procedure is demonstrated on a three-component layer structure Al-Ni-Cu /Table 1/. The analysis was carried out at 100 kV in a TEM of the type JEOL 100 U.

Table 1. Results of the analysis of an Al-Ni-Cu film

	ρD [$\mu g/cm^2$]	c_{Al} [%]	c_{Ni} [%]	c_{Cu} [%]	Σc_i [%]
Without correction	143.6±8.4	17.6±6.2	34.7±4.4	38.5±4.5	90.8±15.1
With correction	148.5±5.0	27.5±1.5	33.5±1.0	37.2±1.5	98.2±4.0

It can be seen from Table 1. that the concentration of Al due to the correction for the AlK_α absorption has changed from 17.6% to 27.5%. At the same time the sum of the concentrations increased from 90.8% to 98.2% thus proving the efficiency of the correction procedure.

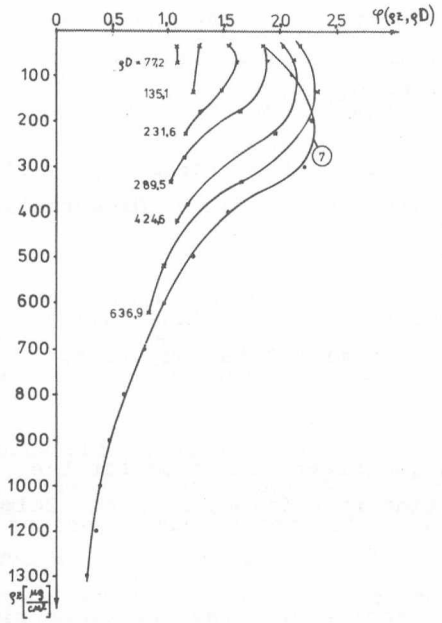

Fig. 1. Depth distribution function for the AuM_{α} line generation in thin Au films measured at 20 kV. /Curve 7 taken from[8] refers to a bulk specimen./

Appendix

When deriving eq. (3) the $\varphi/\rho z,\rho D/$ function was assumed to be constant for mass thicknesses up to 170 $\mu g/cm^2$. We have studied this function experimentally for thin Au films at 20 kV /Fig. 1/ using a Bi tracer of the mass thickness 16.9 $\mu g/cm^2$. In contrast to the bulk specimen the depth distribution function of the X-ray generation depends also on the total film thickness. The constancy of $\varphi/\rho z,\rho D/$ up to ρD = 135.1 $\mu g/cm^2$ at 20 kV suggests its constancy up to 500 $\mu g/cm^2$ at 100 kV, if the energy dependence of the beam broadening is taken into consideration[7].

1. J. Philibert and R. Tixier, Electron probe microanalysis of transmission electron microscope specimens, Physical Aspects of Electron Microbeam Analysis /B.M. Siegel, D.R. Beaman, eds./ pp. 333-354. Wiley, N.Y. 1975.

2. I. Pozsgai and N.P. Ilyin, Quantitative X-ray analysis of thin samples in TEM, Proc. 9. Int. Conf. on Electron Microscopy, Toronto, 1, pp. 500-501, 1979.

3. I. Pozsgai, A quantitative method for the microanalysis of thin samples in the electron microscope, Ph. D. Dissertation, Moscow, 1979.

4. N.P. Ilyin and I. Pozsgai, Quantitative microanalysis of thin samples in the EMMA, Mikrochimica Acta, Suppl. 8, pp. 213-228, 1979.

5. N.P. Ilyin and I. Pozsgai, A quantitative method for the microanalysis of self-supporting thin films, J. Anal. Chimii, 34, pp. 1703-1712, 1979.

6. E.P. Bertin, Principles and Practice of X-ray Spectrometric Analysis, p. 54. Plenum Press, N.Y. 1970.

7. J.I. Goldstein, J.L. Costley, G.W. Lorimer and S.J.B. Reed, Quantitative X-ray analysis in the electron microscope, Scanning Electron Microscopy, Vol. 1. pp. 315-324, Chicago, Illinois, USA, 1977.

8. R. Castaing and J. Deschampes, On the physical basis of localized /ponctuelle/ analysis by X-ray spectrography, J. Radium, 16, p. 304, 1955.

CHANGES IN THE GRAIN BOUNDARY STRUCTURE OF TUNGSTEN WIRES DURING HEAT-TREATMENT

G. Radnóczi

The grain boundary /GB/ structure of heavily deformed tungsten wires has been studied in the as-received state and after heat-treatments lasting 15 mins in the temperature interval 600-1800 K. Recently some results were published on similar topics but on other materials[1,2].

The most important feature of W wires drawn to ϕ /0.2-0.3/ mm is their large deformation causing the formation of a fibre structure with an average fibre diameter of 0.1-0.2 μm. The fibres have moderate dislocation densities in their bulk and narrow boundaries showing a complicated deformation contrast /Fig. 1/. Especially in thinner wires /ϕ = 0.2 mm/ the misorientation around the common /110/ direction is quite large[3], thus the fibre boundaries can be accepted as large angle GB-s. According to their contrast they accomodate large stresses. As a consequence thickness contours never occur on the images of these boundaries.

According to the type of strain contrast we may propose that it originates from dislocations and/or small inclusions. The deformation contrast can be regained by torsion, carried out after heat-treatment[4] this giving an experimental evidence of its dislocation origin, but small inclusions of the oxide type can also be expected[5].

Dislocation strain contrast on the GB-s originates from absorbed lattice dislocations which came to the GB in different slip planes /systems/ and form a narrow but unpenetrable barrier for slip. The elongated inclusions in doped wires may also contribute to the stopping power of GB-s but may cause the formation of new boundaries by accumulating dislocations on themselves.

This stressed state of fibre boundaries changes upon heat-treatment only above 850 K where an ordering process begins.

Arbitrarily choosing the occurence of thickness contours on the images as a sign of ordering of the GB structure, it can be concluded that at 1100 K about 80% of the GB-s is ordered. The appearance of thickness contours as a criterion of structural ordering is rather subjective, but it has a physical background namely that the movement of GB-s can be observed after thickness contours have appeared on them. In situ experiments resulted in 1050 K as the temperature of this stress relaxation. This is in good agreement with the 1100 K observed on samples heat--treated in the wire form.

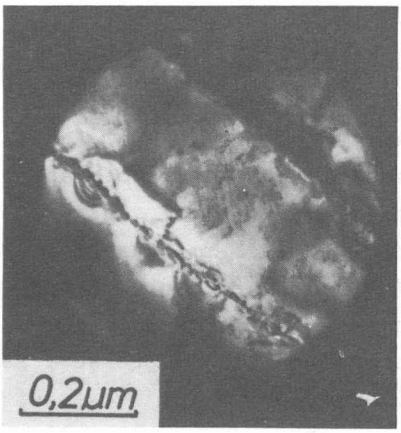

Fig. 1. Strain contrast of GB-s in the as-received state of wires

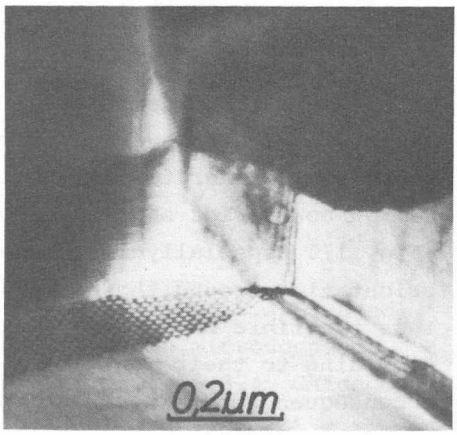

Fig. 2. GB dislocations and networks in wires heat--treated at 1500 K

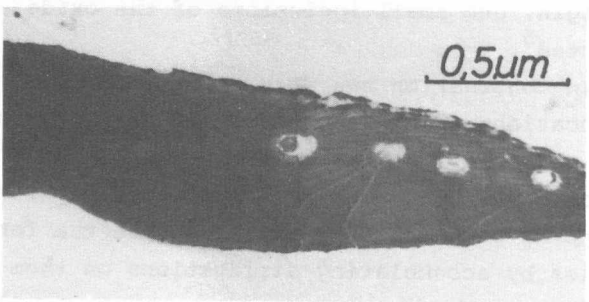

Fig. 3. GB dislocations showing signs of movements and interaction with inclusions

Heat-treatments at higher temperatures /T 1700 K/ cause the formation of GB dislocations in GB-s. At temperatures where the disintegration of the fibre structure is going on intensively /above 1800 K/ the most GB-s show periodic arrays of one or more systems of GB dislocations /Fig. 2/. There are evidences of movement of GB dislocations during GB movements /Fig. 3/.

Dislocations lying in the GB surface can be considered as steps. Tangential movement of these steps results in a movement of the GB in the direction of its normal. In the interaction between GB-s and second phase inclusions /e.g. potassium bubbles/ the GB dislocations also have a part to play. From Fig. 3 we can see, that during their movement the GB dislocations do not intersect these inclusions but overcome them by a clim mechanism.

Summarizing we can conclude that GB structures and their changes effect the structure changes by influencing the mobility of GB-s. The GB-s become mobile as a result of a GB stress relaxation process above 1050 K. We may propose also that this process contributes to the stage IV of recovery of electrical resistivity[6] and it may effect the mechanical properties for example the fracture mechanism and the creep properties of wires, as well.

1. A.R. Jones, P.R. Howell and B. Ralph, Changes in grain boundary structure during the initial stages of recrystallization, Phil. Mag. 35 603-611 /1977/

2. R.A. Varin, Spreading of extrinsic grain boundary dislocations in austenitic steel, Phis. stat. sol. /a/ 52 347-356 /1979/

3. Á. Barna, I. Gaál, O. Geszti-Herkner, G. Radnóczi and L. Uray, The fibre structure of K-Si-Al doped tungsten wires, High Temperatures-High Pressures 10 197-205 /1978/

4. Á. Szőkefalvi-Nagy, G. Radnóczi, A. Kele and I. Gaál, The structure of torsion-deformed tungsten wires, In Proc. of 1st Rls. Int. Symp. on Metallurgy and Mat. Sci. 1980. Ed. by N. Hansen, A.R. Jones, T. Leffers, p. 269-274.

5. G. Radnóczi, On the role of second phases in the recrystallization of tungsten wires, in Proc. of 7th European Congress on Electron Microscopy, The Hague, 1980. Vol. 1 196-197

6. Á. Szőkefalvi-Nagy, G. Radnóczi, L. Lipták, J. Major and I. Gaál, Grain boundaries and flow stress in tungsten, to be published in Proc. of the 10th Plansee Seminar.

MEASUREMENT OF EBIC CONTRAST AND RESOLUTION OF DISLOCATIONS IN Si

A.L. Tóth

As the crystal defects affect the quality of semiconductor devices the analysis of their structural and electrical nature is considered with increasing interest. The electrical activity of single defects can be investigated using the electron beam induced conductivity /EBIC/ mode of the scanning electron microscope.

The experimental setup of the SEM-EBIC used for imaging localized defects is such as to allow the energetic /1-40 keV/ electron beam to penetrate through the thin Schottky barrier /or shallow p-n junction/ and to generate electron-hole pairs in the semiconductor. These carriers are separated and collected by the built-in field and can be displayed as an EBIC image of the SEM.

The electrically active defects appear as dark spots or lines due to the enhanced recombination. Several studies have been made by this technique monitoring precipitates, dislocations, stacking faults and inpurity striations. However, these studies were mostly qualitative ones. This paper describes quantitative EBIC contrast and resolution measurements that can be compared with predictions of computer simulations of Donolato[1].

Schottky barriers were made by evaporating 200 nm Al onto a p-type Si substrate /200 ohm.cm; 10^3-10^4 dislocation/cm^2 obtained from etch-pit measurements/. The diodes of 200 μm diameter have been cut, assembled and gold wired, then measured in a JSM-35 type SEM. The EBIC signal was fed into a Keithley 427 current amplifier, then recorded in the data memory of an ORTEC EEDS-II analyser system, where digital line scans were obtained.

Minority carrier diffusion length in the material was determined by plotting the collection efficiency $\underline{e}$ of the barrier /measured on a dislocation free area/ as a function of the beam

energy E_o, as proposed by Wu and Wittry[2]. Comparing our measurements with their calculated curves, the minority carrier diffusion length was found to be L = 5 μm /Fig. 1/.

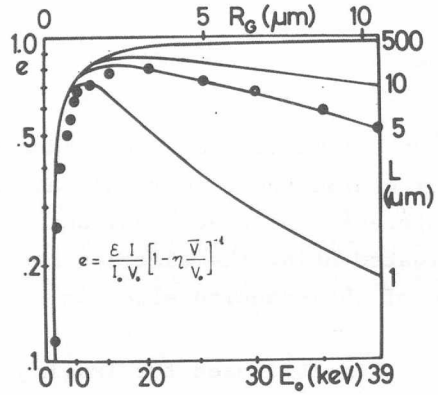

Fig. 1. EBIC collection efficiency e as a function of the beam energy E_o for Al-Si/p/ Schottky barrier diodes

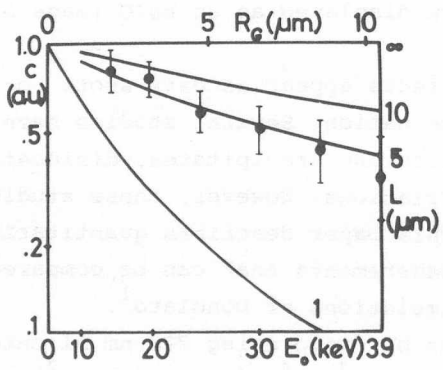

Fig. 2.a.

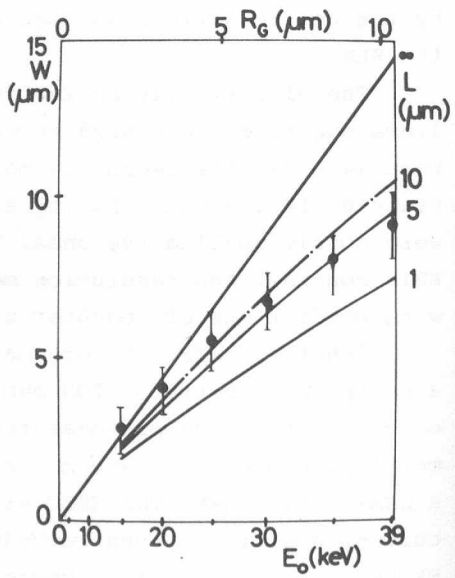

Fig. 2.b.

Fig. 2. EBIC dislocation resolution /a/ and contrast /b/ as a function of the beam energy E_o

The contrast and resolution /FWHM/ values were obtained from digital line scan measurements with different values of E_o across the dislocations perpendicular to the surface. A good agreement was found between the measured points and the computer simulated curves for a diffusion length of L = 5 μm as can be seen from Fig. 2. Further measurements on materials having different L values are in progress.

1. C. Donolato, Contrast and resolution of SEM charge collection images of dislocation, Appl. Phys. Lett. 34 80 /1979/

2. C.J. Wu and D.B. Wittry, Investigation of minority carrier diffusion lengths by electron bombardment of Schottky barriers, J. Appl. Phys. 49 2827 /1978/

ENERGY DISPERSIVE X-RAY MICROANALYSIS /EDS/ OF PHOSPHO-SILICATE GLASSES /PSG/

A.L. Tóth, J.É. Puskás[+]

Controlled deposition of SiO_2 on silicon wafers is a basic procedure of IC production. The oxide acts as a mask or protective or insulating layer. The addition of P modifies the properties of the passivation layer /which can be used as a diffusion source, too/.

The maximum concentration of P is rather critical and its determination is important in the production process. The methods of rapid determination of P used in the industry /etch-rate and sheet-resistivity measurements/ are destructive, non-localised and require a calibration procedure.

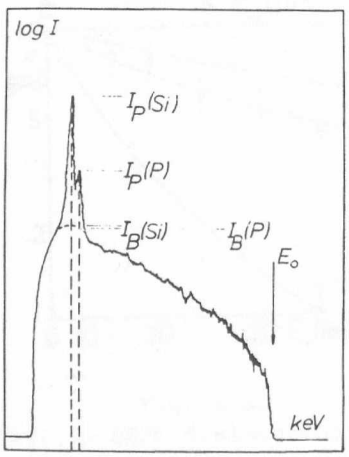

Fig. 1. EDS spectrum of PSG showing the intensities used in the P/Si calculation

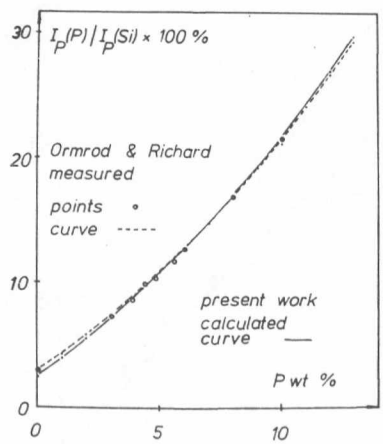

Fig. 2. Measured and calculated working curves for the same parameters

[+]Industrial Research Institute for Electronics /HIKI/

The EDS P/Si ratio method seems to be the best of these procedures taking into consideration the analytical volume, speed, accuracy and non-destructivity. Thin layers /100 nm/ of PSG can be analysed within minutes by calculating the ratio of P and Si peaks of the energy dispersive spectrum and using a working curve to obtain concentration values[1]. The advantage of the method is the unnecessity of standards and its insensitivity to the beam current drifts.

The working curve is measured by a wet chemical and microprobe analysis for a given beam energy and take-off angle. As the depth of the analysis is a function of the beam energy, too many curves would be needed for practical measurements. This problem can be solved by using the theory of correction procedures for the conventional electron probe microanalysis to calculate theoretical working curves[2].

From the definition of the relative intensities as they are used in EDS and WDS calculations the ratio of P and Si peak heights can be expressed:

$$\frac{I_p(P)}{I_p(Si)} = \left[\frac{I_p^{std}(Si) - I_B^{std}(Si)}{I_p^{std}(P) - I_B^{std}(P)}\right] \cdot \frac{k(P)}{k(Si)} \cdot \left[1 - \frac{I_B(Si)}{I_p(Si)}\right] +$$

$$+ \frac{I_B(P)}{I_p(Si)} = A \cdot \frac{B}{C}(1-D) + E$$

The term A, that is the ratio of net intensities from the pure elements can be evaluated by a program developed for no-standard EDS using MAGIC-IV expressions[3]. A is a function of the beam energy E_o and the instrument parameters. The relative intensities B and C are calculated using an inverse ZAF type program /FRAME/[4] as a function of E_o, the X-ray take-off angle and the concentrations. The relative background values D and E are measured values. The obtained working curves are then used as quadratic polynoms. The input data are the P/Si intensity ratio and E_o, the time of calculation is less than 10 s. Furthermore

the whole analysis /collection, readout and correction/ can be executed under computer control. Comparing the results of analyses measured on a large number of PSG samples using different techniques it can be seen that the accuracy of the P/Si method is good, while its precision /and speed/ is superior.

Using our new analytical technique it became possible to verify a proportional relationship between the PH_3/SiH_4 ratio and the P concentration of the deposited PSG.

1. S.E. Ormrod and B.P. Richards, Measurement and interpretation of phosphorus concentration in phosphosilicate glass passivation layers, Microelectronics, 8 /3/, 5 /1977/

2. A.L. Tóth and A.É. Puskás, Energy dispersive X-ray microanalysis of phosphosilicate glasses /PSG/, Acta Phys. Hung. 49 133 /1980/

3. J.W. Colby, Quantitative microprobe analysis of thin insulating films, Adv. in X-ray Anal. 11 287 /1968/

4. K.F.J. Heinrich, R.L. Miklebost, H. Yakowitz and S.D. Rasberry, A simple correction procedure for quantitative electron probe microanalysis, NBS Tech. Note 719. Washington D.C. /1972/

ON THE FAILURE MECHANISM OF NiCr THIN FILM RESISTORS AT DAMP HEAT STEADY STATE TESTS

L. Tóth, Á. Barna, P.B. Barna, J. Szatmári[+]

NiCr thin film resistors deposited onto ceramic substrates should satisfy not only the requirements related to their electrical characteristics /rated resistance, TCR, etc./ but also a number of environmental tests. The resistor should not change its resistance by more than 1% when it is kept in an environment of 93% relative humidity at 40°C and is loaded by a low dc current for 21 days. In the practice many resistors change their resistance by a much greater amount, moreover some of them are damaged due to the damp heat steady state test /Fig. 1/. Based on the investigation of the failured resistors deposited on different ceramic substrates and being of different resistance values the following failure mechanism is assumed. The failure is due to an electrolytic process produced by the ions dissolved from the ceramic substrate by the voltage between the neighbouring resistor strips. This hypothesis is supported by a complex range of experiments including four steps:

a/ Boiling of different kinds of ceramic substrates in clean distilled water.

b/ Measurement of the electrical conductivity of their solution in the function of time. /This is characteristic for the total amount of the dissolved ions./

c/ Electron probe microanalysis of dried droplets of the solutions /Fig. 2/.

d/ Modelling of the electrolysis of NiCr layers using the ceramic solutions as electrolytes.

+ REMIX Manufacturing Co. Electronic Components,

It must be emphasized that the analysis of the droplets was carried out in a transmission electron microscope completed with a wave-length dispersive X-ray spectrometer this being the only way to separate the droplet material capable of creating an electrolyte from the crystalline ceramic grains.

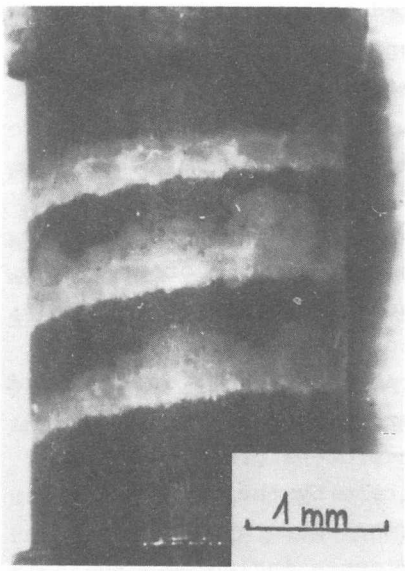

Fig. 1. Optical micrograph of a failured resistor

Fig. 2. Electron micrograph of a dried droplet of the ceramic solution

Basing upon our investigations we can conclude that:

1. the electrical conductivity connected with the ions dissolved from the ceramics correlates well with the failure frequency of the resistors. The boiling and conductometry may well be used as a method for the special qualification of ceramics,
2. the dissolved material forming an amorphous gel in the dried droplet does not reflect the original

ceramic composition, although it is not enriched in alkalines either,

3. NiCr thin films can be well electrolysed with the solutions of the ceramics. At several volts the current is about proportional to the measured conductivity of the solutions.

The results of our investigations have proved the supposed failure mechanism to be valid. The only solution of the problem could be a fully waterproof coating of the NiCr resistors.

DIVISION OF OPTICS AND ELECTRONICS

DIVISION OF OPTICS AND ELECTRONICS

J. Schanda

The Division of Optics and Electronics deals with two complementary fields of research. Most of the information reaching us is transmitted by the eye. Therefore for human information gathering the proper illumination of the environment is of utmost importance. The purpose of the work carried out in the Division is to find the ways and means for characterizing optical radiation reaching the eye in an objective way that corresponds well to the subjective psychophysical response of the human being. The research work done in the Division deals just with this objective measurement, data collection and information processing.

The mean features of our investigations are:

1. Characterization of light sources

Light sources were usually characterized by their efficacy, colour temperature and more recently colour rendering properties. Basic colorimetric work carried out partly in the Institute, partly in other laboratories throughout the world showed that proper characterization of colour had to be modernized. In this respect the CIE XYZ system has been surpassed by CIELAB and CIELUV systems. The colorimetric characterization of light sources does not take this into account. As a result of recent work carried out in the Institute two new methods were developed for describing colorimetric properties of light sources. One dealing with the colour rendering of light sources based on the CIELAB colour space, the other one dealing with colour discrimination properties of light sources. In this respect first the concept of correlated colour temperature has to be reevaluated and it has been shown that a transition from the traditional

colour space to one of the more modern ones influences this concept considerably.

Further visual and mathematical modelling experiments are needed before final international recommendations can be made. We hope, however, that on the basis of this work a light source characterizing system can be worked out that enables a more efficient usage of lighting energy.

2. Development of light and radiation measuring techniques

Besides the above mentioned visual aspects of lighting the objective evaluation of optical radiation is of utmost importance. In this respect not only the visible radiation has to be measured but the near ultraviolet and near infrared radiation as well. Recent biological investigations have shown that the well-being of the human organism depends considerably on the available amount of radiation in these spectral bands. A family of photo-radiometers has been developed for measuring illuminance and irradiance in the above mentioned spectral regions. The instrument will be augmented with further measuring heads permitting the determination of spherical and cylindrical illuminance, colour temperature and daylight factor. The prototype developed at the Institute will be produced by a Hungarian electronic factory.

For characterizing the spatial distribution of light sources and determining the total luminous flux of such sources different instruments have been developed during the past years. A multipurpose microporcessor controlled goniophotometer has been set up in the Institute enabling not only the measurement of the photometric characteristics of light sources, but also to determine the spatial distribution of colorimetric characteristics. For determining the total luminous flux under industrial circumstances a fully automated luminous flux measuring instrument was built for the Hungarian Lamp Factory TUNGSRAM. This microprocessor controlled instrument determines electrical and photometric data of light sources with high speed, without any human participation in the actual measurement.

Total characterization of the illuminated environment is possible only if the material characteristics of light reflecting surfaces are determined as well. For this purpose a prototype of a gloss measuring instrument has been built and a research instrument for determining light reflection indicatrices is under development.

3. Psychological characteristics of light

Besides the characterization of large light sources the importance of alpha-numerical displays in man-machine communication increases. Displays using light emitting diodes gain on importance in these fields. A psychological question is the visibility and readability of such displays. A number of investigations carried out throughout the world showed that the brightness of highly saturated colours differs from the luminance measured using the CIE photometric system. We showed - using direct visual scaling experiments - that this brightness to luminance discrepancy reflects itself in the readability of numeric displays, but the optimum of light colour for readability differs from that of brightness. Although red lights are brighter than yellow ones for equal luminance, experiments have shown that readability is best in the yellow-orange spectral region, where a compromise is found between the brightness effects and chromatic aberration effects of the human eye. Green displays showed the lowest readability. Also the colorimetric characterization of the displays needs some revision. In the deep red part of the spectrum an evaluation according to the standard colorimetric system shows discrepancies compared with the visual observation. We proposed the use of an alternative colorimetric system developed for visual research, as this gives better congruence with the visual data.

4. Data collecting and evaluating systems

All the above measurements - and a number of further problems raised in the Institute - require the evaluation of

large numbers of experimental results. Therefore data collecting and evaluating systems were worked out. First generations of such equipment used off-line techniques but recent developments were built using microprocessors. The light distribution measuring goniophotometer and the total luminous flux measuring instruments were mentioned already as examples for these techniques. Further electronic work was put into the measurement of very low currents and the development of special equipment for measuring the electrical characteristics of light sources.

PHOTO-RADIOMETER WITH MULTIPURPOSE DETECTORS

R. Brósz, G. Czibula, S. Ferenczi, J. Lánc

In recent years the application of optical energy in different branches of surgery, agriculture, photochemistry, etc. gained importance because of their accuracy and good repeatability.

A radiometer with a number of detectors was developed at our Institute. It consists of a single central unit and changeable measuring heads, for the determination of the intensity or the distribution of radiation in different spectral regions.

In designing the instrument the following starting points were taken into consideration:

1. Using Si detectors /in UV spectrum, too/
2. Easy manufacturing and high accuracy $V(\lambda)$ fitting
3. Single central unit for the different detectors.

The correctly built, filtered, etc. detectors realize the following optical-electrical transformation[1]:

$$K \int_c^\infty E_{e\lambda} \, B(\lambda) \, d\lambda = U \pm \Delta U$$

or in the measurement of distribution temperature (blue-red ratio) or spatial homogeneity:

$$\frac{K1 \int_c^\infty E_{e\lambda} \, B_1(\lambda) \, d\lambda}{K2 \int_c^\infty E_{e\lambda} \, B_2(\lambda) \, d\lambda} = \frac{U_1 \pm \Delta U_1}{U_2 \pm \Delta U_2}$$

where $E_{e\lambda}$ is the spectral irradiance distribution;
$B(\lambda)$ is a biological action spectrum;
K is a proportionality factor and
U is the output voltage
ΔU its error voltage.

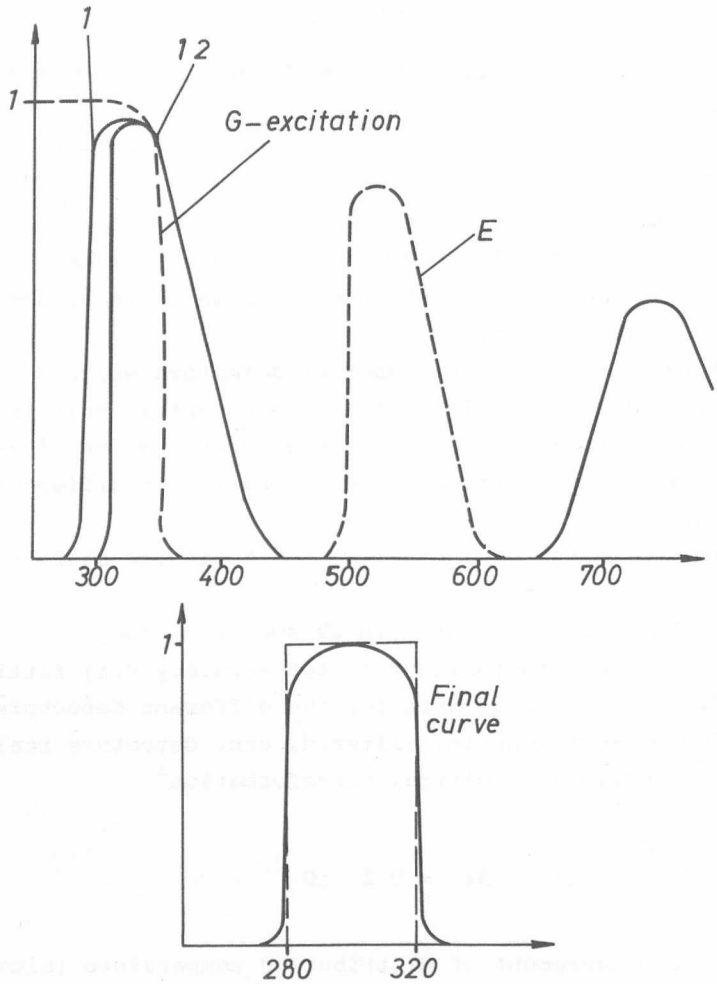

Fig. 1.

The optical-electrical transformation is executed by Si-cells in the UV A, B and C spectrum ranges. The wavelength region can be set on the head. In the optical part of the instrument a wavelength conversion from the UV region to the visible range takes place, therefore a normal silicon photovoltaic cell could be used as a detector. This wavelength conversion is performed by photoluminescent materials. Thus e.g. the UV B head (280-320 nm) functions as follows:

The measured radiation enters the head through a diffuser, which ensures the proportional distribution of the radiation onto two photodetectors. In front of the detectors there are two UV-glass filter combinations. One of them filters out the short-wavelength UV radiation below 280 nm, the other one filters below 320 nm, but the transmission characteristics of the filters are very similar in the longer wavelength region /Fig. 1/.

Behind the UV-glass filters there is a wavelength converter. This is a transparent fluorescent layer, which emits visible radiation, when it is excited. The fluorescent radiation can be separated from the direct visible radiation with further filtering.

The intensity of the fluorescent radiation in each detector channel is proportional to the incident UV radiation. The detectors convert the optical signal to electric ones. Then the photocurrent is amplified. If the sensitivity of the two detector channels is equal, the electrical difference of the signals is proportional to the intensity of the UV-B radiation.

The instrument measures the intensity of the UV radiation in three ranges:

200 $\mu W/cm^2$
2 mW/cm^2
20 mW/cm^2

Repeatability of the measurement is approximately ±1%. The accuracy of the measurement depends mainly on the accuracy of the calibration.

The equipment is often used as an illuminance meter. To realize $V(\lambda)$ fitting the spectral responsivity of the applied Si cell $[s_o(\lambda)]$ must be known. This is measured by a semi-automatic system, using a CARY 17 instrument.

A full filtering is applied, where the thickness of the filters is calculated by a computer programme that minimalizes the following equation[2]:

$$F(h_1, h_2 \ldots h_4) = \int_{380}^{780} \left[\frac{\bar{t}(\lambda)}{\int_{380}^{780} \bar{t}(\lambda)\,d\lambda} - \frac{s(\lambda)}{\int_{380}^{780} s(\lambda)\,d\lambda} \right]^2 d\lambda$$

where $\bar{t}(\lambda) = \bar{x}_{1,2}(\lambda), \bar{y}(\lambda)$ or $\bar{z}(\lambda)$
and $s(\lambda)$ = filtered spectral responsivity of the detector.

The first term in the square brackets is the CIE tristimulus function normalized for its area. The second term is the actual corrected responsivity function again normalized to its area. This depends on the thicknesses of the filters. Fig. 2 shows the realized and the ideal curves.

The equipment, as an illuminance meter, has four ranges:

20.00	lux	full scale
200.0	lux	" "
2000	lux	" "
20000	lux	" "

Accuracy: $\pm 0.1\% \pm 1$ digit
Accuracy of the temperature stability of the head: $\pm 0.2^{\circ}C$.

In our instrument different measuring heads can be connected to the same analogue and digital bus. So the connection of a given head determines the necessary gain, the displayed dimension and also initiates an automatic zeroing /if the measuring surface of the head is in the dark/.

For measuring the spatial homogeneity or the blue-red ratio we must use the central unit with two channels /numerator--denominator/, but the A/D converter of the measuring and zeroing cycle of the numerator and denominator is the same in the time multiplex mode.

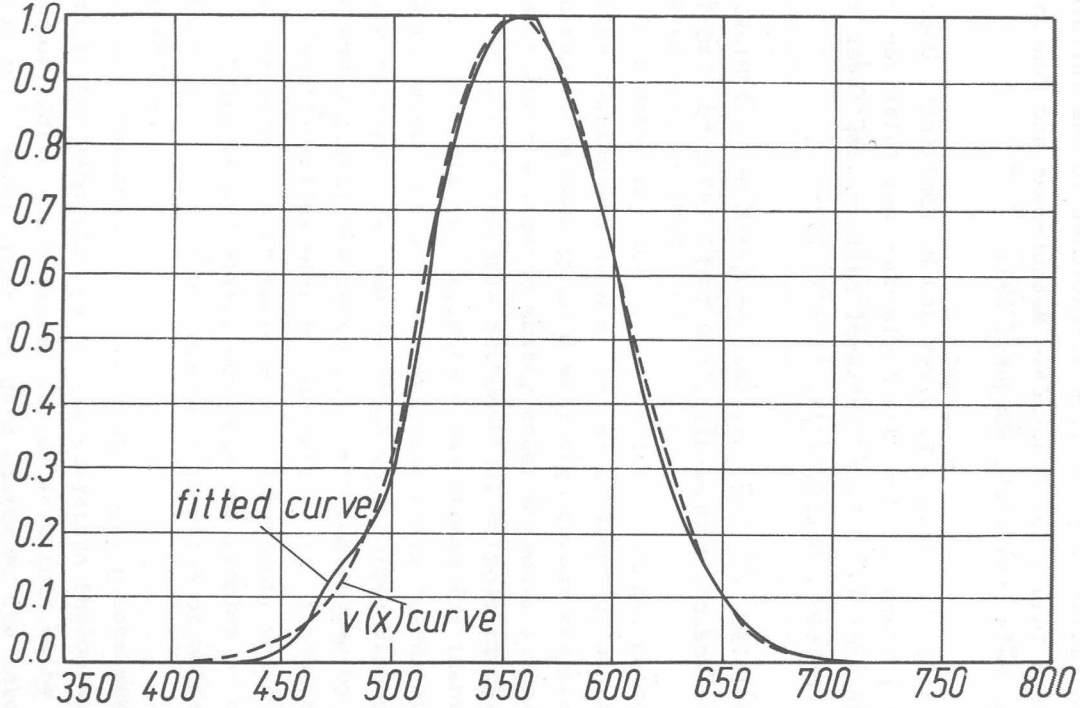
1.0
0.9
0.8
0.7
0.6
0.5
0.4
0.3
0.2
0.1
0.0
fitted curve
v(x) curve
350
400
450
500
550
600
650
700
750
800

Fig. 2.

1. R. Brósz, I. Lánc, S. Ferenczi and M. Vanyek, New approach to measure radiation power from ultraviolet to the infrared ranges, 16th Industrial Electronic Measurement and Control Symposium, Balatonszéplak, Hungary, 1979.

2. G. Geutler, J. Krochmann, Z. Özver and W. Röhrlicht, Über die Kennzeichnung der Güte des Angleiches der relativen spektralen Empfindlichkeit lichtempfindlicher Empfänger an die V(λ)-Funktion, Optik, 43/5, 453-69 /1975/.

3. D.M. Himmelblau, Applied nonlinear programming, 4.2 Flexible polyhedron search. McGraw-Hill, New York, 1972. pp. 148-57.

COLOUR IDENTIFICATION BY COLOUR PRINTS

M. Dányi

Colour constancy of real objects, when changing illuminant chromaticity, is well known. In colorimetrics chromatic adaptation transformations should take care of this effect[1], but no transformation equation describes the effect of large changes of illuminant chromaticity well enough, to be used, if no ambiguity is permitted.

Colour constancy has to be considered in all colour reproduction techniques, as e.g. in aerial mapping, where the picture taking is made under a very high colour temperature illuminant and the viewing mostly under standard illuminant A. Due to the lack of reliable mathematical methods of chromatic adaptation corrections a technique was chosen for identifying colours in manned space flight missions using colour atlases. Satellite pictures are usually taken with colour dissector cameras and pictures are restored in the laboratory by using colour identifications made by the astronauts. If colour atlases are used both in space and in laboratory using the same colour photography primaries, not only the problem of chromatic adaptation is eliminated but also the question of metamerism is much reduced.

For this reason a high number of colour prints were prepared in the laboratories of the Hungarian Photographic Film Factory Forte and measured in our Institute using a high precision colorimeter under standard source A. The coloured samples were arranged into CIELAB chroma-lightness charts[2] for different metric hue angles.

Fig. 1. shows the gamut area reproducible with these colour prints in a CIE /x,y/-diagram for different lightness levels. Here the Mac Adam optimal colour gamuts have also been reproduced[3].

These are maximal gamut areas which can be reproduced at a given lightness level. As seen the practically achivable gamut is much smaller then the theoretical one, nevertheless it is high enough to serve as a good basis for all practical uses.

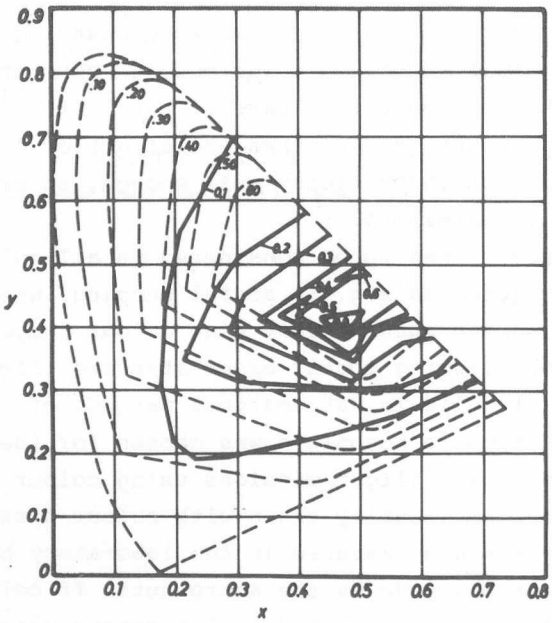

Fig. 1.

The colour atlas produced by ordering the colours according to their CIELAB C^{x}_{ab} chroma and L^{x}_{ab} lightness for the selected H^{o}_{ab} hue angles, a perceptually reasonably equidistant systematisation of the colour samples, it was easy to memorize the location of a colour in the atlas, so that if a given real object colour was seen the apropriate nearest sample in the atlas could be easily located and identified. In preparing the colour composition reproductions the colour of the selected object can then be set to the selected colour in the restoration process.

The colour atlas was produced by measuring the tristimulus values of over 500 colour samples from which 300 were used in preparing the atlas.

1. J. Schanda, to be published in Proc. Lux Europa, Granada,

2. CIE Publ. 15. Suppl. 2.

3. Mac Adam, D.L., Maximum visual efficiency of colored materials, JOSA, 25, 1935, 361 p.

GONIOPHOTOMETER

G. Eppeldauer, K. Kántor, J. Lánc

Efficacy of modern light sources has increased quite considerably during the past decades. However, a large portion of the produced light never reaches the target due to poor construction of the luminaires, low efficiency and improper light distribution. To improve this situation the spatial distribution of emitted light has to be determined by goniophotometric measurements. The total description of light distribution needs several hundred data per luminaire, calling for a properly automated measuring system. Lamps used in practice show small irregular fluctuations of their light output, which we tried to eliminate from the measurement results by using a ratioing technique. Further demand is to record not only the photometric, but also the electrical data of the lamp, i.e. voltage, current and power.

The goniometer

Instead of the known solutions[1,2,3,4] we have chosen as measuring principle the so called two-axis system, where the luminaire is rotated both around a horizontal and a vertical axis. As a rotation around a horizontal axis changes the position in Earth gravitational field, such a rotation might introduce systematic errors; to eliminate these - and to cancel the influence of lamp instability a ratioing system has been used enableing to normalize all the measurements on the value determined in normal ground position.

The mechanical build-up of the instrument is seen in Fig. 1. The rotation around the vertical axis is realised by the help of a worm gear of 144 teeth. This way during one turn of the input driving shaft the light source turns 2.5^{o} around the vertical axis. The rotating mechanism of the horizontal axis can be adjusted manually and is mounted on the moving part of a

slide. The slide rests on a frame rotating around the vertical axis. With the help of the slide the optical centre of the lamps or luminaires to be measured can be brought into the vertical axis. The light of the horizontal axis above the frame is 1300 nm. The horizontal shaft has a diameter of 120 mm for fixing both the different light sources or luminaires and the secondary light detector holder.

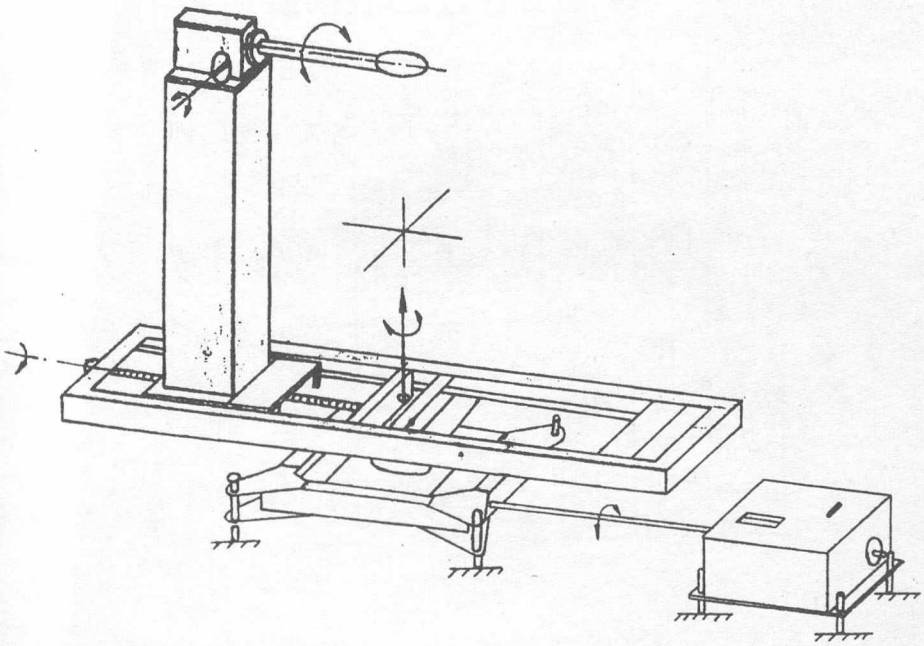

Fig. 1. The mechanical build-up of the goniophotometer

The control and measuring system

The block-scheme of the control and measuring system is shown in Fig. 2.

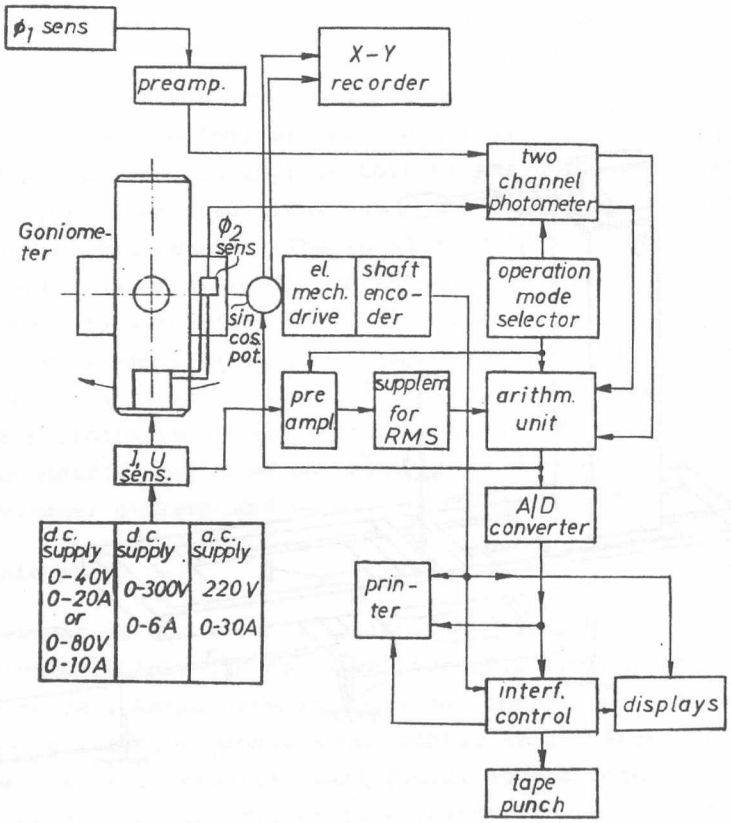

Fig. 2. The block-scheme of the control and measuring system

The light source can be fed from home made d.c. and a.c. regulated supplies up to 22 A and 300 V. The continuously moving

goniometer mechanism is driven by the help of an electro-mechanical driving unit. This unit contains an a.c. driving motor, a gear box with 2-speed motoric and a manual driving possibility together with two adjustable disks for setting the start and end position of the rotation. It also contains a sine/cosine potentiometer to produce registration in polar coordinates. A built-in shaft encoder ensures the absolute measurement of the anglar position during the rotation.

The applied measuring system is suitable to measure the electrical true RMS characteristics of light sources and also the corrected light distributions. The latter is performed with a double beam arrangement, where two detectors, both corrected to the visibility function are used. ϕ 1 is the main light detector, ϕ 2 is the secondary one. The double beam arrangement eliminated the errors originating from the changing position and the fluctuations of the light source.

The response time of the measurement and that of the data registration is resonably short to win correctly all the data during the continuous rotation of the goniometer mechanism.

The RMS measurements and the ratio type light distribution measurements are performed by the help of a hybrid arithmetric unit. This unit works in multiplying operation mode during the RMS measurements and measures the ratio of the signals of light detector ϕ 1 and ϕ 2 in the light distribution measuring mode according to the command of the operation mode selector.

After the RMS measurements the corrected goniometer light distribution measurement begins. This time the two channel photometer measures the short circuit currents of the light detectors[5] ϕ 1 and ϕ 2. ϕ 1 is followed by a preamplifier and ϕ 2 is in a thermostat with a built in preamplifier in order to eliminate the drifts caused by the heat of the light source. The photometer works in two operation modes. In the first mode by using only ϕ 1 it measures the illuminance from 4 lux fs. to 40 kilolux fs. with a resolution of 1 mlx to 10 lx, respectively. In the other mode also ϕ 2 is used and the calculated Cd/klm value can be set accurately in the meter. The light distribution measurement is accomplished in this operation mode.

The analogue output signals are converted to digital ones. The binary coded output signal of the analogue-to-digital converter is further converted to BCD and thereafter printed together with the BCD output code of the absolute shaft encoder. The start signal comes from the electromechanical drive unit at every full turn of the goniometer input driving shaft. This way the results are printed at each 2.5^{o} position. We use a common interface control unit for the strobed LED displays and the tape punch. The latter punches the results in standard ASC II code.

The sine/cosine potentiometer also receives the input signal of the analogue-to-digital converter. Its two output signals are connected to the X and Y inputs of a X-Y recorder. The light distribution is continuously registered during the forward rotation of the goniometer.

The patented instrument[6] was made for the bigest hungarian luminaire manufacturing company VBKM where it is successfully used for product control.

1. K.E. Fairbanks and A.R. Jaeger, A New concept photometer, J. of IES 2, 55 /1972/

2. J. Krochmann and P. Marx, Ein digitales Messgerät zur Ermittlung des Lichtstromes aus der Lichtverteilung, Lichttechn. 21, 92A /1969/

3. G.A. Horton, R.C. Speck, P.A. Zaphyr and R.E. Wendt, Automatic Photometer for Street Lighting Luminaires, Illum. Engng. Nov. 1958. 591-97

4. J.S. Franklin, Automated Universal Distribution Photometer, Illum. Engng. 53 Dec. 1958. 667-678.

5. G. Eppeldauer, J. Gráner, J. Lánc and K. Németh, Design problems of the photocurrent measurement of photovoltaic cells, MFKI Publications, O-16, 1975 p. 123-140.

6. G. Eppeldauer, J. Schanda, J. Lánc and K. Németh Hungarian Patent No. MA-2777

MEASUREMENT OF LOW PHOTOCURRENT USING PHOTOVOLTAIC CELLS

G. Eppeldauer, J. Lánc

In photometric and colorimetric work the most important practical photodetector is the Si-photovoltaic cell. Instrument performance is highly influenced by the proper choice of the input stage of the electronic circuits. Present paper summarizes the results of our investigations in this field.

DC methods

Before choosing a suitable operational amplifier and measuring circuit, the most important characteristics of the photovoltaic cells used have to be known. E.g. the shunt resistance of the cell depends on the ambient temperature significantly.

Mostly, the manufacturer's data sheets do not contain all the necessary values and characteristics of photovoltaic cells which are needed for proper and accurate design.

According to our measurements the value of the shunt resistance changes from 1 kohm to 100 Mohm. The temperature dependence of that is in the order of 10%/^{o}C.

The measured capacitance, which is parallel with the photovoltaic cell, may cause instabilities in the photocurrent measuring circuit. It can be compensated by an external capacitor coupled parallel to the feedback resistor.

There are totally different design aspects in the case of low or high internal resistance photovoltaic cells. When we measure with an old type silicon photovoltaic cell having low internal resistance, the amplification of the operational amplifier for the input error voltages is high.

If we do not use range change compensation the output zero voltage error originating from the change of the feedback resistor can be calculated. The input bias currents of the inverting and noninverting inputs cause voltage drops on the resultant resistance coupled to the two inputs.

As the feedback resistor may be changed by 4 to 7 orders of magnitude in a light-meter, the resultant resistance coupled to the inverting input can also change a few orders of magnitude.

The compensation of the errors caused by the previously mentioned range change can be achieved in different ways.

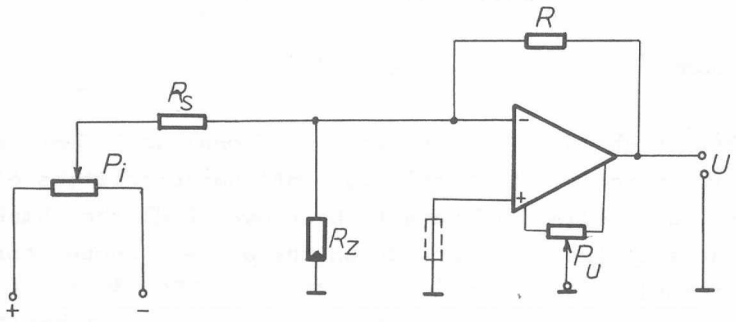

Fig. 1.

A generally usable solution for range change error elimination is the method of double zeroing. In this case after zeroing the offset voltage, the input bias current of the inverting input is also compensated while the photovoltaic cell is in the dark. This is shown in Fig. 1. If the temperature changes R_z has to be applied on the noninverting input or a thermostat has to be used for both the amplifier and the photovoltaic cell.

Using a silicon photovoltaic cell with a high shunt resistance better results can be obtained. In this case the amplification for the input error voltages is low. Consequently the main task here is to use such an operational amplifier which has a low input bias current. With electrometer type

-ultra low bias current operational amplifiers input bias current are 10^{-14} A. Using such amplifiers the dominant error originates from the drift and noise voltages if the photovoltaic cell has a shunt resistance less than 1000 MΩ. At present this value is significantly higher than the realized best values. With such amplifiers, a photocurrent sensitivity of theoretically 10^{-14} A can be achieved. When the shunt resistance of the photoelement is 100 MΩ the obtained sensitivity is 10^{-13} A.

AC methods

In several applications when the light is modulated the previously discussed d.c. errors can be eliminated by using usual a.c. measuring circuits.

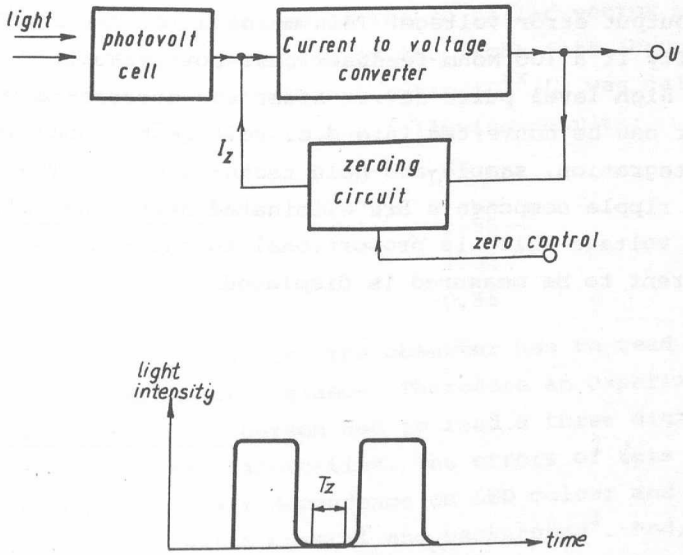

Fig. 2.

In most cases the d.c. error signals appear only in the output signals of the demodulators. The disadvantage is the restricted accuracy and resolution because of the errors originating from the demodulator.

A circuit built in our laboratory uses a light chopper or pulse operated light sources and ensures high accuracy and resolution at high sensitivity. The block diagram of the current to voltage converter and the time dependence of the photocurrent of the photovoltaic cell can be seen in Fig. 2.

The zeroing circuit, during the zeroing time T_Z, closes the zero control loop and regulates the output voltage U to zero. Between two T_Z intervals the zeroing circuit is in the hold state and produces a continuous compensating current I_Z.

The chopping frequency should be different from the line frequency or the harmonics of the latter in order not to have zero error in the measurement.

Using this method photometric instruments were built with $\sim$10 μV output error voltage. This means a 10^{-13} A photocurrent sensitivity if a 100 Mohm feedback resistor is applied.

The high level pulse series after the current-to-voltage converter can be converted into d.c. voltage by known methods /e.g. integration, sample-and-hold technics etc./. The unwanted ripple components are eliminated here. Thereafter the d.c. voltage which is proportional to the short circuit photocurrent to be measured is displayed.

VISIBILITY OF DIFFERENT COLOURED LED DISPLAYS

J. Schanda

Displays based on light emitting diodes LED's find widespread application in many types of electronic instruments. Due to technological reasons these displays are produced in red, yellow and green colour. The luminance attained by such displays is determined primarily by their technology and the evaluation of their performance is usually done by comparing their luminance, not taking into consideration the differences between luminance and visibility induced by the chromaticity of the display.

The CIE Technical Committee dealing with the visual aspects of light recommended the use of the so called vector brightness /L^{xx}/ taking the chromaticness of the light into account.

The brightness-to-luminance ratio (L^{xx}/L) was calculated for typical LED's and led to the following results:

	L^{xx}/L
Red	1.55
Yellow	1.08
Green	0.98

In practical situations the observer has to read the results of a display at a glance. Therefore an experiment was set up, where the test person had to read a three digit LED figure, flashing for a short time. The errors of this reading were recorded with their dependence on LED colour and contrast among lit numeral, unlit numeral and background[2]. Red, yellow and green LED displays were optically filtered and electrically biased to give approximately equal luminance and contrast values. The luminance of the filtered displays was set to 40 cd m^{-2} with a surrounding luminance of 20 cd m^{-2}.

Table 1 shows the optical data of these displays. Experiments were carried out on 51 people having normal colour vision, each performing 50 or 100 single tests with each colour. An arbitrary 3 digit numeral was lit for a short time /~50 ms/, and the number of wrong readings was counted. Figure 1 shows the experimental results in a triangular coordinate system. Every cross represents an average mistake rate of one person. Near to the green corner a cross means a lot of mistakes were made by reading the green numbers, but none by reading the red or yellow. A cross in the middle means an equal error rate for all the three colours.

Table 1. Optical data of filtered displays

Display colour	Red	Yellow	Green
Filters used	RG1/2mm	OG5/2mm+ +VG6/2mm	VG3/2mm
Average luminance of display /cd m^{-2}/	40.2	40.4	40.0
Percentual deviation from average luminance among numerals and within one display	±25%	±15%	±25%
Luminance of non-activated display segment /cd m^{-2}/	1.0	1.1	2
Luminance of non-active display surface /cd m^{-2}/	1.2	1.5	1.6

As a characteristic number of LED display readability, the probability that a typical observer reads the three digit displays with an error was adapted. This was called the "probability of errors". The distribution of observing an error of the flashing numbers produces a system of full occurrences, thus its distribution follows Bernoulli's law. Due to the large number of individual observations this can be substituted with a Gauss distribution.

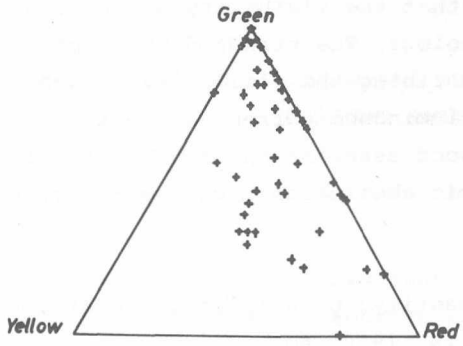

Fig. 1. Triangular coordinate system for depicting the error rates

Table 2. Relative frequency of errors and their standard deviations

	Red	Yellow	Green
$\bar{p}$	0.060	0.025	0.130
$\bar{\sigma}_{emp}$	0.057	0.033	0.127

Table 2 shows the numerical results achieved by using this technique of evaluation. Here $\bar{p}$ is the relative frequency of errors /number of errors divided by the number of experiments/:

$$\sigma = \frac{\sum_{i=1}^{M} (p_i - \bar{p})^2}{M-1} \; ; \; \bar{p} = \frac{1}{M} \sum_{i=1}^{M} p_i$$

is the standard deviation, where p_i is the relative frequency of errors for one person, M is the number of persons participating in the experiment.

Comparing the relative probability of an error reading with the brightness-to-luminance values referred to in the introduction, it can be seen that the 50% lower error reading of the red LED, compared to the green one, can be explained on the basis of the differences in their brightness-to-luminance ratio. The higher readability of the yellow display compared to the red one might be explained by chromatic aberration effects[3].

The experiments showed that the visibility of LED displays is highly dependent on LED colour. The standard photometric system is inadequate for describing the visibility of such displays, but brightness-to-luminance corrected "vector--brightness" seems to be a good description of LED visibility. For red LED displays chromatic aberration might be a further disturbing factor.

1. Light as a true visual quantity: principles of measurement, CIE Publ. 41 /TC-1.4/ Paris, 1978, 40

2. E.W. Pálmai, J. Schanda and G. Heine, Visibility of different coloured LED displays, Displays, Oct. /1980/ 123-127.

3. L.R. Ronchi, S.R. Stefanacci, R. Macii and M. Bassan, Luminance and brightness of heterochromatic test fields, Naz di Ottica /Florence-Arcetri, March, 1979/.

NEW DESCRIPTION OF COLOR DISCRIMINATION PROPERTIES OF LIGHT SOURCES

J. Schanda, G. Czibula

Many practical situations require a correct and easy color discrimination. Thus light sources should be evaluated according to a scale of color discriminating capability. However, no such internationally agreed scale exists.

Several authors proposed to use the gamut area of the eight CIE test colors measured in the CIE 1960 UCS-diagram for this purpose[1-7].

There are, however, both conceptual and practical problems with this: A color discrimination task is generally not one where among a large variety of object colors one seeks maximal difference, this would rather increase the "color-fullness" of the scene. The other is that the presently available uniform chromaticity scales are not equidistant enough for meaningful evaluations.[5]

Boyce and Simons[6,7] used the Farnsworth-Munsell 100 hue test for visual colour difference evaluation.

A new color discrimination index based on color differences between a "central color sample" and eight samples with slightly differing spectral reflectance factors was introduced recently by one of the authors.

Our basic assumption was that the color discrimination index should describe how well adjacent colors can be discriminated, thus color difference has to be calculated between colors differing only slightly. For this purpose the eight CIE test colors, as defined with their spectral reflectance factors 13.2 were used[9] as "central color samples" and around each of these eight variations were constructed by slightly increasing or decreasing the spectral reflectance factor of the samples by a given amount in given wavelength ranges.

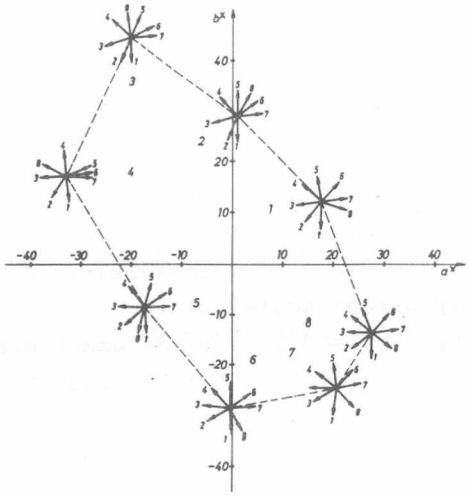

Fig. 1.

Fig. 1 shows the 8 CIE test samples and 8x8 varied samples for D_{65} illuminant in the a*, b* plane[8]. Color differences are calculated between each of the color points lying at the tips of the arrows and the centrally located test sample (ΔE_{ik}^*, where i refers to sample i and k to its variation) both illuminating the samples with illuminant D_{65} (as shown in Fig. 1) and the test illuminant: $\Delta E_{ik}^*(D_{65})$ and $\Delta E_{ik}^*(S)$. The special color discrimination index (sCDI); is constructed from the color differences and their standard deviations (σ_i):

$$sCDI_i = \frac{\sum_{k=1}^{8} \frac{\Delta E_{ik}^*(S)}{\Delta E_{ik}^*(D_{65})}}{8} - a\sigma_i$$

where a has been calculated to give optimal fit of the sCDI to the visual color dicrimination error scores of Boyce and Simons[7].

Experiments showed that using a value of a = 1.2 a good correlation with visual data could be obtained even for the "Grolux" lamp, whose gamut area is extremely high and the "Triband" lamp having a relatively large gamut area and a high color rendering index, but performing not too well in visual color discrimination tasks. Table 1 shows the correlation between the visual error scores of the Boyce and Simons experiment and the suggested CDI, gamut area and color rendering index, respectively.

Table 1.

	Cor. Coeff.
CDI	0.90
Gamut area	0.41
CRI	0.57

1. W.A. Thornton, Color-discrimination index, J. Opt. Soc. Amer, 62 191-194 /1972/

2. W.A. Thornton, The quality of white light, Lighting Design and Appl. 2/12 51-52 /1972/

3. H.H. Haft and W.A. Thornton, High performance fluorescent lamps, J. IES 2 29-35, /1972/

4. W.A. Thornton, Fluorescent lamps with high color-discrimination capability, J. IES 3 61-64, /1973/

5. M.B. Halstead, Colour rendering systems and their applications, Light and Lighting 69 244-247 /1976/

6. P.R. Boyce, Illuminance, lamp type and performance on a colour discrimination task, Ltg Res. and Technol. 8 195-199 /1976/

7. P.R. Boyce and R.H. Simons, Hue discrimination and light sources, Ltg Res. and Technol, 9 125-140 /1977/

8. J. Schanda, Ein neuer Farbdiskriminations-index, Licht Forschung 1/1 17-23 /1979/

9. CIE Publ. No. 13. 2 /TC-3.2/ 1974, Verfahren zur Messung u. Kennzeichnung der Farbwiedergabe-Eigenschaften von Lichtquellen /2. Ausgabe, Bur. Centr. CIE, Paris, France/

LIST OF PUBLICATIONS

1979.

M. Andrási, G. Forgács, A. Lőrinczy, The effect of potassium contamination of tungsten on filament-metallized devices. Phys. Stat. Sol. /a/ 51, 573 /1979/

W. Beyer, A. Barna, H. Wagner, Highly doped evaporated amorphous silicon by alkali implantation. Appl. Phys. Lett. 35, 539 /1979/

Á. Csanády, Á. Barna, P.B. Barna, The direct observation and investigation of the oxidation of aluminium in the transmission electron microscope. Oxid. Met. 13, 245 /1979/

Á. Barna, P.B. Barna, G. Radnóczi, F.M. Reicha, L. Tóth, Formation of aluminium thin films in the presence of oxygen and nickel. Phys. Stat. Sol. /a/ 55, 427 /1979/

M. Pasemann, Á. Barna, P. Werner, H.J. Hagel, Electron optical identification of precipitations in silicon semiconductor devices. Krist. und Tech. 14, 553 /1979/

L. Bartha, Gy. Gyarmati, B.A. Kiss, T. Németh, A. Salamon, T. Szalay, Complex studies on intermedier decomposition products of ammonium paratungstate. Acta Chim. Hung. 101, 127 /1979/

M. Farkas-Jahnke, P. Gács, Changes in structure of ZnS crystals due to mechanical stresses. Krist. und Tech. 14, 1475 /1979/

M. Gál, Temperature modulated photoluminescence of semiconductors, applied to GaP:N. J. Lumin. 18/19, 771 /1979/

M. Gál, B.C. Cavenett, P. Smith, New evidence for the two--electron $O^{=}$ state in GaP. Phys. Rev. Lett. 43, 1611 /1979/

T. Görög, E. Lendvay, Synthesis and crystal growth of $A^{III}B^{V}$ compounds from elements. Acta Phys. Hung. 47, 25 /1979/

R. Groh, T. Millner, L. Bartha, Einwirkung von Lithiummetall auf das Gefüge von oxidisch dotierten Wolframdrähte. Acta Chim. Hung. 100, 15 /1979/

P. Harmat, J. Major, A high-temperature dilatometer for thin wires. J. Phys. E.: Sci. Instrum. 12, 1067 /1979/

G. Hoffmann, A. Lőrinczy, M. Németh-Sallay, I.C. Szép, Room temperature transformations in Si_2O layers induced by chemical compounds. II. Thin Solid Films, 59, 319 /1979/

G. Hoffmann, L. Puskás, M. Lőrinc, A. Nagy, Determination of the phosphorus content of doped SiO_2 films by IR absorption and activation analysis. J. Phys. D: Appl. Phys., 12, 569 /1979/

G. Hoffmann, T. Veszprémi, A. Nagy, Properties of IR spectra of phosphorus doped SiO_2 films. Period. Polytech. Chemical Eng. 23, 175 /1979/

J. Kertész, Effective-field approach to transverse correlations in simple liquids. J. Phys. C: Solid State Phys. 12, 1985 /1979/

L. Kozma, Influence of photographic and photometric effects on spectrographic evaluation, II. Microdensitometer for spectrographic research and practice. Acta Chim. Hung. 102, 267 /1979/

L. Kozma, W.J. Huppmann, Experimental method for determining transport paths in liquid phase sintering. Int. J. Powder Metall. and Powder Technol. 15, 115 /1979/

L. Kertész, Cs. Lénárt, M. Kovács-Treer, DTA studies in the Al-Mg-Si alloys III. Crystal Lattice Defects 8, 99 /1979/

E. Lendvay, Crystal growth at the Research Institute for Technical Physics. Acta Phys. Hung. 47, 13 /1979/

I. Hornyák, E. Lendvay, Fluorescence and sensitization properties of linear polyphenyls. J. Lumin. 18/19, 444 /1979/

F. Hecks, A. Lőrinczy, J. Ponomarenko, Probleme bei der Entwicklung von Speicherbauelementen von Typ. FAMOS. Nachrichtentech, Elektron. 29, 248 /1979/

M. Menyhárd, Potassium on the fracture surface of tungsten wires studied by AES. Surf. and Interface Anal. 1, 175 /1979/

M. Menyhárd, Investigation of tungsten wires by AES. In: Proceedings of the surface analysis 1979 conference. /D. Stulik/ Karlovy Vary, 1979. Vol. 2. pp. 38/1-6.

I. Mojzes, T. Sebestyén, B.P. Barna, G. Gergely, D. Szigethy, Gallium plus metal contacts to gallium arsenide alloyed in an arsenic molecular beam. Thin Solid Films, 61, 27 /1979/

E. Beregi, E. Sterk, E. Pál, M. Farkas-Jahnke, Crystal defects in flux grown lithium ferrite, $LiFe_5O_8$ single crystals. Acta Phys. Hung. 47, 263 /1979/

J. Pfeifer, L. Csontos, M. Gál, N doping in the liquid phase epitaxial growth of GaP:N light emitting diodes. Acta Phys. Hung. 47, 45 /1979/

B. Pődör, J. Pfeifer, Residual donors in liquid phase epitaxial GaP. Acta Phys. Hung. 47, 75 /1979/

N.P. Ilyin, I. Pozsgai, Capabilities of X-ray microanalysis in the analytical electron microscopy. In: XI. All-Soviet conference on electron microscopy. Vol. 1.: Physica. Moscow, 1979.-p. 68. /in Russian/

N.P. Ilyin, I. Pozsgai, A quantitative method for the microanalysis of self-supporting thin films, J. Anal. Chimii, 34, 1703 /1979/ /in Russian/

N.P. Ilyin, I. Pozsgai, Quantitative microanalysis of thin samples in the EMMA. Mikrochimica Acta, Suppl. 8, 213 /1979/

T. Sebestyén, Thin phase epitaxy of III-V compound semiconductors. Acta Phys. Hung. 47, 51 /1979/

T. Sebestyén, E. Lendvay, T. Görög, Quick and automatic determination of the dopant concentration profils of GaAs epitaxial layers. Acta Phys. Hung. 47, 33 /1979/

K. Somogyi, J. Chevallier, J.M. Rommeluere, J. Marine, B. Schaub, Luminescence and electrical properties of $Mg_xZn_{1-x}Te$ alloys. IEEE Trans. Electron Devices ED-26, 1198 /1979/

M. Somogyi, M. Farkas-Jahnke, G. Mezey, J. Gyulai, Investigations of surface layers produced by chemical treatment of GaP. Thin Solid Films 60 , 377 /1979/

M. Füstöss-Wégner, P. Sviszt, Thermally stimulated polarization and depolarization measurements in metal-free phtalocyanine thin layers. KFKI Report /92/: 1-8 /1979/

A. Szász, Á. Tichy-Rács, Photoemission investigation of Ni near the Curie temperature. Phys. Stat. Sol. /b/ 93, K13 /1979/

1980.

M. Andrási, Etched profile control in photolitographic pattern etching. Thin Solid Films 67, 229 /1980/

G. Aszódi, J. Szabon, I. Jánossy, V. Székely, Uniform high resolution thermal mapping of microcircuits using nematic liquid crystals. KFKI Report /36/:1-12 /1980/

A. Belu, A. Dévényi, R. Manaila, L. Miu, C. Rusu, Á. Barna, P.B. Barna, G. Radnóczi, L. Tóth, Structure and electrical properties of amorphous Ge-Mo films. Acta Phys. Hung. 49, 207 /1980/

A. Barna, G. Radnóczi, Specimen preparation methods of thin tungsten wires for transmission electron microscopy. Zavodskaya Laboratoriya 46, 741 /1980/ /in Russian/

P.B. Barna, Á. Barna, Z. Paál, Surface chemical phenomena influencing the growth of thin films. Acta Phys. Hung. 49, 77 /1980/

M. Lomniczy, P.B. Barna, A. Barna, Effect of trimming on the structure of NiCr thin films /abstract/. Acta Phys. Hung. 49, 253 /1980/

P.B. Barna, F.M. Reicha, The effect of oxygen uptake of crystallographic faces on the growth and coalescence of crystals in Al films. In: Proceedings of the 8th International vacuum congress, Cannes, 1980. Vol.1: Thin films. pp. 165-168.

B.P. Barna, L. Tóth, B. Petretis, R. Rinkunas, The effect of charge density in the molecular beam on the structure and properties of selenium films. Acta Phys. Hung. 48, 315 /1980/ /in Russian/

I. Nagy, T. Tarnóczy, M. Hossó, T. Nagy, P.B. Barna, Z. Frait, Magnetic phenomena in amorphous films with large scale inhomogenities /abstract/. Acta Phys. Hung. 49, 215 /1980/

L. Bartha, L. Gombos, T. Németh, T. Szalay, A.B. Kiss, Surface chemical reactions on molibdenum oxides in aqueous media. In: 9th International symposium on the reactivity of solids. Cracow, 1980. pp. 287-291

Z. Csépes, I. Gaal, Thermotransport of volatile impurities. Phys. Stat. Sol./a/ 62, 705 /1980/

M. Farkas-Jahnke, T. Grósz, E. Benes, K. Vadasdi, Structural changes accompanying repeated dehydration-hydration processes in APT.$4H_2O/[NH_4]_{10}\ H_2W_{12}O_{42}.4H_2O/$. In: 10th Hungarian diffraction conference, Balatonaliga, 1980. Coll. abstr. pp. A60-61.

I. Gaál, H.E. Exner, Interfacial instability in peritectic reactions. In: Interfaces and kinetics in materials phenomena. National Physics Laboratory, Teddington 8-10 December 1980. Abstracts p. 14.

G. Gergely, Some problems of quantitative AES in fractography. Acta Phys. Hung. 49, 87 /1980/

K. Romhányi, Zs. Szász-Csih, G. Gergely, M. Menyhárd, Auger spectrometric studies on fracture surfaces of tool steel. Krist. und Tech. 15, 471 /1980/

G. Gergely, B. Gruzza, M. Menyhárd, Backscattering spectra of medium energy electrons Acta Phys. Hung. 48, 337 /1980/

G. Gergely, B. Gruzza, M. Menyhárd, Backscattering spectra for quantitative AES of thin overlayers. In: Proceedings of the 4th international conference on solid surfaces and 3rd European conference on surface. Vol. 2.: pp. 1392-1395. Supplément á la revue "Le Vide, les Couches Minces" no. 201. 1980.

L. Gutai, Characterization of highly compensated semi-insulated GaAs substrates. Acta Phys. Hung. 48, 119 /1980/

P. Harmat, J. Major, I. Gaál, The influence of oxygen on the volume and growth kinetics of potassium bubbles in tungsten. In: Interfaces and kinetics in materials phenomena. National Physical Laboratory, Teddington 8-10 December 1980. Abstracts p. 34.

O. Horacsek, Properties and failure modes of incandescent tungsten filaments. IEE Proc. A 127, 134 /1980/

Zs. J. Horváth, Memory hysteresis measurements on silicon oxynitride films. Solid-State Electron. 23, 1053 /1980/

Zs. J. Horváth, G. Stubnya, P. Tüttő, Resistivity measurements on chemically vapour-deposited Si_3N_4 films. Thin Solid Films 69, L51 /1980/

A. Kele, M. Menyhárd, On the fracture of doped tungsten. Acta Phys. Hung. 49, 127 /1980/

J. Kertész, T. Vicsek, Orientated bond percolation. J. Phys. C: Solid State Phys. 13, L343 /1980/

F. Koltai, G. Radnóczi, Investigation of grain orientation in tungsten wires by scanning electron microscopy. In: 10th Hungarian diffraction conference, Balatonaliga, 1980. Coll. abstr. pp. A85-86.

I. Markó, On the determination of the gold acceptor level concentration in the small area p^+-n silicon junction from the steady-state phase of the TSC curve. Phys. Stat. Sol. /a/ 58, 367 /1980/

I. Markó, P. Sviszt, Effect of excitation temperature of TSC in semi-insulating GaAs:O. Phys. Stat. Sol. /a/ 58, K93 /1980/

M. Menyhárd, On the detection of small inclusions by AES. In: Proceedings of the 4th international conference on solid surfaces and the 3rd European conference on surface science. Vol. 2.: pp. 1388-1391. Supplément á la revue "Le Vide, les Couches Minces" no. 201. 1980.

I. Mojzes, Electrical modelling of ohmic contacts formation on metal-n-GaAs systems. Acta Phys. Hung. 48, 131 /1980/

M. Németh-Sallay, R. Szabó, I.C. Szép, P. Tüttő, Charge motion in silicon MOS structures. Thin Solid Films 70, 37 /1980/

E.K. Pál, A.J. Vértesy, Electrical measurements and lattice defects in silicon p-n junctions. In: 10th Hungarian diffraction conference, Balatonaliga, 1980. Coll. abstr. pp. A12-13.

I. Pozsgai, Correction for X-ray absorption in thin film microanalysis. In: Electron microscopy 1980 /EUREM'80/ Proceedings of the 7th European Congress on Electron Microscopy /P. Brederoo, V. Cosslett/ Leiden, 1980. Vol. 3. pp. 150-151.

É. Radácsi, I. Mojzes, J. Pfeifer, Comments on the properties of an NH_4OH-H_2O etch on epitaxial GaAs. Krist. und. Tech. 15, 717 /1980/

G. Radnóczi, On the role of second phases in the recrystallization. In: Electron microscopy 1980 /EUREM'80/ Proceedgins of the 7th European Congress on Electron Microscopy. /P. Brederoo, V.G. Boom/ Leiden, 1980. Vol. 1. pp. 196-197.

F.M. Reicha, P.B. Barna, On the mechanism of hillocks formation in vapour deposited thin films. ActaPhys. Hung. 49, 237 /1980/

T. Sebestyén, I. Mojzes, D. Szigethy, Use of Ga in metal-GaAs contacts to eliminate large As loss peaks. Electron. Lett. 16, 504 /1980/

I. Skopal, Eddy-current loss in powder metallurgical tungsten rods. Powder Metall. Int. 12, 75 /1980/

M. Somogyi, Investigation of oxidized $A^{III}B^{V}$ surfaces by photoresponse. Acta Phys. Hung. 48, 153 /1980/

A. Laugier, B. Montegu, D. Barrier, J. Chevallier, J.C. Guillaume, K. Somogyi, Band structure of $Mg_xZn_{1-x}Te$ alloys. Phys. Stat. Sol. /b/ 99, 319 /1980/

B. Szentpáli, A new DLTS method. Acta Phys. Hung. 48, 161 /1980/

D. Szigethy, G. Gergely, I. Mojzes, T. Sebestyén, M. Riedel, Mass spectrometric study of semiconductor layer structures. Acta Phys. Hung. 49, 199 /1980/

Á. Szőkefalvi-Nagy, G. Radnóczi, A. Kele, I. Gaál, The structure of torsion-deformed tungsten wires. In: Recrystallization and grain multiphase and particle containing materials. /N. Hansen, A.R. Jones, T. Leffers/ Proceedings of the 1st Riso International symposium on metallurgy and materials science. Roskilde, 1980. pp. 269-270.

I. Kondor, T. Temesvári, L. Herényi, Resummation of the 1/n expansion through a self-consistent approach. Phys. Rev. B /Condensed Matter/ 22, 1451 /1980/

A.L. Tóth, J.É. Puskás, Energy dispersive X-ray microanalysis of phosphosilicate glasses /PSG/. Acta Phys. Hung. 49, 133 /1980/

T. Vicsek, Simple variational method for the closures of the Ornstein-Zernike equation: a study of liquid instability. Physica 102A, 523 /1980/

A. Lindegaard-Andersen, G. Christiansen, L. Zsoldos, On the geometrical conditions for X-ray topographs of large crystal slices. J. Appl. Crystallogr. 13, 1 /1980/

L. Zsoldos, Determination of strain distribution in surface layers of bent crystals by double-crystal X-ray topography. In: 10th Hungarian diffraction conference, Balatonaliga, 1980. Coll. abstr. pp. A21-22.

É. Zsoldos, L. Zsoldos, Determination of thickness of thin epitaxial garnet films from double-crystal rocking curve. In: 6th European crystallographic meeting, Barcelona, 1980. p. TU-P66.

PATENTS

L. Bartha, I. Hangos, K. Vadasdi: Halogen incandescent lamp and a method for its production. Hung. pat. No. 167 329 /1975/; BDR Pat. No. 2 431 250 /1977/; GB Pat. No. 1 541 949 /1979/

R. Brósz, G. Eppeldauer, J. Schanda, M. Vanyek: Digital output short circuit current meter. Hung. Pat. No. 173 090 /1978/; Pat. Appl. GDR, Poland

G. Eppeldauer, J. Schanda, G. Lux: Equipment for the determination of tristimulus values and chromaticity coordinates. Hung. Pat. No. 168 258 /1975/; GDR Pat. Appl. No. 117 736 /1974/; French Pat. No. 7 418 053.

G. Ferenczy, P. Horváth, F. Tóth, J. Kiss, J. Boda: A method for deep level transient spectroscopy scanning and apparatus for carrying out the method. Hung. Pat. Appl. No. 1439/80; European Pat. Appl. No. /For BGFR, UR, Netherland, Sweden, France/ 81302531.9; GDR Pat. Appl. No. 226-420.

I. Gaál, P. Ivanov, J. Major, E. Hauszner, D. Zsámbók: Method and apparatus for the contactless measurement of mechanical stresses in ferromagnetic materials. Hung. Pat. No. 174 945 /1980/; Pat. Appl.: France, BDR, GDR, The Netherland, Sweden, Luxemburg, Great Britain.

K. Németh, Cs. Lénárt, E. Nagy, L. Bartha: Process and equipment for the thermal analysis of materials. Hung. Pat. No. 175 262 /1980/; Pat. Appl: USSR, Poland, GDR, USA, Switzerland, France, BDR, GB.

T. 13.